

**IN VIVO ARCHITECTURE OF THE GASTROCNEMIUS AND SOLEUS
MUSCLES IN HEALTHY BOYS AND THOSE WITH DUCHENNE MUSCULAR
DYSTROPHY**

by

Christopher Yuen

**A thesis submitted in conformity with the requirements
for the degree of Master of Exercise Science
Graduate Department of Exercise Science
University of Toronto**

© Copyright by Christopher Yuen 2008



Library and
Archives Canada

Bibliothèque et
Archives Canada

Published Heritage
Branch

Direction du
Patrimoine de l'édition

395 Wellington Street
Ottawa ON K1A 0N4
Canada

395, rue Wellington
Ottawa ON K1A 0N4
Canada

Your file *Votre référence*
ISBN: 978-0-494-45030-7
Our file *Notre référence*
ISBN: 978-0-494-45030-7

NOTICE:

The author has granted a non-exclusive license allowing Library and Archives Canada to reproduce, publish, archive, preserve, conserve, communicate to the public by telecommunication or on the Internet, loan, distribute and sell theses worldwide, for commercial or non-commercial purposes, in microform, paper, electronic and/or any other formats.

The author retains copyright ownership and moral rights in this thesis. Neither the thesis nor substantial extracts from it may be printed or otherwise reproduced without the author's permission.

AVIS:

L'auteur a accordé une licence non exclusive permettant à la Bibliothèque et Archives Canada de reproduire, publier, archiver, sauvegarder, conserver, transmettre au public par télécommunication ou par l'Internet, prêter, distribuer et vendre des thèses partout dans le monde, à des fins commerciales ou autres, sur support microforme, papier, électronique et/ou autres formats.

L'auteur conserve la propriété du droit d'auteur et des droits moraux qui protègent cette thèse. Ni la thèse ni des extraits substantiels de celle-ci ne doivent être imprimés ou autrement reproduits sans son autorisation.

In compliance with the Canadian Privacy Act some supporting forms may have been removed from this thesis.

Conformément à la loi canadienne sur la protection de la vie privée, quelques formulaires secondaires ont été enlevés de cette thèse.

While these forms may be included in the document page count, their removal does not represent any loss of content from the thesis.

Bien que ces formulaires aient inclus dans la pagination, il n'y aura aucun contenu manquant.

■ ■ ■
Canada

In vivo architecture of the gastrocnemius and soleus muscles in healthy boys and those with Duchenne Muscular Dystrophy

Christopher Yuen
Master of Science, Department of Exercise Science
Faculty of Physical and Health education, University of Toronto, 2008

Abstract

Purpose: To quantify and visually compare *in vivo* ultrasound changes in pennation angles, fibre bundle length and muscle thickness of medial (MG) and lateral (LG) gastrocnemius, and posterior soleus (PS) in Duchenne Muscular Dystrophy (DMD) and in controls. **Methods:** 18 DMD and 18 control boys were recruited. Architectural measurements were quantified from images in relaxed and maximally contracted states. A new qualitative scale was developed to grade images and compared with timed function tests (TFT). **Results:** Compared to controls, PS of DMD showed significant changes in architecture on contraction in all parameters ($p < 0.05$). MG/LG exhibited less change than PS. Muscle thickness was significantly greater ($p < 0.05$) in DMD at all sites. Qualitative scores were well correlated with TFTs (walking: $\rho = 0.670$; stairs: $\rho = 0.816$). **Conclusion:** MG/LG changes in muscle architecture are different than those of PS. The new grading scale may be a useful clinical tool to monitor DMD disease progression.

Acknowledgements

"At times our own light goes out and is rekindled by a spark from another person. Each of us has cause to think with deep gratitude of those who have lighted the flame within us."

--Dr. Albert Schweitzer--

I will forever be indebted to my mentors, Dr. Nancy McKee and Dr. Anne Agur: theirs were the flames that lighted the path when my own was insufficient to show me the way. While their knowledge and experience made it possible for me to complete this thesis, it is their dedication, patient nurturing, and above all, humanity that truly shepherded me through graduate school. Both of them transcend the meaning of the word "mentor". Quite simply: thank you Anne, thank you Nancy.

I am also very grateful to Dr. Scott Thomas for agreeing to be a part of my advisory committee, and to Drs. Bareket Falk (external examiner) and Marius Locke (chair) for their contributions during my oral defence.

My personal odyssey through academia has not only made me into a better researcher, but I dare say, a better person. This is due, in no small measure, to the excellent students and colleagues that came into my life and indelibly enriched it. Your camaraderie brought a little sunshine into the windowless basement of MSB. One colleague in particular, Kajeandra Ravichandiran, deserves a special note of gratitude. His technical expertise facilitated many things and helped to keep my stress levels at a minimum. I have no doubt that he will achieve his dreams.

Many thanks must go to the staff at Bloorview MacMillan Children's Center for giving me the opportunity to work among them. Their assistance with recruiting patients (Dr. Doug Biggar and Ms. Vivien Harris) and obtaining the ultrasound scans (Mr. Joe Chan) was also invaluable and should be recognized.

Special credit goes to Dr. Roger Leekam for sharing his expertise on musculoskeletal ultrasound imaging with us.

My family, of course, deserves great distinction and appreciation. They have allowed me the time and freedom to explore my options, and that is what any person facing an ambiguous future could ever really hope for.

Finally, I must thank my wonderful wife, Karen, who inexplicably saw the best in me even while I was at my worst. Her unwavering support and heroic tolerance harboured my ship during the stormy times, and reminded me that the sky always clears after the rain passes. I love you Karen.

**This thesis was made possible by generous funding from the Hospital for Sick
Children foundation and Kids Action.**

Table of Contents

	Page
Abstract	ii
Acknowledgements	iii
Table of Contents	v
List of Figures	viii
List of Tables	xi
List of Abbreviations	xiv
Chapter 1: Introduction	1
1.1 Overview	1
1.2 Contents of thesis	2
Chapter 2: Background	4
2.1 Skeletal muscle	4
2.2 Structure of skeletal muscle	4
2.3 Muscle architecture	10
2.4 Relation of architecture to function	13
2.5 Physiological Cross-sectional Area	16
2.6 Architecture of Gastrocnemius and Soleus	17
2.6.1 Cadaveric studies	18
2.6.2 <i>In vivo</i> ultrasound studies	19
2.6.2.1 Introduction	19
2.6.2.2 <i>In vivo</i> studies of normal soleus and gastrocnemius in adults	21
2.6.2.3 <i>In vivo</i> studies of normal soleus and gastrocnemius in children	27
2.7 Duchenne Muscular Dystrophy	29

2.7.2 Etiology	32
2.7.3 Pathophysiology	33
2.8 Quantitative ultrasound studies of muscle architecture in children with Duchenne Muscular Dystrophy	37
2.9 Qualitative rating of ultrasound images	38
Chapter 3: Purpose and Hypothesis	40
3.1 Purpose	40
3.2 Hypothesis	40
Chapter 4: Methods	41
4.1 Subjects	41
4.2 Protocol	42
4.3 Measurements	45
Chapter 5: Results	50
5.1 Control group	50
5.1.1 Fiber Bundle Length	50
5.1.2 Angles of Pennation	52
5.1.2.1 Posterior Pennation Angle	52
5.1.2.2 Anterior Pennation Angle	53
5.1.2.3 Change in Pennation Angle on contraction	54
5.1.3 Muscle Thickness	54
5.2 DMD group	55
5.2.1 Fiber Bundle Length	56
5.2.2 Angles of Pennation	58
5.2.2.1 Posterior Pennation Angle	58
5.2.2.2 Anterior Pennation Angle	58
5.2.2.3 Change in Pennation Angle on contraction	59
5.2.3 Muscle Thickness	60
5.2.4 Correlation between muscle architectural parameters	61
5.3 Control group vs. DMD group	62

5.3.1 Fiber Bundle Length	62
5.3.2 Angles of Pennation	63
5.3.2.1 Posterior Pennation Angle	63
5.3.2.2 Anterior Pennation Angle	65
5.3.3 Muscle Thickness	66
5.4 Qualitative Rating	67
5.4.1 Overview	67
5.4.2 Age distribution of scans	67
5.4.3 Rating scores	68
5.4.3.1 Comparison by age	68
5.4.3.2 Comparison of qualitative rating scale with Timed Function Tests	70
5.4.3.3 Fiber bundle curvature	72
5.4.3.4 Deformity of aponeurosis	72
Chapter 6: Discussion	75
6.1 Quantitative muscle architecture of control group	75
6.2 Quantitative muscle architecture of DMD group	77
6.2.1 Quantitative results and Timed Function Tests	81
6.3 Qualitative rating of ultrasound	82
6.3.1 Qualitative rating scores and Timed Function Tests	86
Chapter 7: Conclusion	87
Chapter 8: Future directions	89
References	90
Appendix A: Sample size of DMD subjects by age	97
Appendix B: Sample size of control subjects by age	98
Appendix C: Architectural parameters by age	99
Appendix D: Calculations for Specificity and Sensitivity	116
Appendix E: Consent and Assent forms	117

List of Figures

	Page
Chapter 2:	
Figure 2.1. Gross structural arrangement of skeletal muscle.	5
Figure 2.2. Electron micrograph of skeletal muscle.	6
Figure 2.3. Muscle proteins.	7
Figure 2.4. Sarcomere and myofibril proteins.	8
Figure 2.5. Muscle contraction.	9
Figure 2.6. Fascicular architecture of skeletal muscle.	11
Figure 2.7. Schematic illustration of architectural parameters.	12
Figure 2.8. Pennation angle and axis of force.	14
Figure 2.9. Force-length relationship.	15
Figure 2.10 Normalized force-velocity curve.	16
Figure 2.11 Dissections of the posterior compartment of right leg.	18
Figure 2.12 Ultrasound scan of calf muscles.	21
Figure 2.13 Pictorial series demonstrating Gowers' sign.	31
Figure 2.14 Dystrophin-Glycoprotein complex.	33
Chapter 4:	
Figure 4.1. Ultrasound scanning sites.	43
Figure 4.2. Ultrasound image of the medial gastrocnemius.	44
Figure 4.3. Scale markers on the ultrasound image.	45
Figure 4.4. Ultrasound image with completed lines for measurement.	46
Figure 4.5. Ultrasound scans of relaxed medial gastrocnemius.	49

Chapter 5:

Figure 5.1.	Ultrasound scans from one control subject.	51
Figure 5.2.	Ultrasound scans of one DMD subject.	57
Figure 5.3.	Bar graphs of mean fiber bundle lengths for control vs. DMD groups.	63
Figure 5.4.	Bar graphs of mean posterior pennation angles (Post PA) for control vs. DMD groups.	64
Figure 5.5.	Bar graphs of mean anterior pennation angles (Ant PA) for control and DMD groups.	65
Figure 5.6.	Bar graphs of mean muscle thicknesses (MT) for control and DMD groups.	67
Figure 5.7.	Ultrasound scan of posterior soleus rated “out of plane”.	69
Figure 5.8.	Excessive curvature of DMD muscle fibers.	73
Figure 5.9.	Deformity of DMD aponeurosis.	74

Appendix C

Figure C.1.	Bar graphs of mean fiber bundle lengths (FBL) by age for the control group.	100
Figure C.2.	Bar graphs of mean anterior pennation angles (Ant PA) by age for the control group.	101
Figure C.3.	Bar graphs of mean posterior pennation angles (Post PA) by age for the control group.	102
Figure C.4.	Bar graph of mean muscle thicknesses (MT) by age for the control group.	104
Figure C.5.	Bar graphs of mean fiber bundle lengths (FBL) by age of the DMD group.	105
Figure C.6.	Bar graphs of mean anterior pennation angles (Ant PA) by age of the DMD group.	106
Figure C.7.	Bar graphs of mean posterior pennation angles (Post PA) by age of the DMD group.	107

Figure C.8.	Bar graphs of mean muscle thicknesses (MT) by age for the DMD groups.	109
Figure C.9.	Bar graphs of mean fiber bundle lengths by age for control vs. DMD groups.	110
Figure C.10.	Bar graphs of mean posterior pennation angles (Post PA) by age for control vs. DMD groups.	113
Figure C.11.	Bar graphs of mean anterior pennation angles (Ant PA) by age for control and DMD groups.	114
Figure C.12.	Bar graphs of mean muscle thicknesses (MT) by age for control and DMD groups.	115

List of Tables

	Page
Chapter 2:	
Table 2.1. Architectural data of gastrocnemius and soleus from cadaveric specimens.	19
Table 2.2. Architectural data for medial gastrocnemius in adults.	22
Table 2.3. Architectural data for lateral gastrocnemius in adults.	25
Table 2.4. Architectural data for posterior soleus.	26
Table 2.5. Estimated posterior PA and MT data from Binzoni et al. (2001)	28
Table 2.6. Duchenne's clinical description of DMD.	30
Table 2.7. Typical pattern of muscle weakness in children with DMD.	30
Table 2.8. Previously established qualitative rating scale for US images of diseased muscle (Heckmatt et al., 1982).	39
Chapter 4:	
Table 4.1. New qualitative rating scale for ultrasound images.	48
Chapter 5:	
Table 5.1. Mean fiber bundle lengths (FBL) for the control group.	52
Table 5.2. Anterior (Ant) and Posterior (Post) Pennation angle (PA) data for the control group.	53
Table 5.3. Mean muscle thicknesses (MT) for the control group.	54
Table 5.4. Mean fiber bundle lengths (FBL) for the DMD group.	56
Table 5.5. Mean anterior (Ant) and posterior (Post) pennation angles (PA) for the DMD group.	59
Table 5.6. Mean muscle thicknesses (MT) for the DMD group.	60

Table 5.7.	Pearson's correlation values between pennation angle and muscle thickness for the DMD group.	61
Table 5.8.	Pearson's correlation values between pennation angle and muscle thickness for the control group.	61
Table 5.9.	Mean fiber bundle lengths for Control vs. DMD groups.	62
Table 5.10.	Mean posterior pennation angle (Post PA) for control and DMD groups.	64
Table 5.11.	Mean anterior pennation angles (Ant PA) for control and DMD groups.	65
Table 5.12.	Mean muscle thicknesses (MT) for control and DMD groups.	66
Table 5.13.	Distribution of quantifiable images in the relaxed state for the DMD group.	68
Table 5.14.	Distribution of qualitative ratings in the DMD group by age and muscle.	69
Table 5.15.	Mean results on timed function tests (TFT).	71
Table 5.16.	Pearson's correlation (r values) between qualitative rating scores and age, TFT (walk), and TFT (stairs).	71
Table 5.17.	Comparison of qualitative data to timed function tests (TFT) for younger DMD children (≤ 10 years).	71
Table 5.18.	Comparison of qualitative data to timed function tests (TFT) for older DMD children (≥ 11 years).	72
Chapter 6:		
Table 6.1.	Comparison of mean architectural parameters of MG and LG between studies.	76
Table 6.2.	Percentage difference of architectural parameters between DMD and control subjects in the relaxed state.	79
Table 6.3.	Percentage difference between DMD and control subjects in the amount of change in architectural parameters on contraction.	80

Table 6.4.	Comparison of the amount of change on contraction of MG, LG, and PS architectural parameters to TFT scores in the young and old DMD groups.	82
Table 6.5.	Qualitative rating scale developed by Heckmatt et al. (1982) for US images of diseased muscle.	83
Table 6.6.	New qualitative rating scale of US images for children with DMD.	84
Appendix A		
Table A.1.	Number of legs (MG) quantified for each architectural parameter categorized by age for DMD subjects.	97
Table A.2.	Number of legs (LG) quantified for each architectural parameter categorized by age for DMD subjects.	97
Table A.3.	Number of legs (PS) quantified for each architectural parameter categorized by age for DMD subjects.	97
Appendix B		
Table B.1.	Number of legs (MG) quantified for each architectural parameter categorized by age for control subjects.	98
Table B.2.	Number of legs (LG) quantified for each architectural parameter categorized by age for control subjects.	98
Table B.3.	Number of legs (PS) quantified for each architectural parameter categorized by age for control subjects.	98
Appendix D		
Table D.1.	Number of legs (DMD and control) for specificity and sensitivity calculations.	116

List of Abbreviations

Ant PA	Anterior pennation angle
DMD	Duchenne Muscular Dystrophy
FBL	Fiber bundle length
LG	Lateral gastrocnemius
MD	Muscular dystrophies
MG	Medial gastrocnemius
MT	Muscle thickness
MVC	Maximal voluntary contraction
Post PA	Posterior pennation angle
PS	Posterior soleus
US	Ultrasound

Chapter 1: Introduction

1.1 Overview

Muscular dystrophies (MD) are a group of genetic disorders characterized by progressive skeletal muscle weakness and degeneration of muscle fibers (Dubowitz 1995). Muscular dystrophies are *primary* myopathies because they result from a defect within the muscle itself that is not secondary to other pathologies (e.g., metabolic disorders). The genotype and phenotype of different MD are used to define and classify them; each type of MD varies in severity and pattern of muscle weakness. Presently, MD cannot be cured.

Duchenne Muscular Dystrophy (DMD) is one severe form of MD that begins to affect boys at a very young age, typically about 2-3 years old. It is the most common neuromuscular disease in children, and even with treatment, the average life expectancy of these boys is in the low to mid twenties (Dubowitz 1995). While the genetic defect responsible for DMD has been discovered (Kunkel, Monaco et al. 1986), the exact cause of muscle weakness and deterioration remains unclear. Moreover, it is not known why certain muscles are affected earlier and to a greater degree than others.

Numerous studies have looked into these issues dealing with the pathogenesis and treatment of DMD (Brussock, Haley et al. 1992; Campbell and Jacob 2003; Bogdanovich, Perkins et al. 2004), but comparatively few have investigated the anatomical features of the disease such as the internal structure of dystrophic muscle. This internal structure or architecture refers to how muscle fibers are assembled to make up the whole muscle. Insight into the architecture of skeletal muscle is essential to understanding its function

(Kawakami, Abe et al. 1995); for patients with DMD, knowledge of muscle architecture can shed specific light on how the disease process alters muscle function.

The current thesis documents the architecture of the gastrocnemius and soleus in children with DMD using non-invasive ultrasound imaging. These two plantarflexors were chosen because 1) they are relevant to ambulation, and 2) they maintain functional strength longer than many other lower limb muscles, which allows their contraction characteristics to be studied. This thesis will include analysis and discussion of architectural and qualitative data obtained from cadaveric and in vivo studies. A better understanding of normal muscle architecture and the progression of architectural changes that occur in DMD subjects may enable clinicians to develop evidence-based guidelines for monitoring functional changes through the use of ultrasound.

1.2 Contents of thesis

This thesis consists of eight chapters presented in the following sequence:

- Chapter 1 provides an introduction to DMD and its effects on skeletal muscle structure and function.
- Chapter 2 consists of a review of the literature in the areas of normal skeletal muscle structure and function, and DMD. Existing literature of the architecture of human gastrocnemius and soleus of healthy and DMD subjects are reviewed. Finally, ultrasound imaging of muscle architecture is discussed.
- Chapter 3 states the purpose and hypothesis for this thesis.
- Chapter 4 describes the recruitment of subjects, methods, and protocols that were used to acquire and analyze the data.

- Chapter 5 presents the results of this study. Ultrasound data of the gastrocnemius and soleus from control and DMD subjects are analyzed and compared.
- Chapter 6 discusses the findings and limitations of this study.
- Chapter 7 and 8 consists of the conclusions and future directions of this work

Chapter 2: Background

2.1 Skeletal Muscle

The muscular system consists of approximately 650 individual muscles and accounts for about forty percent of total body weight in adults. Muscles vary considerably in size and shape, and act on the skeleton to provide movement and stability to the body. A muscle's output - the amount of force and motion it can generate - depends largely on the arrangement of contractile and connective tissue elements within (Fukunaga, Kawakami et al. 1997). This internal organization is called muscle architecture.

2.2 Structure of Skeletal Muscle

Skeletal muscle is composed of connective tissue and contractile elements. Connective tissue include tendons, aponeuroses, and protective coverings (i.e., epimysium, perimysium, endomysium), while contractile elements are the myofibrils that make up the muscle belly (Sherwood 2001). There are also vascular and neural tissues associated with muscle.

Tendons are fibrous cords with minimal elasticity that connect the fleshy part of a muscle to its bony attachment. Aponeuroses are flat, expanded tendons that also attach muscle fibers to bone.

The entire muscle belly is enveloped by a connective tissue sheath called the epimysium (Fig. 2.1).

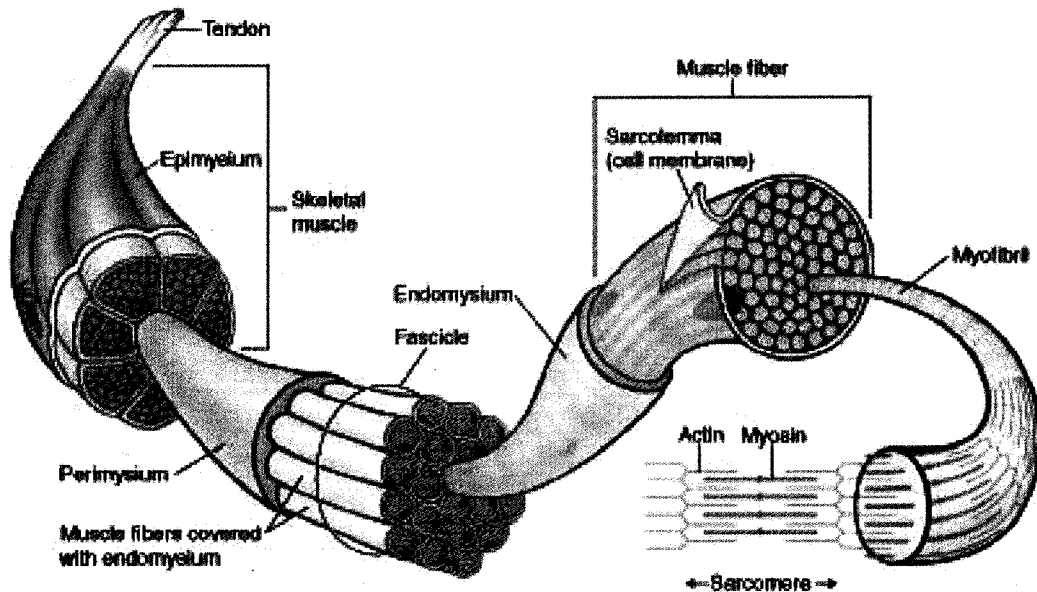


Figure 2.1. Gross structural arrangement of skeletal muscle.
 (Reproduced with permission from Lippincott, Williams, & Wilkins, *Essential Clinical Anatomy* (2007), Fig. I.10)

Extensions from the epimysium enter the substance of the muscle, dividing the muscle into distinct bundles of fibers called fascicles. Each fascicle is surrounded by perimysium and contains many muscle fibers (muscle cells) arranged in parallel; individual fibers or cells are covered by endomysium. A single muscle fiber (~10-100 μ m diameter) is made up of *myofibrils* which have a characteristic appearance of alternating light and dark bands under high-powered magnification (Fig. 2.2). These bands result from the interdigitation of two basic structural components within myofibrils: *actin thin filaments* (7-9nm diameter) and *myosin thick filaments* (12-15nm diameter).

Myosin thick filaments are constructed of myosin molecules which have a long rod-like body and a globular head that projects out at an angle from the body (Figs. 2.3A & 2.3B). Myosin molecules are assembled into filaments with their tails connecting to a common anchorage point called the M-line (Fig. 2.4). For a contraction to occur, the

myosin heads must connect to attachment sites on actin filaments to form reversible connections or cross-bridges.

Actin thin filaments consist of twin strands of actin molecules wound together into a spiral (Fig. 2.3C). The analogy of two parallel strings of pearls twisted on each other is a common description for this design (Buller 1978). Two regulatory proteins are also associated with actin filaments: long strands of *tropomyosin* and globular *troponin* (Fig. 2.3C). These proteins act as gatekeepers to the myosin attachment sites, allowing actin-myosin cross-bridges to form only in the presence of calcium.

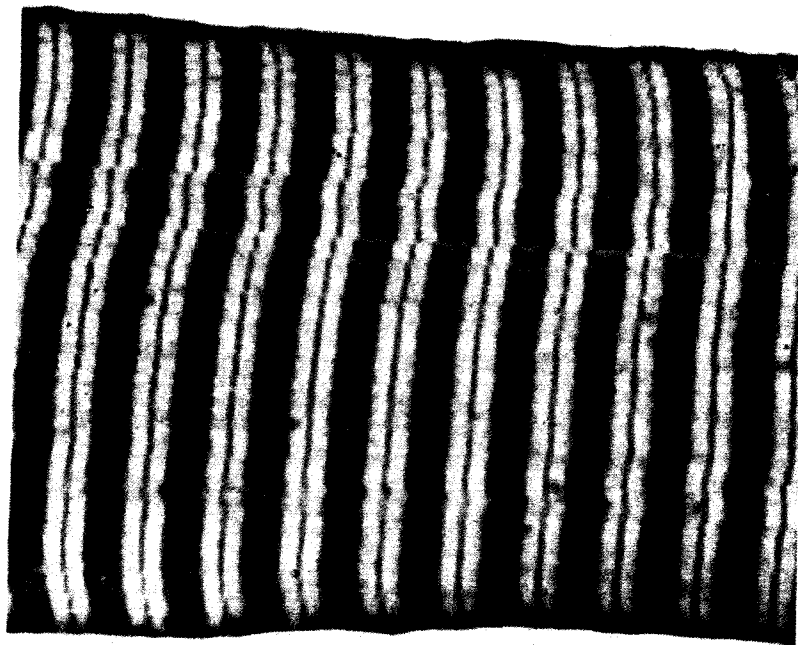


Figure 2.2. Electron micrograph of skeletal muscle. Distinctive light and dark bands are clearly visible. (Reproduced with permission from Cormack (1987) Fig. 15-4).

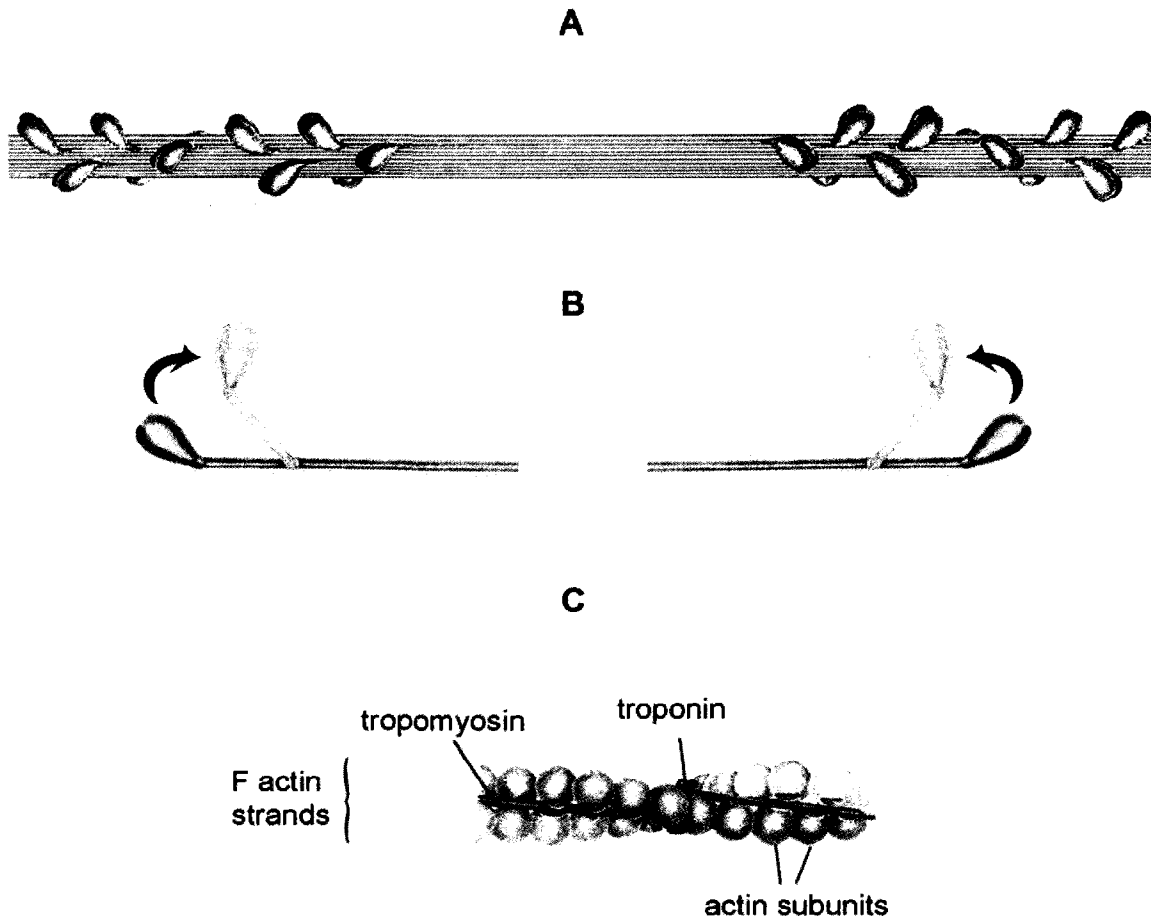


Figure 2.3. Individual muscle proteins. (A) Myosin thick filament. (B) Individual myosin proteins. Arrows demonstrate the swinging action of myosin heads during muscle contraction. (C) Actin filament with associated proteins, tropomyosin and troponin. (Reproduced with permission from Cormack (1987) Figs 15-18, 15-19, and 15-20)

The alternating light and dark pattern previously described on the myofibrils are divided into discrete zones, producing useful landmarks for the study of muscle contractions. The dark A-band contains myosin thick filaments overlapped with actin thin filaments, whereas the lighter I-band contains only actin thin filaments. The line bisecting the I-band is the Z-line (Z-disc), which anchors actin filaments and marks the boundaries of a single contractile unit, the sarcomere (Fig. 2.4).

Within a sarcomere the basic mechanism of muscle contraction takes place.

Following the arrival of an action potential, stored calcium is released within the muscle.

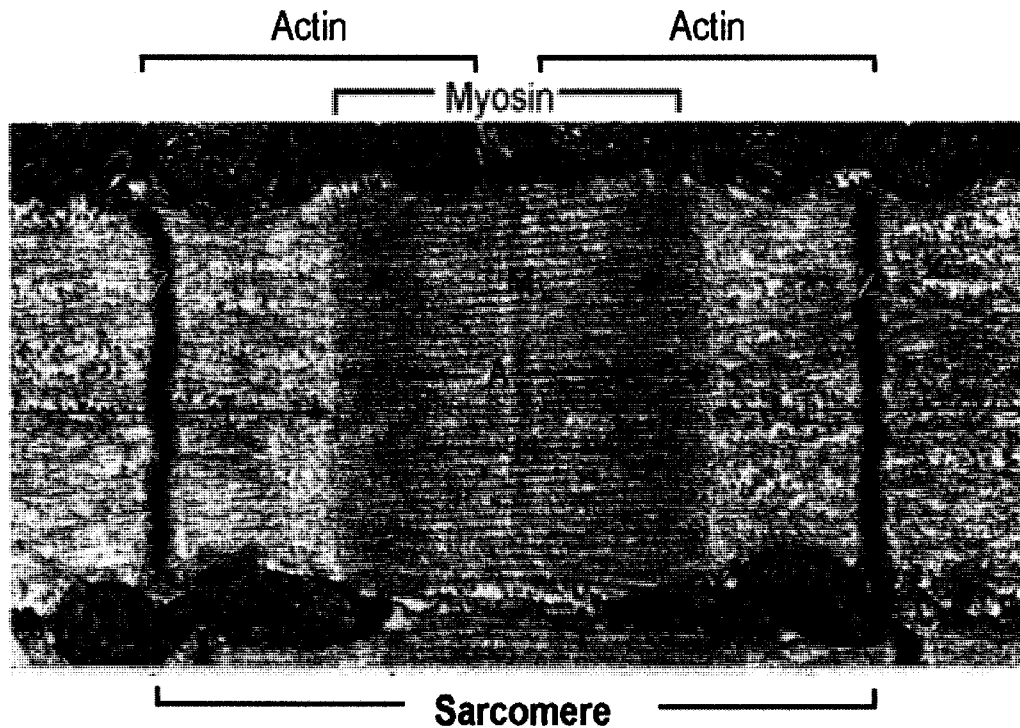


Figure 2.4. Sarcomere and myofibril proteins. M = M line, A = A band, I = I band, H = H zone (Reproduced with permission from Cormack (1987) Fig 15-6)

Calcium alters the troponin-tropomyosin complex, so that myosin attachment sites on actin are uncovered, and myosin can form cross-bridges with actin. Once cross-bridges are established, a change occurs in the conformation of the myosin heads – provided ATP is present – which causes them to swing toward the A band. This motion slides actin and myosin filaments past each other, bringing adjacent Z lines closer together and shortening the sarcomere (Fig. 2.5). The large number of sarcomeres connected in series is sufficient to generate functional ranges of motion (Lieber 1999).

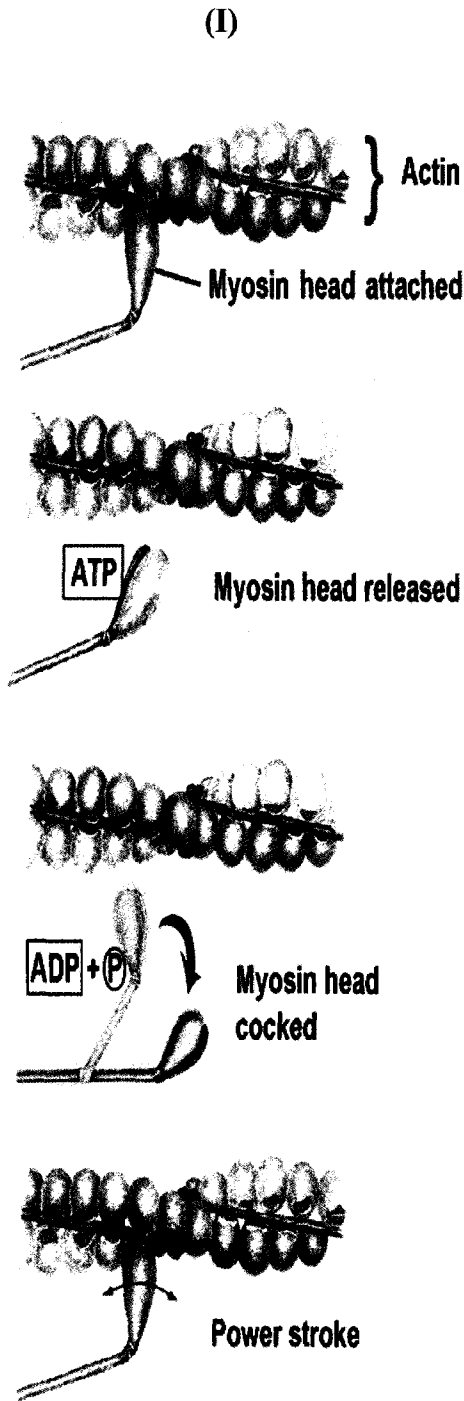
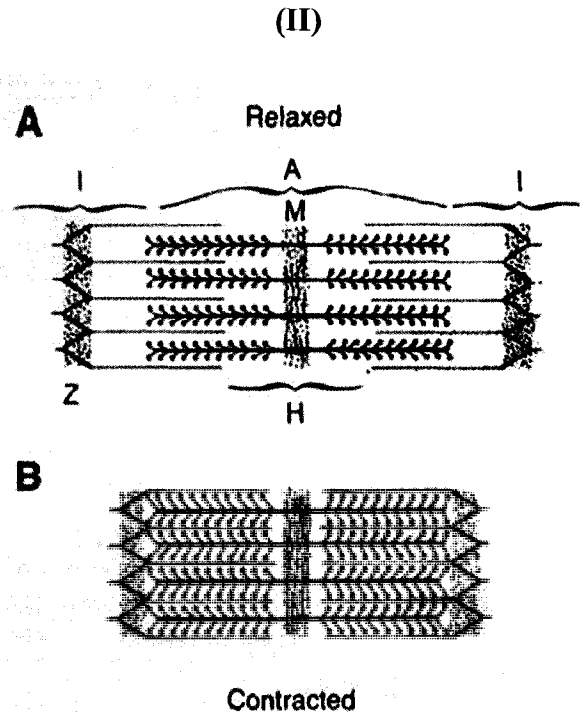


Figure 2.5. Muscle contraction. (I) The crossbridge cycle. Myosin remains attached to actin at the end of a previous muscle contraction. ATP attaches to the myosin head and releases it from actin. Hydrolysis of ATP changes the conformation of the myosin head, priming it for power generation (cocked). Calcium release within the muscle allows myosin to reattach to actin, forming the cross-bridge. Upon cross-bridge formation, the myosin head flexes (power stroke) and “pulls” actin towards the M line. The cycle can repeat at this point. (II) Diagram of sarcomeres illustrating the position of actin thin filaments in relaxed (A) and maximally contracted conditions (B). Note how actin slides across myosin towards the M line (M). (Reproduced with permission from Cormack (1984) Fig. 10-6; (1987) Fig. 15-18).



2.3 Muscle Architecture

Architecture of skeletal muscle refers to the internal arrangement of muscle fibers (Lieber and Brown 1992). In general, muscle fibers may be arranged in numerous patterns within a muscle belly. Some of the more common arrangements found, for example, in the muscles of the upper and lower limb are fusiform, spiral, and pennate as shown in Figure 2.6 (Moore and Agur, 2007).

In a fusiform muscle (e.g., biceps brachii) the fibers are arranged parallel to the long axis of the muscle. Spiral muscles usually coil around bone to their attachment and generate rotational force (e.g., supinator). Pennate muscles have fibers that are oblique to the long axis of the muscle. They can be further sub-divided into unipennate, bipennate, and multipennate muscles (Fig. 2.6). Unipennate muscles have oblique fibers attaching to one side of the tendon only, so they resemble half a feather (e.g., medial gastrocnemius). Bipennate muscles resemble the whole feather because they have oblique fibers on both sides of the tendon (e.g., rectus femoris), while multipennate muscles have additional septa within the muscle which divide it into several feather-like portions (e.g., soleus). The obliquity of fibers in pennate muscles allows for more fibers to attach to its tendon, giving more force generating capacity, but less excursion than fusiform muscles (Maganaris, Baltzopoulos et al. 1998). More specifically, muscle architectural parameters include muscle length, muscle volume, cross-sectional area, fiber bundle length and angle of pennation.

Muscle length is defined as the distance from the origin of the most proximal fibers to the insertion of the most distal fibers (Lieber 2002). This measurement is

different from whole muscle length, which includes the length of the tendon as well as the muscle belly.

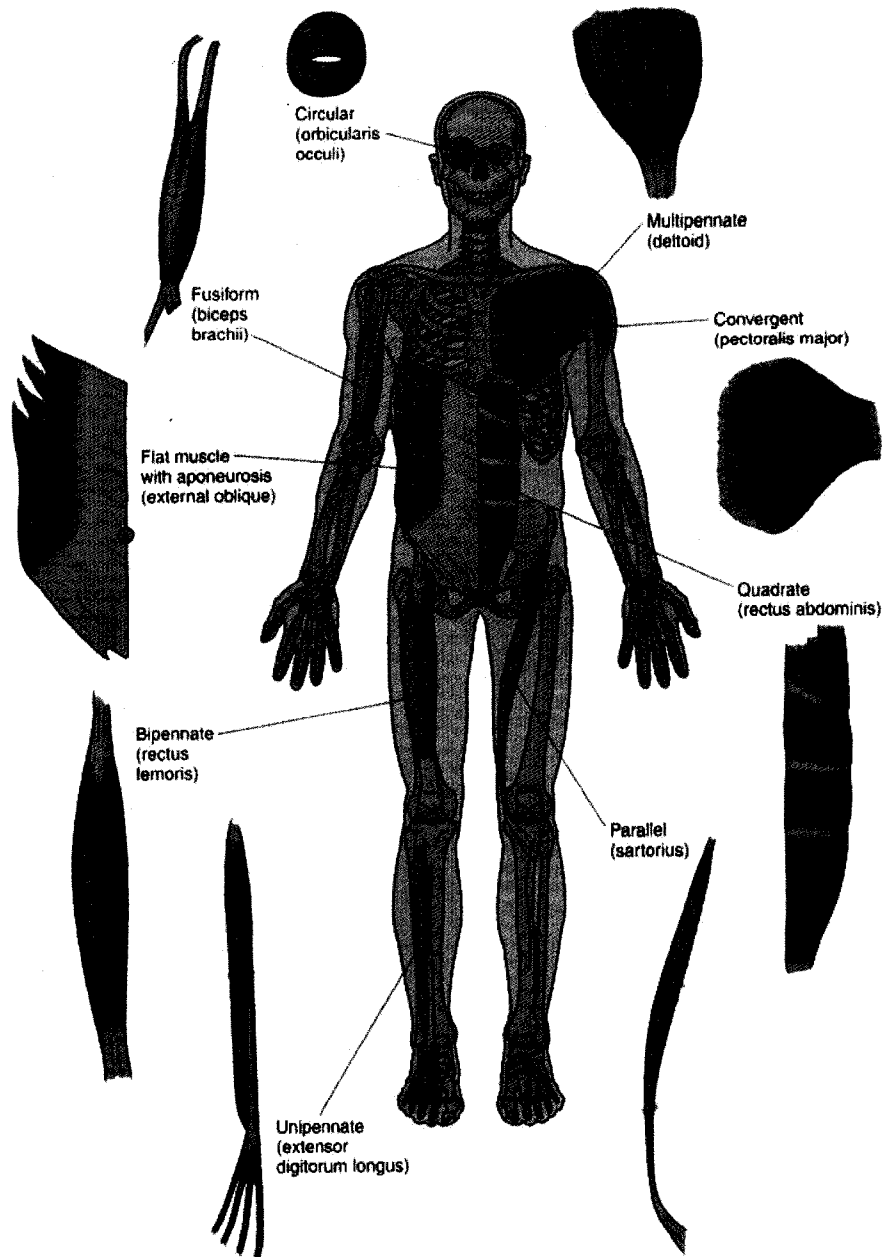


Figure 2.6. Fascicular architecture of skeletal muscle.
(Reproduced with the permission from Lippincott, Williams & Wilkins, Essential Clinical Anatomy (2007), Figure I.9)

Muscle volume is calculated by dividing a muscle's mass by its density. This gives an estimate of muscle size, but yields no information about its internal architecture. Cross-sectional area (CSA), another descriptor of muscle size, is the area of a slice, in the transverse plane, through the belly of a muscle. Since it is a two-dimensional measurement, CSA can be obtained directly from an image, making it easier to calculate than muscle volume. Similarly, the thickness of a muscle can be determined from an image by measuring the distance between its superficial and deep boundaries as shown in Figure 2.7.

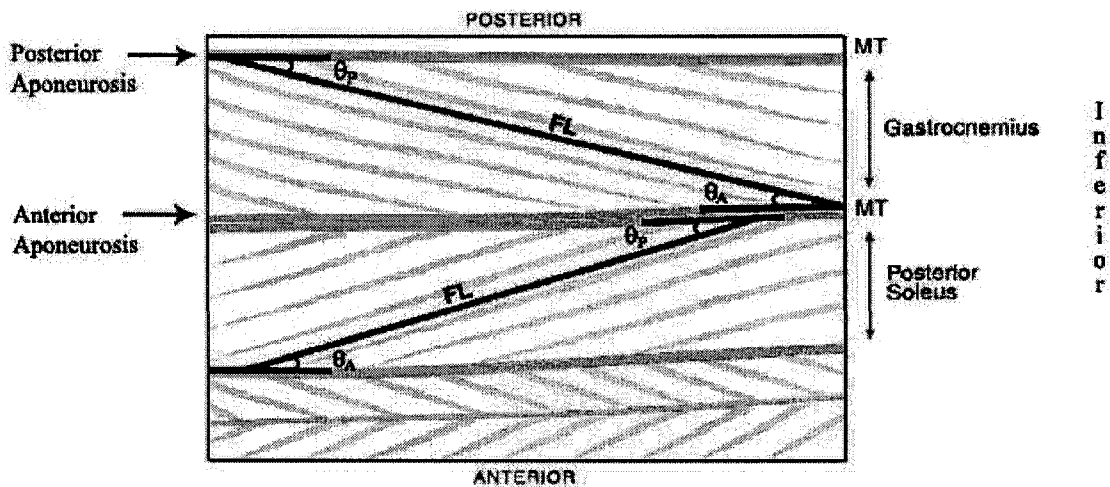


Figure 2.7. Schematic illustration of architectural parameters. FL = Fiber bundle length θ_A = anterior angle of pennation, θ_P = posterior angle of pennation, MT = muscle thickness.

The fiber bundle length (FL) is defined as the length of a fiber bundle between its two attachment sites (e.g., aponeuroses, bone). The pennation angle (PA) is the angle at

which muscle fiber bundles intersect their attachment sites. For most muscles (e.g., the gastrocnemius and soleus), two angles may be measured corresponding to the anterior and posterior attachment sites on the aponeuroses of these muscles. This yields an anterior and a posterior angle of pennation.

2.4 Relation of architecture to function

Lieber and Friden (2000) stated that architectural variations are good predictors of force characteristics in different muscles. Numerous other studies have also documented the importance of architecture as a determinant of function (Wickiewicz, Roy et al. 1983; Friederich and Brand 1990; Roy and Ishihara 1997; Narici 1999). Fiber bundle length, angle of pennation, and measures of muscle size (i.e., CSA, thickness) all influence the output of skeletal muscle.

Muscles with fiber bundles that contain longer fibers are capable of greater excursion (i.e., additive effect of a higher percentage of sarcomeres arranged in series) compared to muscles with shorter fibers with sarcomeres arranged in parallel (Lieber 2002). On the other hand, the amount of pennation within a muscle determines the number of contractile elements that can be packed along a tendon; a greater PA allows more fiber bundles to fit into a given volume to contribute to force production. However, since the FB are pulling at an angle relative to the axis of force, only a component of its force (i.e., cosine of the angle) will be transmitted to the tendon (Fig. 2.8). This reduced force is offset by the greater number of fiber bundles in pennate muscle so that overall, pennate muscles still generate more force than fusiform muscles. A greater PA also means that the length of the FB will be shorter than in a similar muscle with less pennation (i.e., fibers that run more parallel). Generally speaking, FL affects a muscle's

excursion and PA modifies muscular force. Consequently, both PA and FL also indirectly affect the length-tension and force-velocity relationships of skeletal muscle (van Donkelaar, Willems et al. 1999).

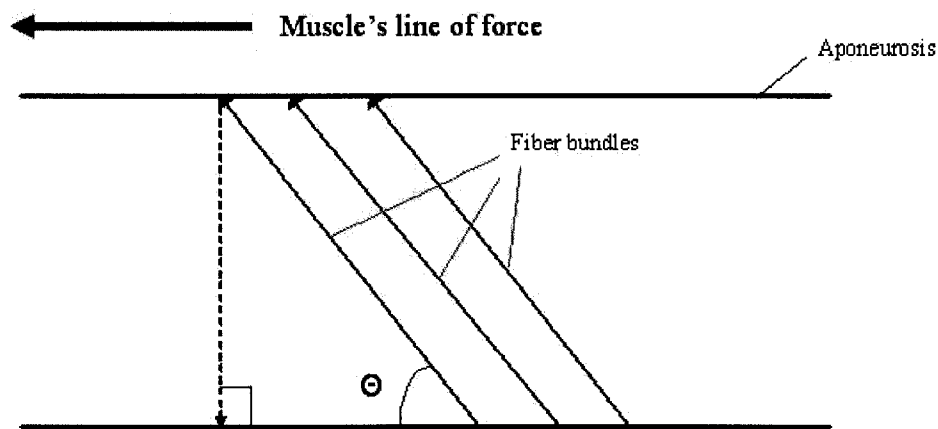


Figure 2.8. Pennation angle and axis of force. Fiber bundles acting at an angle (Θ) to the muscle's line of force. The amount of force transmitted to the aponeurosis by the fiber bundles is modified by $\cos \Theta$.

The length-tension relationship refers to the effect the length of a muscle has on its ability to generate force. There is an optimum length during a muscle's contraction where the overlap between actin and myosin filaments allows for a maximum number of cross-bridges between actin and myosin to form. Since all available cross-bridges are connected at this length, maximum force is produced in the muscle. The greater the deviation from its optimal length (i.e., shorter or longer), the less force a muscle will be able to generate (Fig. 2.9).

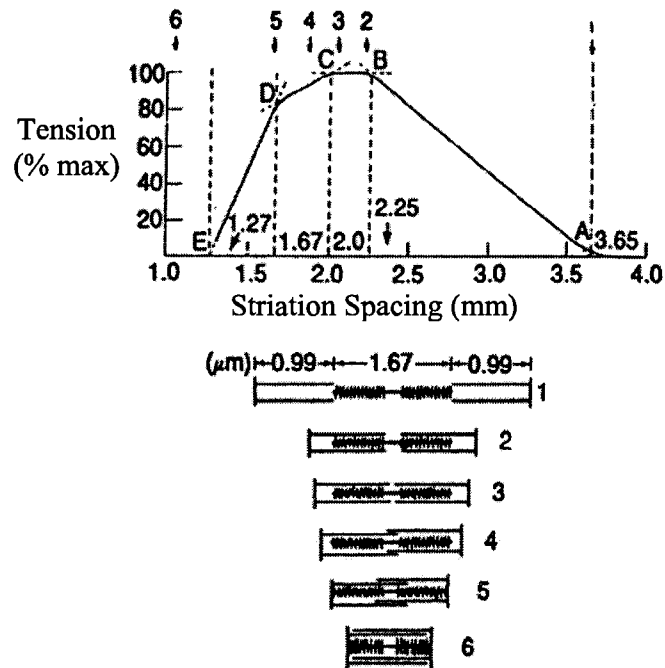


Figure 2.9. Force-length relationship. Graph of theoretical force-length relationship based on data from isolated frog skeletal muscle fibers. The amount of filament overlap at various locations on the curve is shown below the graph. The plateau region of the curve (B-C) represents the portion of the force-length curve used *in vivo*. (Reproduced with permission from McMahon (1984), Figure 3.7)

The speed of a muscle contraction also affects the amount of force a muscle can generate; fast contractions yield less force than slow ones (Fig. 2.10). This is described as the force-velocity relationship of muscle. One explanation for this phenomenon is that there is less time for cross-bridges to form during fast contractions, so not all available actin-myosin connections are made. Furthermore, energy is diverted to move the muscle at a faster rate rather than to generate force (Low and Reed, 1996).

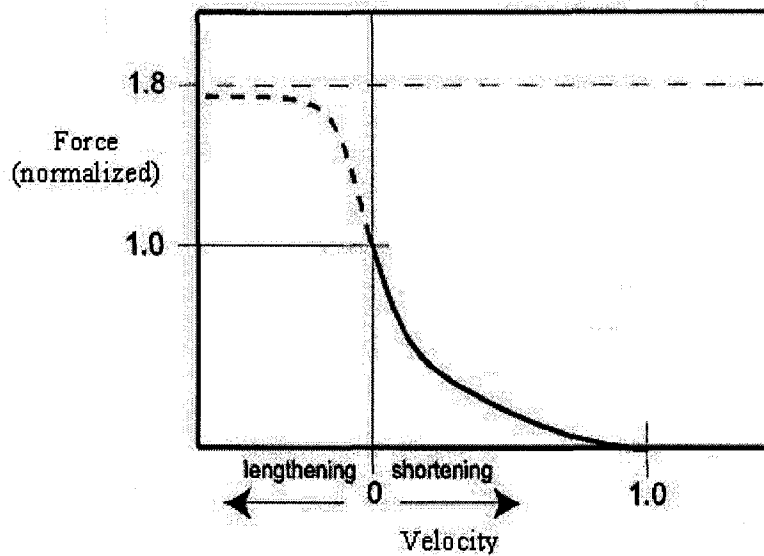


Figure 2.10. Normalized force-velocity curve. The “shortening” portion on the x-axis relate to concentric contractions while the “lengthening” part pertains to eccentric contractions. (Reproduced with permission from Ng-Thow-Hing, 2001).

2.5 Physiological Cross-Sectional Area

Physiological cross-sectional area (PCSA) is commonly used to estimate a muscle's maximal force. PCSA theoretically represents the sum of the cross-sectional areas of all the fibers within a muscle (Narici 1999). It is calculated using the architectural parameters fiber length, pennation angle, muscle mass, and density in the following equation,

$$\text{PCSA} = (\text{mass (g)} * \cos\Theta) / (\text{density (g/cm}^3\text{)} * \text{fiber length (cm)})$$

(Lieber 2002)

Note that one average value for fiber length and one for pennation angle are used in the calculation of PCSA for the entire muscle. In other words, the formula assumes all fibers in a muscle have equal length and equal pennation angles. Also, the muscle density value typically used for determining PCSA comes from studies performed on dogs and rabbits (Mendez and Keys 1960); a density value for human muscle was not obtained experimentally until recently (Ward and Lieber 2005). These assumptions are potential sources of error in PCSA calculations (Enoka 1988), and suggest further study is needed to find alternate ways to express muscle size as related to architectural characteristics (Agur 2001).

2.6 Architecture of Gastrocnemius and Soleus

The Gastrocnemius (*G. gaster*, belly-shaped + *kneme*, leg) is the most superficial muscle in the posterior compartment of the leg (Fig. 2.11A). It has a lateral and a medial head (the larger of the two) that originate from the posterior surfaces of the medial and lateral femoral condyles respectively, and from the underlying capsule of the knee joint (Moore 1999). Distally, both heads attach to an aponeurosis, which, together with the aponeurosis of the underlying soleus, forms the calcaneal (Achilles) tendon. The gastrocnemius acts to plantarflex the ankle joint, and is also capable of flexing the knee joint.

The Soleus (*L. solea*, a sandal or sole-like) is a broad, flat muscle lying deep to the gastrocnemius (Fig. 2.11B). Proximally, the soleus arises from the head of the fibula, the soleal line, and the medial border of the tibia. Distally, its aponeurosis fuses with the overlying aponeurosis of gastrocnemius to form the calcaneal (Achilles) tendon, which

inserts onto the posterior surface of the calcaneus. The soleus also acts as a plantarflexor of the ankle joint and stabilizes the leg on the foot (Moore 1999).

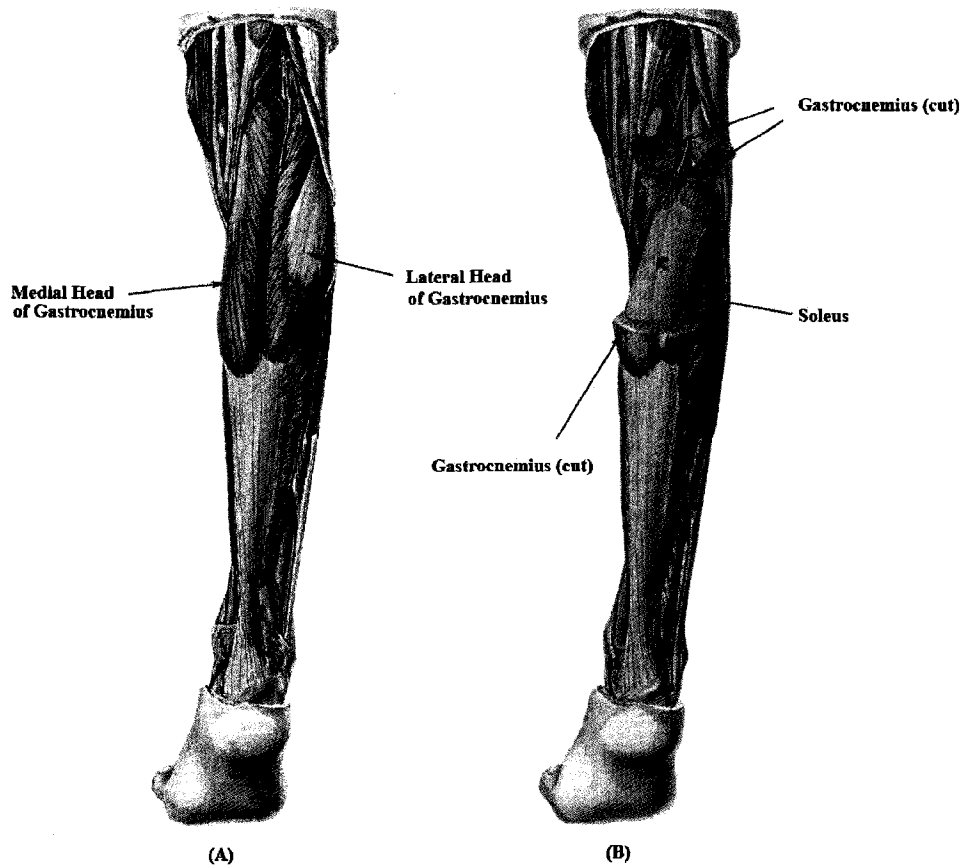


Figure 2.11. Dissections of the posterior compartment of right leg. (A) Medial and lateral heads of the gastrocnemius. (B) Gastrocnemius has been partially removed to show the Soleus beneath. (Reproduced with permission from Lippincott, Williams & Wilkins, Grant's Atlas (2009), Figs. 5.60B and 5.60C)

2.6.1 Cadaveric Studies

Architectural parameters of gastrocnemius and soleus have been investigated using cadaveric specimens in *in situ* studies. Table 2.1 summarizes architectural data obtained from cadavers.

Author (year)	N (lower limbs)	Muscle	FL (mm)	Mean PA (degrees)	Ant PA (degrees)	Post PA (degrees)
Agur et al. (2003)	1	PS	42.5(±5.0)	n/a	15.4(±7.5)	17.5(±6.4)
Friederich & Brand (1990)	2	S	30.3	32	n/a	n/a
		MG	38.85	6.5	n/a	n/a
		LG	60.55	17.5	n/a	n/a
Spoor et al. (1991)	3	PS	25.8	34	n/a	n/a
		MG	42.6	11	n/a	n/a
		LG	52.1	8.7	n/a	n/a
Wickiewicz et al. (1983)	3	S	19.5	25	n/a	n/a
		MG	35.3	16.6	n/a	n/a
		LG	50.7	8.3	n/a	n/a

Table 2.1. Architectural data of gastrocnemius and solues from cadaveric specimens. N = sample size, FL = fiber length, PA = angle of pennation, Ant = anterior, Post = posterior, PS = posterior soleus, S = soleus, MG = medial gastrocnemius, LG = lateral gastrocnemius, n/a = not available.

The lateral gastrocnemius has the longest FL in the studies shown, and has the smallest PA in all but the study by Friederich & Brand (1990). Soleus has the largest PA out of the three sites tested. The vast majority of studies reporting architectural data on healthy skeletal muscle involve adult or older adult cadavers.

2.6.2 Ultrasonographic studies

2.6.2.1 Introduction

Ultrasound (US) can be used to produce images of deep tissue structures by directing high frequency acoustic waves into the body and recording the returning reflections (Dorland 2003). Since the range of human hearing is between 15 Hz and 20 kHz, US, by definition, is any acoustic frequency above 20 kHz. Factors such as the density of a material or the angle of the scanning beam will affect the transmission of US and therefore the final image. Skeletal muscle tissue, for example, is made up of

approximately 76% water, making it an excellent conductor of acoustic energy (i.e., relatively little energy is reflected back to the US transducer). The lack of a return signal from the target is displayed as a dark area on an US image. Conversely, connective (e.g., epimysium, perimysium, endomysium) and adipose tissues are echogenic. These types of tissues reflect a strong signal back to the machine and show up as light areas on the US image. In this way, the pattern of connective tissue sheaths and tendons can be visualized on US as a gray-scale image, revealing the internal architecture of a muscle (Fig. 2.12). US can also tolerate some movement during image capture relative to other imaging modalities (e.g., MRI) without seriously compromising image quality. This enables it to record pictures of *in vivo* muscle contractions in real time, typically at frequencies between 2 and 13 megahertz. The advantages of ultrasound include its relatively low cost, non-invasiveness, lack of ionizing radiation, and ease of use (Narici, Binzoni et al. 1996).

US has been used to examine normal and pathological muscle (Heckmatt, Dubowitz et al. 1980; Heckmatt, Leeman et al. 1982). Fischer and Stephens (1988) attempted to establish optimal US techniques in normal muscle anatomy of the upper and lower limbs on 30 subjects (age 1 day to 59 years). No specific quantitative data are reported in this study, but they do present US images obtained in their study that may be used for reference. The accuracy of US for studying human muscle architecture has been verified by Narici, Binzoni et al. (1996).

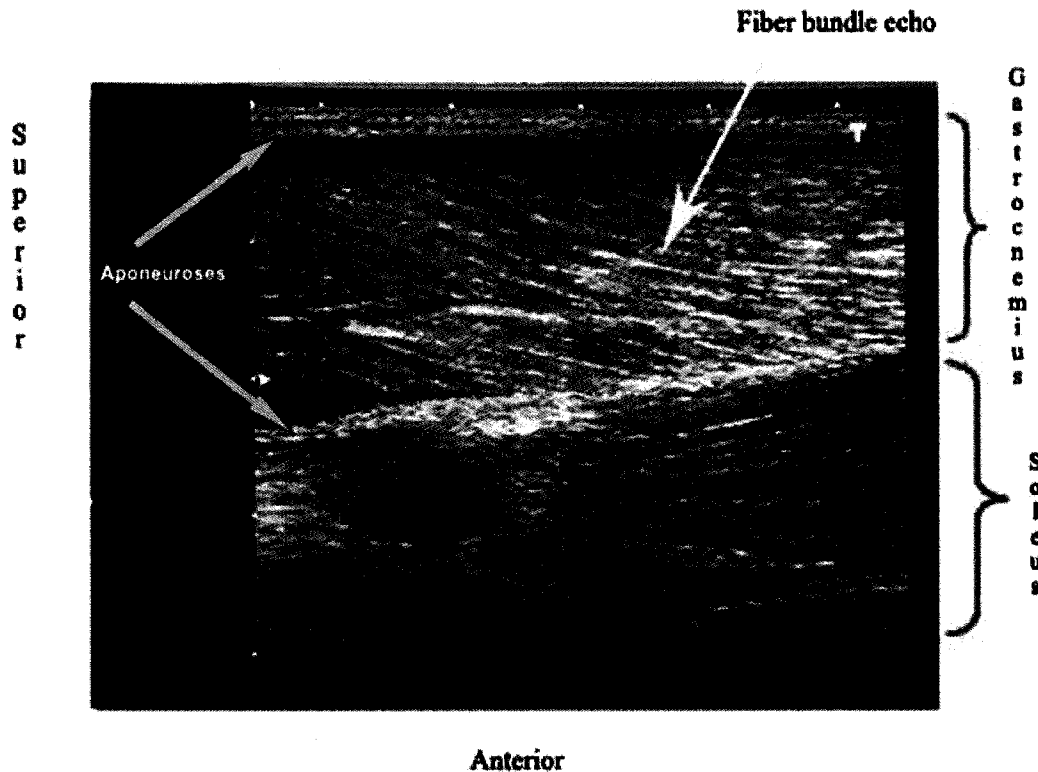


Figure 2.12. Ultrasound scan of calf muscles. The pattern of fiber bundles and location of aponeuroses can be identified.

2.6.2.2 In vivo studies of normal soleus and gastrocnemius in adults

Many researchers have used US to investigate gastrocnemius and soleus architecture *in vivo* in adult subjects. The results of these studies for medial gastrocnemius (MG), lateral gastrocnemius (LG), and posterior soleus (PS) are summarized in Tables 2.2, 2.3, and 2.4 respectively. The architectural parameters studied include fiber bundle length (FL), pennation angle (PA), and muscle thickness (MT) in relaxed and contracted states.

Few US studies of MG have complete data on all of the parameters, especially in the contracted state (Table 2.2). Mean relaxed FL was between 43.0-52.0mm, whereas

mean contracted FL was between 25.0-27.7mm. The longest FL was found in the central or mid region of the sagittal plane; the shortest in the medial region of the sagittal plane.

Author (year)	N (age)	Site (Sag)	Mean PA Relaxed (degrees)	Mean PA Contracted (degrees)	Mean FL Relaxed (mm)	Mean FL Contracted (mm)	Mean MT Relaxed (mm)	Mean MT Contracted (mm)
Martin et al. (2001)	9 X (70-92y)	Prox	Ant: 18.6±3.6 Post: 14.4±3.6	Ant: 30.3 ±8.5 Post: 28.7±9.0	43.6±8.6	27.7±5.6	n/a	n/a
Narici et al. (1996)	6 M (30-46y)	Prox	16.2±5.9	35.0±7.8	n/a	n/a	21.1±3.4	18.2±2.6
		Cent	17.3±2.6	35.3±4.1	50.8±3.6	32.9±2.6	19.8±2.3	18.5±3.1
		Dist	13.0±2.3	30.4±5.8	n/a	n/a	17.2±3.2	16.5±2.5
Kawakami et al. (1998)	6 M (21-53y)	Mid	Ant: 24.0 ±2.0 Post: n/a	n/a	52.0±7.0	n/a	n/a	n/a
Maganaris et al. (1998)	6 M (25-31y)	Medial Prox	21.4±1.1	42.5±2.5	43.0±2.0	25.0±1.5	16.3±2.0	16.8±2.0
		Mid Prox	21.5±2.0	43.4±2.9	45.9±3.1	25.0±3.0	17.6±2.6	17.0±2.5
Chow et al. (2000)	19 M (22-66y)	Mid Prox	Ant: 18.7 (±3.0) Post: 15.8±3.8	n/a	50.8±10.3	n/a	14.7±2.8	n/a

Table 2.2. Architectural data for medial gastrocnemius in adults. Data is summarized from *in vivo* ultrasonographic studies. N = sample size, Post PA = posterior pennation angle, FL = fiber bundle length, MT = muscle thickness, M = male, X = gender not specified, Sag = sagittal plane, Prox = proximal, Cent = central, Dist = distal, Mid = middle, n/a = not studied.

The reported mean posterior PA of MG was between 15.8°-21.5° (relaxed) and between 28.7°-43.4° (contracted). Narici et al. (1996), Chow et al. (2000), and Martin et al. (2001) all reported similar mean values for relaxed PA (16.2°, 15.8°, and 14.4°, respectively), but Maganaris et al. (1998) found a larger mean PA (21.4°).

The change of PA reported on contraction was 14.3° (Martin et al. 2001), 18.8° (Narici, Binzoni et al., 1996) and 21.1° (Maganaris, Baltzopoulos et al., 1998). It should be noted that the subjects in Martin et al.'s study (2001) were the oldest of all the studies (Table 2.2).

Maganaris et al. (1998) found that MT of MG did not differ ($P>0.05$) between rest and maximal voluntary contraction, and Narici et al. (1996) report no significant change in MT of MG following isometric contraction. Muscle thickness data is summarized in Table 2.2.

Three of the previous studies reported architectural data for LG (Maganaris et al. (1998); Chow et al. (2000) ; and Martin et al. (2001). In addition, Morse et al. (2008) also reported FBL and anterior PA of LG for 12 men (25.3 ± 4.4 years). The data is summarized in Table 2.3.

Morse et al. (2008) reported the longest relaxed FBL of LG out of the five studies, 88.0 ± 22 mm, which is 1.2 times longer than the FBL from Maganaris et al. (1998), and 2 times longer than the FBL reported by Martin et al. (2001) and Chow et al. (2000). On contraction, mean FBL of Maganaris et al. (1998) and Martin et al. (2001) became more similar (33.2 ± 2.5 mm – 35.4 ± 1.5 mm and 30.0 ± 6.1 mm, respectively), but the mean FBL of Morse et al. (2008) remained three standard deviations away from the next longest FBL in Maganaris et al. (1998).

For PA, Chow et al. (2000) and Martin et al. (2001) were the only two studies to measure both anterior and posterior PA, and they found similar mean values for the two angles (Table 2.3). Kawakami et al. (1998) and Morse et al. (2008) only measured the anterior PA, and the relaxed means they reported were comparable to each other, but smaller than Martin et al. (2001). In contrast, Maganaris et al. (1998) investigated only the posterior PA of LG and reported a relaxed mean of $10.8^{\circ 1}$. On contraction, the older adults from Martin et al.'s study (2001) produced the smallest percentage change in PA compared to Maganaris et al. (1998) and Morse et al. (2008).

A single study reported MT of LG in relaxed and contracted states (Maganaris et al., 1998). The MT increased on contraction from an average of 15.4mm (relaxed) to an average of 21.5mm (contracted).

Five studies, summarized in Table 2.3, reported architectural data for PS. Mean relaxed fiber bundle length for PS was between 29.7mm and 42.5mm. On contraction, Martin et al. (2001) reported a 31.3% decrease in FBL, whereas Maganaris (2001) found a 14.7% decrease in FBL. In comparison, Martin et al. (2001) report 36.5% (MG) and 51.9% (LG) change in FL, while Maganaris et al. (1998) report a change of 43.8% (MG) and 51.7% (LG).

The mean PA (relaxed) for PS was similar in all the studies (Table 2.4). Mean relaxed PA of PS ranged between 21.0° - 25.0° . In comparison, the mean relaxed PA of MG (15.8° - $21.5^{\circ 2}$) and LG ($10.8^{\circ 1}$ - 12.6°) were smaller.

¹ This is an average value of the two sites reported in Maganaris et al. (2001).

² All PS scan sites were Sag Mid so the corresponding scan sites, or next closest site, for MG and LG were used for comparison here.

Author (year)	N (age)	Site (Sag)	Mean PA Relaxed (degrees)	Mean PA Contracted (degrees)	Mean FL Relaxed (mm)	Mean FL Contracted (mm)	Mean MT Relaxed (mm)	Mean MT Contracted (mm)
Morse et al. (2008)	12 M (21-30y)	Mid	Ant : 11.5±2.3 Post : n/a	Ant : 18.0±3.5 Post : n/a	88.0±21.8	55.0±11	n/a	n/a
Martin et al. (2001)	9 X (70-92y)	Dist	Ant: 16.4±2.6 Post: 12.1±3.4	Ant: 24.7±4.9 Post: 21.4±6.5	41.6±7.4	30.0±6.1	n/a	n/a
Kawakami et al. (1998)	6 M (21-53y)	Mid	Ant: 13.0±1.0 Post: n/a	n/a	56.0±8.0	n/a	n/a	n/a
Maganaris et al. (1998)	6 M (25-31y)	Mid Dist	Ant: n/a Post: 10.5±1.9	36.5±0.9	73.3±3.8	35.4±1.5	15.5±1.5	22.0±2.9
		Lat Dist	Ant: n/a Post: 11.1±0.6	36.1±3.0	72.8±3.0	33.2±2.5	15.3±0.6	21.0±0.8
Chow et al. (2000)	19 M (22-66y)	Mid Dist	Ant: 16.4±2.0 Post: 12.6±2.8	n/a	44.6±8.2	n/a	11.0±1.8	n/a

Table 2.3. Architectural data for lateral gastrocnemius in adults. Data is summarized from *in vivo* ultrasonographic studies. N = sample size, Post PA = posterior pennation angle, FL = fiber bundle length, MT = muscle thickness, M = male, X = gender not specified, Sag = sagittal, Mid = middle, Dist = distal, Lat = lateral, n/a = not available.

Maganaris (2001), the only study to report MT of PS, found the mean relaxed MT was 15.1mm, and a mean contracted MT of 21.0mm.

It is important to note that adult subjects were used in all of the above mentioned *in vivo* US studies of MG, LG, and PS. In the context of examining DMD, it is obviously most desirable to gather data on younger children and have it analyzed without confounding information obtained from adults.

Author (year)	N (age)	Site (Sag)	Mean PA Relaxed (degrees)	Mean PA Contracted (degrees)	Mean FBL Relaxed (mm)	Mean FBL Contracted (mm)	Mean MT Relaxed (mm)	Mean MT Contracted (mm)
Martin et al. (2001)	9 X (70-92y)	Midmid	Ant: 23.7±6.3 Post: 22.2±7.2	Ant: 35.5±9.7 Post: 34.2±10.3	29.7±11.1	20.4±6.1	n/a	n/a
Kawakami et al. (1998)	6 M (21-53y)	Mid	Ant: n/a Post: 21.0±3.0	n/a	38.0±4.0	n/a	n/a	n/a
Maganaris et al. (1998)	6 M (25-31y)	Midmid	Ant: n/a Post: 25.0±2.6	40.0±3.3	42.5±1.5	n/a	n/a	n/a
Maganaris (2001)	6 M (24-32y)	Midmid	n/a	32.0±3.0	35.4±3.5	30.2±1.9	15.1±2.2	21.0±2.7
Chow et al. (2000)	19 M (22-66y)	Midmid	Ant: 24.1±4.0 Post: 22.2±7.1	n/a	32.3±7.7	n/a	12.1±3.6	n/a

Table 2.4. Architectural data for posterior soleus in adults. Data is summarized from *in vivo* ultrasonographic studies. N = sample size, Ant = Anterior Post = posterior, FBL = fiber bundle length, MT = muscle thickness, M = male, X = gender not specified, Sag = sagittal, Midmid = midline middle, Mid = middle, n/a = not available.

2.6.2.3 In vivo studies of normal soleus and gastrocnemius in children

There were three studies found that utilized US to investigate healthy gastrocnemius and soleus architecture in children.

In the same study that Morse et al. (2008) looked at the muscle architecture of LG in 12 men (25.3 ± 4.4 years), they also measured the architectural characteristics of 11 healthy boys (10.9 ± 0.3 years) and compared them to the adults. Anterior PA and FBL of LG were determined from ultrasound scans and mean values, in relaxed and contracted states, were reported. In the relaxed condition, anterior PA for the boys was $10.8 \pm 2.5^\circ$ and FBL was 7.0 ± 0.8 cm. In the contracted condition, anterior PA was $16.6 \pm 4.6^\circ$ and FBL was 4.2 ± 0.8 cm.

Kearns et al. (2001) studied the difference in MG architecture of dominant and non-dominant legs of junior soccer players (mean age 16.5 ± 0.5 y), and compared the characteristics with college freshmen (mean age 18.3 ± 0.6). Therefore this study deals with the older adolescents, not children. No quantitative architectural data for the MG was provided, only p and r values. It was concluded that the differences between dominant and non-dominant legs for FBL and MT were significantly greater in soccer players than in the college freshmen (controls). No significant differences were found for PA.

Binzoni et al. (2001) investigated the PA (posterior angle) and MT of relaxed MG of 100 plus (number of subjects reported in the abstract was 162; in methods, 134 subjects). Age of subjects ranged from newborn to 70 years, but a numeric breakdown of the age groups was not included and no quantitative architectural data were reported. Instead, results were presented solely in scatterplots. Pennation angle and muscle

thickness was estimated from the scatterplots for boys 5-15 years of age (approximately 30 males) and summarized in Table 2.5. The purpose of Binzoni et al. (2001) was to quantify changes in human skeletal muscle PA during growth and adult life. They found that both PA of MG and MT increased from birth to the adolescent growth spurt, and then reached a plateau. Kearns et al. (2001) also supported this finding of plateauing of PA in MG after adolescence.

There have been very few studies that investigated *in vivo* architecture of gastrocnemius and soleus in healthy children. The muscle architecture of the MG, LG, and PS in children has not been adequately explored. Due to the lack of studies for children, there is a paucity of healthy and pathological muscle architecture data that could be used in functional/clinical studies.

Age (Years)	N	Posterior PA (degrees)	N	MT (mm)
5	2	6.5; 15	2	9; 12
6	4	10; 10.5; 15; 9	4	8.5; 9.5; 13; 10.5
7	4	8; 14; 18; 15	2	7; 10
8	1	14.5	6	9; 9.5; 14.5; 15; 15; 15.5
9	4	11; 13.5; 14; 17.5	2	9; 12
10	4	8.5; 11; 12; 13	4	9; 9; 11; 12
11	3	14; 14.5; 20	3	12.5; 12.5; 14
12	1	10	0	-
13	1	17	5	10; 10.5; 12; 13; 16.5
14	4	13.5; 14; 15.5; 18	1	16
15	1	17	0	-

Table 2.5. Estimated posterior PA and MT data from Binzoni et al. (2001). Values are from MG of boys aged 5-15 years. N = Sample size.

2.7 Duchenne Muscular Dystrophy

2.7.1 General description

Duchenne Muscular Dystrophy (DMD) is the most common inherited neuromuscular disease affecting approximately 1 in 3500 male births (Bogdanovich, Perkins et al. 2004). DMD causes rapid progressive degeneration of skeletal muscle, which eventually leads to fibrosis and fatty infiltration of muscle tissue.

Boys with DMD are asymptomatic at birth, and typically achieve early motor milestones (e.g., rolling, standing). Parents often do not notice problems with their child until 2-3 years of age, when the child begins to fall behind his peers in physical activities. The child is often presented in clinic with complaints that he is “clumsy” or not able to run like other children.

The clinical signs of DMD were first described comprehensively by Duchenne in the 1850s (Duchenne 1868). These have changed very little over the decades and are summarized in Table 2.6 (Tyler 2003). The muscle weakness experienced by DMD patients typically begins in the proximal muscles (e.g., trunk muscles, around the pelvic girdle) before spreading distally into the limbs as the disease progresses. Usually the lower limbs are affected earlier than the upper limbs (Table 2.7). Muscle weakness will continue to develop until the child has difficulty getting up from a seated or lying position. Patients intuitively learn a characteristic method of pushing against themselves to achieve an upright position (Fig. 2.13). The ability to ambulate is eventually lost requiring the child to use a wheelchair. Finally, respiratory muscles also fail and artificial respiration must be used to help the child breathe.

Clinical signs of DMD
<ul style="list-style-type: none"> • Muscle weakness starting with the lower extremities • Lordosis and wide base of support • Hypertrophy of involved muscles • Progressive nature of the disease eventually spreading to whole body • Decreased response of the muscle to electrical stimulation in advance stages of disease • No accompanying sensory defects, fever, or bladder/bowel issues

Table 2.6. Duchenne’s clinical description of DMD.

Typical pattern of muscle weakness
<ul style="list-style-type: none"> • Proximal muscles affected earlier than distal muscles • Lower extremity affected before upper extremity (quadriceps, gluteals, iliopsoas affected earliest) • Ankle plantarflexors preserved longer than dorsiflexors

Table 2.7. Typical pattern of muscle weakness in children with DMD.

The age at which these events occur varies, but prior to modern medical intervention, most children lost the ability to walk before the age of ten and death was common in the early teens (Dubowitz 1995).

Presently, with the use of steroids, children with DMD can remain ambulatory until 12-13 years of age (Alman, Raza et al. 2004). Steroids also help to preserve pulmonary function, which is vital for preventing secondary infections (e.g., pneumonia). However, as with most drugs, steroids have unwanted side effects such as excessive hair growth, osteoporosis, and cataracts (Manzur, Kuntzer et al. 2004). Despite the use of

these drugs, most patients with DMD still die of secondary complications (e.g., cardiorespiratory issues, infection) in their early 20s.

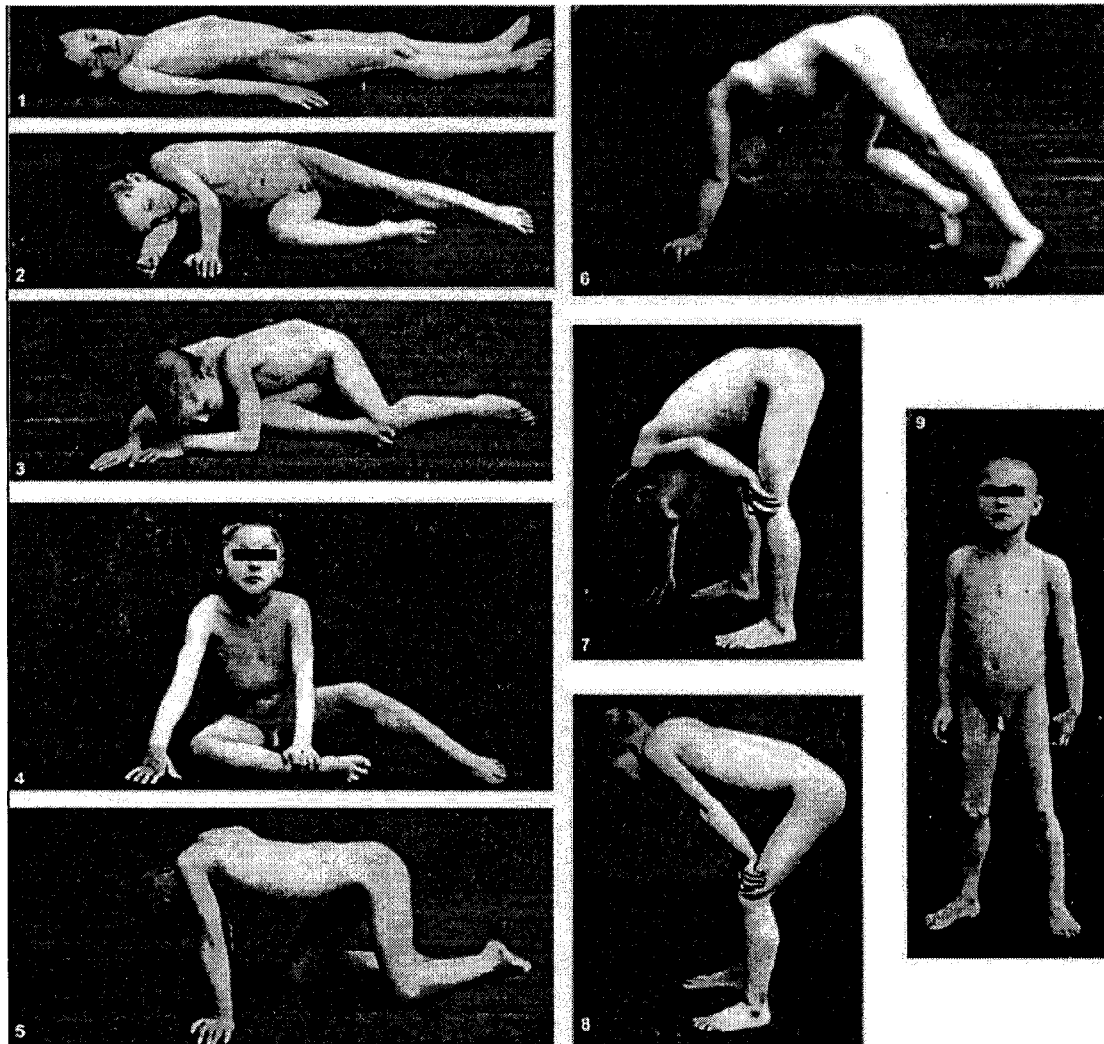


Figure 2.13. Pictorial series demonstrating Gowers' sign. Weakness of muscles around the trunk, pelvic girdle, and thigh (e.g., erector spinae, glutei, and quadriceps) prohibits this boy with DMD from standing up without helping with his arms. (Reproduced with permission from John Wiley & Sons, Inc. Tyler 2003, Fig. 10)

2.7.2 Etiology

Our understanding of DMD dramatically improved with the advent of more sophisticated techniques in molecular biology and genetics. The gene responsible for DMD was cloned in 1987 (Koenig, Hoffman et al. 1987) and its protein product, Dystrophin, identified shortly after (Hoffman, Brown et al. 1987). In addition to Duchenne's clinical description, it is now known that DMD is an x-linked, recessive disorder mapped to position 21.2 on the short (p) arm of the X chromosome (Xp21.2). The defect in the majority of cases is due to a single deletion in the reading frame of the mRNA, producing a severely truncated or absent dystrophin protein (Culligan, Mackey et al. 1998). Dystrophin is a small protein (3684 amino acids, 427 kD) found just below the muscle cell membrane connecting actin filaments to a protein complex within the sarcolemma (Fig. 2.14).

While the precise role of dystrophin and how its absence leads to muscle damage have yet to be explained, there is strong evidence to support dystrophin's function as a structural support for the muscle cell (Samitt and Bonilla 1990; Pasternak, Wong et al. 1995; Rybakova, Patel et al. 2000; Krag, Gyrd-Hansen et al. 2001). It is also known that dystrophin helps to localize other components in and around the sarcolemma (e.g., nNOS, sarcoglycans), and failure of these components to assemble properly leads to various dysfunctions (e.g., abnormal cell signaling, muscle ischemia) of the muscle cell (Culligan, Mackey et al. 1998).

While the mechanism of disease progression has yet to be determined, it is likely that DMD pathogenesis is multifactorial and cannot be attributed to any one process.

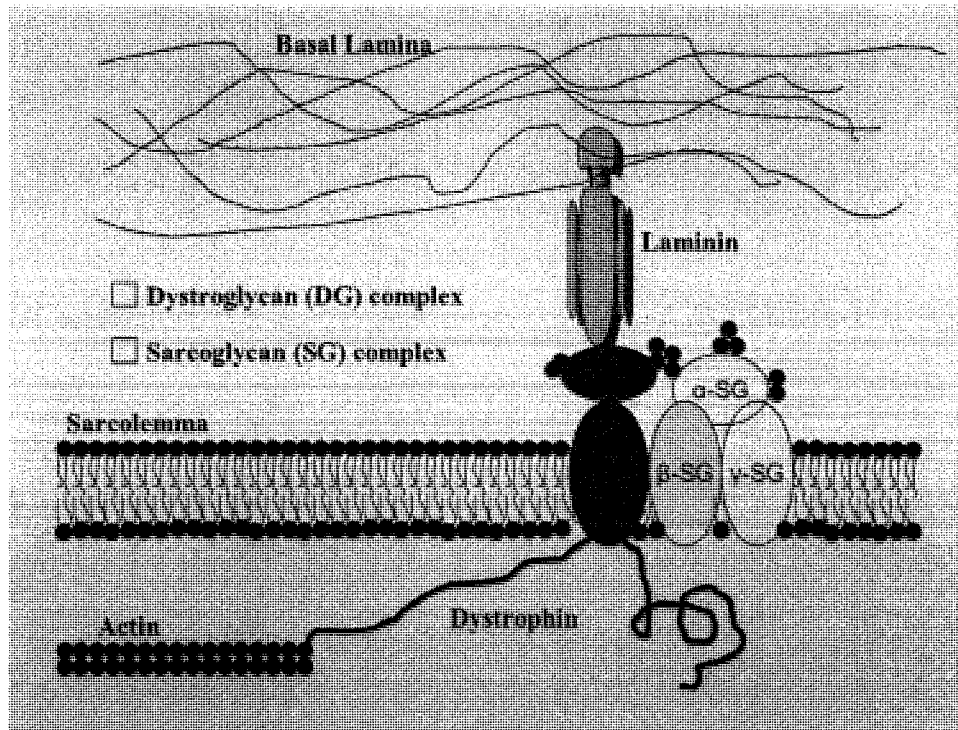


Fig. 2.14. Dystrophin-Glycoprotein complex (DGC). Associated molecules and proteins are also shown. F-Actin is connected to the DGC and sarcolemma via dystrophin.

Current theories on the mechanism of DMD muscle damage can be classified into five main categories: 1) Mechanical stress 2) Oxidative stress 3) Alteration of intracellular calcium 4) Abnormal cell signaling and 5) Muscle ischemia (Petrof 2002).

2.7.3 Pathophysiology

1. Mechanical stress

There is strong indirect evidence indicating that dystrophin provides mechanical support to the sarcolemma (Petrof 1998). *In vitro* experiments have shown dystrophin to be concentrated in areas of high mechanical stress such as the I-band, M-line, and myotendinous junction (Porter, Dmytrenko et al. 1992). Also it has been found that dystrophic muscles have an unusually high level of sarcolemmal damage during muscle

contraction compared to healthy muscle (Moens, Baatsen et al. 1993; Petrof, Shrager et al. 1993). *In vivo* studies involving animals (e.g., mdx mice) have also confirmed a greater susceptibility in dystrophic muscles to membrane damage following exercise compared to controls (Brussee, Tardif et al. 1997; Vilquin, Brussee et al. 1998). Therefore, dystrophin-deficient muscles seem to have weaker sarcolemma and may be less able to withstand normal muscle contraction forces.

2. Oxidative stress

Oxidative stress is a known cause of cellular damage in the human body (Disatnik, Dhawan et al. 1998). Elevated markers of oxidative stress have been found following a variety of demanding situations including strenuous exercise, injury, and illness (Krotkiewski and Brzezinska 1996; Laplace, Huet et al. 2005; Kirkham and Rahman 2006). Similar studies investigating the level of oxidative stress in animal and human dystrophic muscles have all reported increased amounts of stress indicators in dystrophic subjects compared to controls (Disatnik, Chamberlain et al. 2000; Kumar and Boriek 2003; Rodriguez and Tarnopolsky 2003).

Further evidence of oxidative stress as a mechanism for muscle damage in dystrophic muscle comes from studies using antioxidants. In Kumar & Boriek's (2003) study of mdx mice diaphragm, they found that pretreatment of the mice with a free radical inhibitor, N-acetyl cysteine, blocked the stretch-induced activation of the inflammatory marker NF-Kappa_B. Both Buetler et al. (2002) and Dorchies et al. (2006) successfully used green tea extract, known for its antioxidant effects, to decrease muscle necrosis in mdx mice. However, the role of antioxidants as a protective factor against muscle damage remains unclear in humans. Beaton et al. (2002) report that vitamin E –

another well-known antioxidant – supplementation did not protect muscle against the damaging effects of eccentric exercise in healthy adult males. Thus, oxidative stress is certainly a potential mechanism of muscle damage in individuals with DMD, but further study is needed to elucidate this process definitively.

3. Alteration of intracellular calcium

In vitro experiments using dystrophin-deficient muscle cells from humans and mice show altered Ca^{2+} handling by these cells, which result in significantly higher levels of intracellular Ca^{2+} compared to controls (Turner, Westwood et al. 1988; Deval, Levitsky et al. 2002; Mallouk and Allard 2002). The mechanisms that contribute to higher levels of calcium in dystrophic muscle include Ca^{2+} channel leakage, abnormal ion channels, and decreased calcium reuptake (Fong, Turner et al. 1990; Franco and Lansman 1990; Nicolas-Metral, Raddatz et al. 2001).

Elevated intracellular calcium concentrations trigger the activity of calcium-dependent proteases called calpains (Belcastro, Shewchuk et al. 1998). This may contribute to muscle wasting in DMD patients through increased proteolysis (Tidball and Spencer 2000). Calpains are also strongly implicated in the regulation of gene expression and in cell apoptosis (Carafoli and Molinari 1998). Significantly high levels of calpains then may disrupt normal processes within a muscle cell, leading to its dysfunction and death.

4. Abnormal cell-signaling:

The dystrophin-glycoprotein complex (DGC) is composed of dystrophin and a number of other proteins localized to the sarcolemma of a muscle cell (Blake, Weir et al. 2002). The DGC has been shown to have cell-signaling properties (Yoshida, Pan et al.

1998; Henry and Campbell 1999), and also associates with a host of molecules such as nitric oxide and calmodulin, that have cell-signaling functions (Sotgia, Lee et al. 2000; Schottelndreier, Potter et al. 2001).

A mutation or lack of dystrophin may cause alterations in cell-signaling in two ways. First, dystrophin itself is involved in signaling so its absence interrupts normal cellular communication (Blake, Weir et al. 2002). Second, proper assembly of the DGC cannot occur without dystrophin, so dystrophic muscle will also have malfunctioning DGC (Petrof 2002). This disruption in signaling is believed to affect a cell's normal survival pathways, which leads to premature apoptosis of muscle cells and degeneration of muscle fibers (Rando 2001). Another consequence of this aberrant signaling is an upregulation of the inflammatory response (e.g., increased chemokines, greater inflammatory gene expression), which compounds the cellular necrosis and muscle damage (Porter, Khanna et al. 2002).

5. Ischemia

The role of ischemia in the pathogenesis of DMD is closely related to cell signaling. Nitric oxide (NO) is a signaling molecule with broad physiological effects (Froehner 2002). It is produced by the enzyme neuronal nitric oxide synthase (nNOS), which is normally bound to a complex associated with dystrophin. The studies by Brenman et al. (1995) and Chang et al. (1996) demonstrated that dystrophin-deficient muscle fails to localize nNOS to its sarcolemma. This leads to a drastic reduction in nNOS, and therefore NO, within the muscle cell. In skeletal muscle, one of the proposed functions of NO is to regulate blood flow during exercise (Lau, Grange et al. 1998). Without NO, studies have shown that functional ischemia, which could lead to muscle

damage, can occur due to an impaired ability to control vasoconstriction (Thomas, Sander et al. 1998; Sander, Chavoshan et al. 2000; Crosbie 2001; Froehner 2002). Furthermore, it appears that NO also plays a role in regulating apoptosis (Grozdanovic 2001) and can ameliorate muscle damage by reducing certain markers of inflammation in dystrophic mice (Tidball, Lavergne et al. 1998).

6. Interaction of pathogenic mechanisms

DMD pathogenesis is a multifaceted process involving a complex interplay between numerous mechanisms. The theories outlined in this section serve as a basic overview of a very involved subject. Interactions of the different pathogenic mechanisms must be considered for a more complete understanding of the disease process. For example, mechanical stress tearing the weakened sarcolemma in DMD muscle will allow an influx of calcium ions into the cell; this in turn causes calcium-mediated damage by calpains. One of the cellular components susceptible to calpains is nNOS – the destruction of which leads to significant disruptions in cell-signaling. The altered cell-signals decrease a muscle cell's ability to regulate key functions such as local vasoconstriction, creating additional cellular stress, which further damages the cell.

2.8 Quantitative US studies of DMD muscle architecture in children

Quantification of morphological changes is important to understanding how the DMD disease process changes the architecture and function of skeletal muscle. Few studies, however, have investigated the *in vivo* architecture of DMD muscle using ultrasound.

Heckmatt et al. (1988) reported values for quadriceps thickness and subcutaneous tissue thickness for children with DMD. In a subsequent study, Heckmatt et al. (1989)

calculated quantitative values of raw echo data obtained directly from the transducer during US imaging of DMD patients. In both cases, they found abnormalities in the US images of DMD muscle – increased muscle thickness and greater echo values – when compared to controls.

Maurits et al. (2004) used US to determine a set of reference values for the subcutaneous tissue thickness and muscle thickness of the biceps and quadriceps in healthy children. They compared these values to 20 DMD patients to test its specificity and sensitivity. They also quantified qualitative characteristics of the US images (e.g., degree of echogenicity, amount of white area) using computer analysis. They reported that it was possible for US to distinguish between DMD muscle and healthy muscle.

The lack of quantitative US studies on gastrocnemius and soleus architecture in the DMD population prompted this investigation.

2.9 Qualitative rating of US images

Ultrasound studies that systematically characterize the qualitative findings in skeletal muscle of DMD patients are also lacking. Heckmatt et al.'s study (1982) was the first to grade the US appearance of diseased muscle using a four-point rating scale (Table 2.5). Zuberi et al. (1999) later used the same criteria to analyze the US images of the thigh, upper calf, arm, and forearm in four DMD patients. None of the patients had a normal grade: two were rated grade IV, one at grade III, and the last one was at grade II. Other imaging studies have also commented on the general ultrasonographic appearance of diseased muscle, but these are often not specific to DMD boys or include a small number of DMD patients within a larger set of other myopathies (Spiegler, Schindler et al. 1985; Fischer, Carpenter et al. 1988; Lamminen, Jaaskelainen et al. 1988; Schedel,

Reimers et al. 1992). Typically, dystrophic muscle on US images is described as having a granular or stippled appearance with a homogenous increase in echogenicity.

Frequently, there is a loss of bone shadowing.

Grade I	Normal
Grade II	Increased muscle echo, normal bone echo
Grade III	Increased muscle echo, reduced bone echo
Grade IV	Increased muscle echo, absent bone echo

Table 2.8. Previously established qualitative rating scale for US images of diseased muscle (Heckmatt et al. (1982)).

Similarly, Liu et al. (1993) have analyzed magnetic resonance (MR) images of DMD muscle and developed a qualitative rating scale for these scans. This rating scale defines DMD disease severity based on three criteria: severity of fatty infiltration of calf muscles, amount of subcutaneous fat, and the number of affected muscles. Liu et al. (1993) reported a strong correlation between the MR qualitative score and the clinical functional grade. Furthermore, the grading system used in Liu et al.'s (1993) study made it possible to continue monitoring DMD disease progression in patients with low functional grades.

The studies mentioned above were consulted during the development of a rating scale for US images in the current thesis.

Chapter 3: Purpose and Hypothesis

3.1 Purpose

1. To determine the architecture (pennation angles [PA], fibre length [FL], and muscle thickness [MT]) of the medial and lateral heads of gastrocnemius and soleus muscles using *in vivo* ultrasound in boys with DMD and in healthy age matched controls.

2. To compare and contrast the quantitative and qualitative *in vivo* changes in architecture between the medial head of gastrocnemius (MG), lateral head of gastrocnemius (LG) and posterior portion of soleus (PS) in DMD and in healthy controls.

3.2 Hypothesis

1. Muscle architecture of MG, LG and PS in boys with DMD is significantly different (e.g., increased pennation angle, greater muscle thickness) than in healthy controls.

2. There is a positive correlation between functional performance and the qualitative score of US images in DMD subjects.

Chapter 4: Methods

4.1 Subjects

A total of 36 boys, 18 with DMD and 18 controls, participated in this study. Ethics approval was obtained from Bloorview MacMillan Children's Center study number 00-062 (Appendix B).

Boys with Duchenne Muscular Dystrophy (DMD) between the ages of 5-15 were recruited from the neuromuscular clinic at Bloorview MacMillan Children's Center (BMCC). Families with scheduled appointments at the clinic between September 2002 and September 2004 were contacted by telephone. The purpose and protocol for the study were explained to a parent/guardian of the child, and verbal consent to participate was obtained. In order to minimize the amount of traveling for the families, ultrasound (US) imaging was booked on the same day as their clinic appointments at BMCC.

Boys for the age-matched control group were recruited from BMCC via posters and from the community by word of mouth. Respondents were contacted by telephone for preliminary screening. Subjects were excluded if they reported a history of lower limb trauma, neuromuscular disease, or any other condition which affect their skeletal muscles. US imaging of these subjects was done at the families' convenience.

The age range of 5-15 years was chosen to encompass the broadest cross-section of children possible. Children younger than 5 years were excluded because of compliance issues, while boys older than 15 years were not included to account for the rapidly declining physical ability of the DMD group.

On the day of US imaging, the study protocol and information sheet were initially reviewed with the parent/guardian and then with the child. Consent and assent forms were then signed by the parent/guardian and the child (Appendix C).

4.2 Protocol

Real-time US imaging was completed at BMCC by a highly experienced staff radiation technologist using a Toshiba Nemio 30 with an 8.0 MHz transducer. To scan the gastrocnemius and soleus muscles, subjects were positioned prone on an examination table with hips in neutral, knees in full extension, and their feet hanging freely off the end of the table to allow unrestricted ankle plantarflexion. The ankle joint was positioned at 90 degrees. After subjects were comfortable, footwear was removed and both calves were exposed as far proximally as the popliteal fossa. The proximal MG, distal LG, and middle PS were each scanned in turn in the relaxed and contracted states, first in the left leg and then in the right.

Thus, two images were acquired for each scanning site, one in the relaxed state with the foot at 90 degrees to the leg, and another in the contracted or plantarflexed position. Prior to scanning subjects were instructed to plantarflex the ankle “as hard as you can” to illicit maximal voluntary contraction (MVC). This movement was practiced for three repetitions to allow the subject to become familiar with the movement. It should be noted that on MVC, the angle of the ankle varied between subjects. Once it was confirmed that the subjects understood the movement and were compliant, they were asked to sustain a MVC when signaled by the researcher. Verbal encouragement was given throughout the contraction to promote maximal effort, but quantitative force

measurements were not taken. Subjects were allowed to rest as needed in between contractions.

The current study's imaging protocol was based on an approach developed for adults by Agur (2001). Agur lists ten different scanning sites on the calf corresponding to different parts of the gastrocnemius and soleus. A pilot study was conducted to develop a similar protocol in children, and while every scanning site was attempted, not all ten were productive in children because their legs are shorter and their muscles smaller. This study utilized three sagittal scanning planes – the proximal medial gastrocnemius (MG), distal lateral gastrocnemius (LG), and mid posterior soleus (PS) – that most consistently yielded quantifiable images (Figure 4.1).

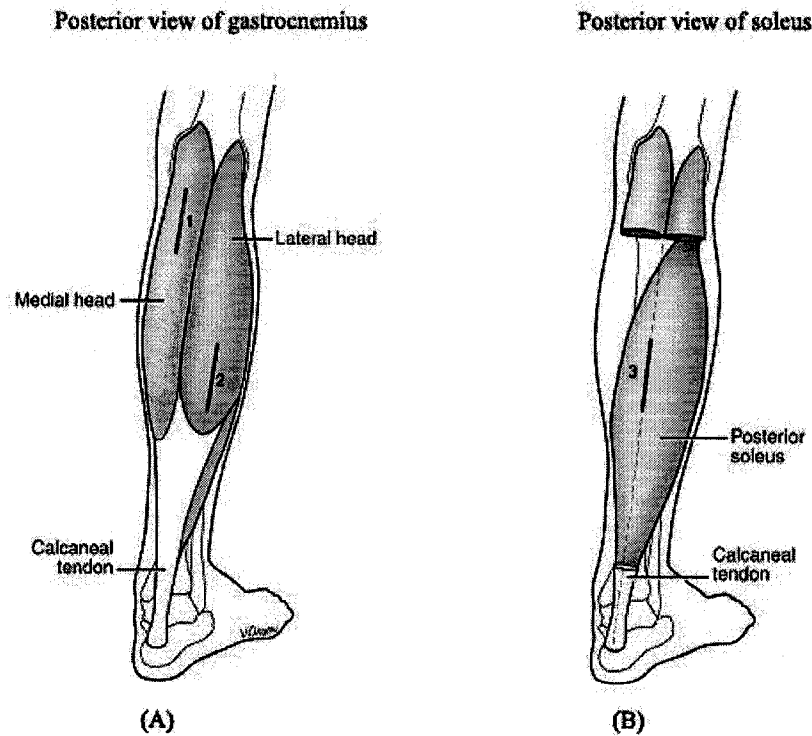


Figure 4.1. Ultrasound scanning sites. (A) gastrocnemius (B) soleus (right leg). Modified with permission from Valerie Oxorn, B.A., M.A., M.Sc.B.M.C.

To locate the scanning planes, an imaginary line connecting the midpoint of the calcaneal (Achilles) tendon to the center of the popliteal fossa served as a reference for the placement of the US transducer. This line divided the leg into medial and lateral halves. To image proximal MG, the US transducer was oriented in the sagittal plane medial to the reference line, along the middle of the medial portion of the leg. For distal LG imaging the transducer was placed lateral to the reference line in the sagittal plane. The distinctive tapering of the distal ends of the medial and lateral gastrocnemius helped to confirm the correct location for this site. Imaging of PS occurred on the reference line, distal to the tapered ends of the medial and lateral heads of gastrocnemius. Once the transducer was positioned on the calf, a visual check of the real-time image was performed to verify the location and scanning plane. Manual adjustments were made to the angle of the transducer to achieve full visualization of entire fiber bundles. All images were printed on film. A typical US image of a muscle in relaxed and contracted conditions is shown in Figure 4.2.

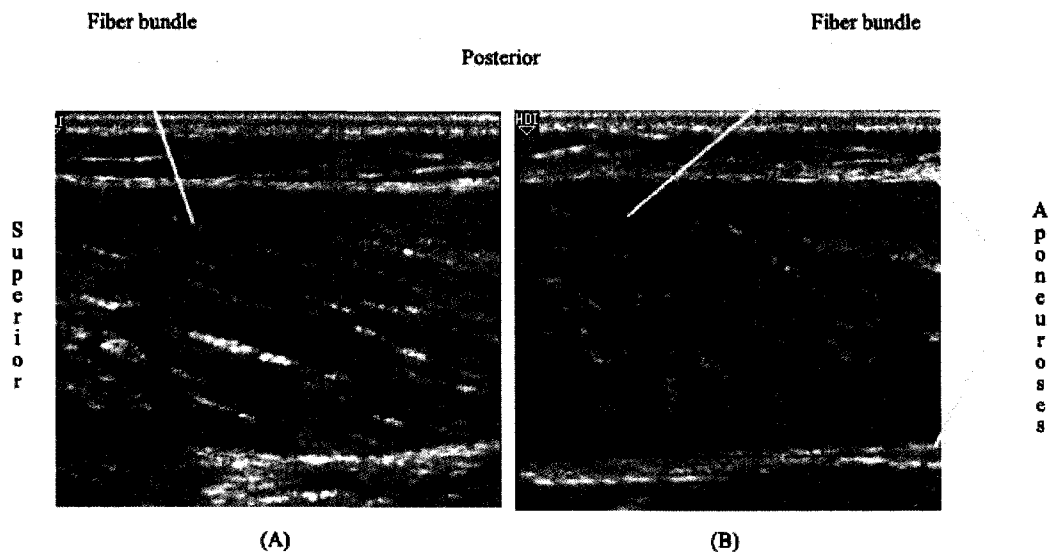


Figure 4.2. Ultrasound image of medial gastrocnemius. (A) relaxed (B) contracted.

4.3 Measurements

All image output from the US machine was stored as JPEG files. Fiber bundle length, anterior and posterior pennation angles, and muscle thickness were measured on each image using software developed at this laboratory. The software used the US image scale markers as calibration points; one unit on the scale – same for both x and y axes – is equal to one centimeter (Fig. 4.3).

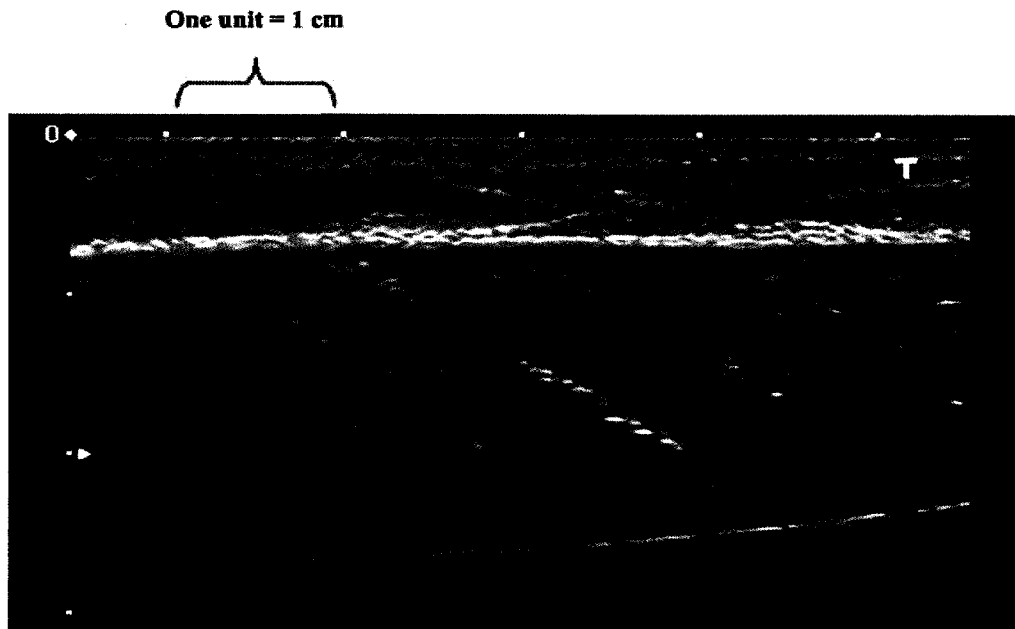


Figure 4.3. Scale markers on an ultrasound image.

For each image, a well-defined fiber bundle was chosen for measurement. The fiber bundle length (FL) is defined as the distance between the attachment points of a muscle fiber into the anterior and posterior aponeuroses, and was measured in centimeters. The angle of pennation (PA) is the angle, in degrees, between the muscle fiber bundle and the two aponeuroses; there is an anterior PA and a posterior PA, defined in relation to the anterior and posterior aponeuroses of the muscle. Muscle thickness

(MT) is the perpendicular distance, in centimeters, between two aponeuroses. This was measured in two locations determined by the scale markers on the x-axis of the US image. The two values for MT were then averaged for each scan.

Each ultrasound image was measured three times by one researcher (C.Yuen), and the average value of FBL, PA, and MT was recorded (Fig. 4.4). No significant difference was found between the three measurements taken for each architectural parameter ($p < 0.05$). To determine interrater reliability, a second rater trained in the use of the new software measured a subset of the images (half). No significant differences were found between the measurements by the two raters ($p < 0.05$).

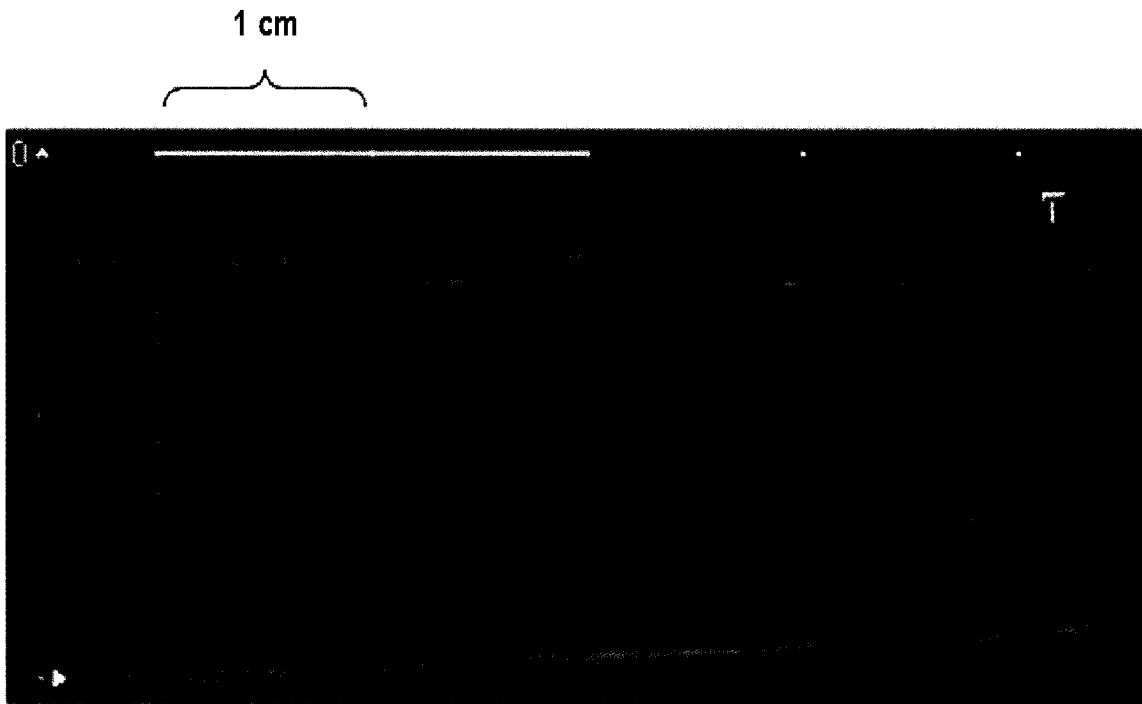


Figure 4.4. Ultrasound image with completed lines for measurement. The custom software automatically measures and extrapolates data from the colour-coded lines.

The custom software used to calculate the architectural parameters was previously validated by comparing its measurements of the US images with measurements of the same images obtained from tools available in Adobe Photoshop 6.0. The validity of *in vivo* US measurements have been demonstrated elsewhere (Narici, Binzoni et al. 1996; Fukunaga, Ichinose et al. 1997).

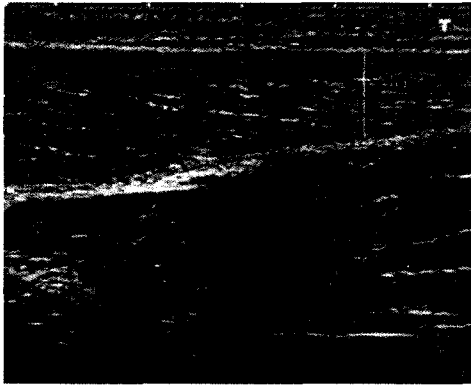
It is evident that the DMD disease process results in fatty infiltration of muscle which replaces fiber bundles. As fatty infiltration increases, fiber bundles become increasingly difficult to visualize using US, so in addition to the quantitative measurements of muscle parameters, a qualitative rating scale was developed to categorize US appearance of each muscle based on the degree of echogenicity, fiber bundle pattern, and structural abnormalities observed in the images (Table 4.1 and Figure 4.5). This classification enabled an assessment of the visual differences in the US images between DMD and control subjects, and between DMD subjects across a range of disease severity. The qualitative rating also provided an alternative means of comparison for images that could not be measured quantitatively due to disease progression. In addition to the author, two other raters, blinded to the condition of the subjects, were trained in the use of the new scale and separately rated the appearance of the US scans.

Qualitative scores for the US images were then correlated to clinical functional performance. The functional indicators chosen for comparison were timed function tests (TFT) for walking 30-feet and climbing 4 steps; non-ambulatory children were not assessed with TFT. This data was acquired from chart reviews of physical therapy assessments done in the neuromuscular clinic at BMCC.

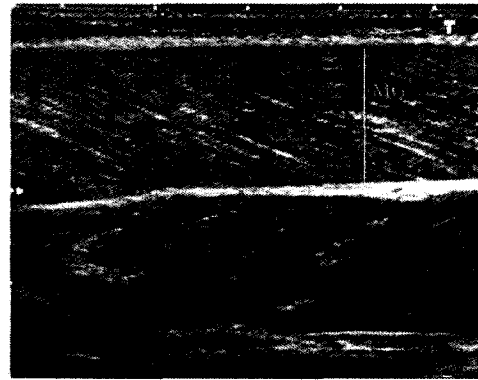
Rating	Characteristics
0 = Normal	<ul style="list-style-type: none"> • “Random” fiber pattern • Mostly “dark” with areas of echogenicity • No abnormalities of tendons or fiber bundles
1 = Mild	<ul style="list-style-type: none"> • Fiber pattern near normal • Slightly increased echogenicity (<1/3 of image area) • No abnormalities of tendons or fiber bundles
2 = Moderate	<ul style="list-style-type: none"> • ↑ visibility of fiber pattern • ↑ brightness (up to 2/3 of image) • May contain abnormalities (e.g., excessive curvature of fiber bundles, disruption of aponeurosis)
3 = Severe	<ul style="list-style-type: none"> • Fiber pattern present but nearly infiltrated • Mostly echogenic tissue; may contain some dark areas • Abnormalities very apparent
4 = Obliterated	<ul style="list-style-type: none"> • No fiber pattern discernible • Entire image is echogenic • Gross abnormalities
OP = Out of plane	<ul style="list-style-type: none"> • Fibers not in plane of image

Table 4.1. New qualitative rating scale for ultrasound images.

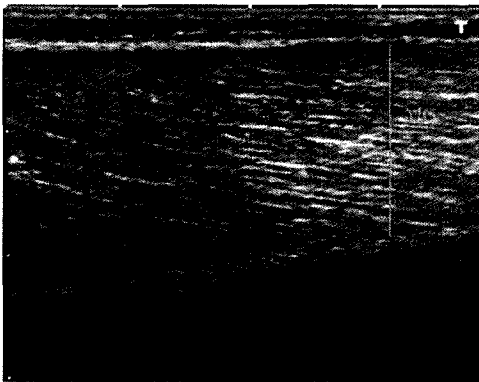
Statistical analysis of the quantitative architectural parameters between the DMD and control groups was performed using two-way ANOVA, and comparison of muscles within the same group was done using one-way ANOVA. Pearson’s correlation coefficient was also used to test the relationship between the quantitative variables. The relationship between qualitative rating scores and TFT was explored using Spearman’s rank correlation. Significance of rating scores was assessed by the Wilcoxin Rank Sum test. Interrater reliability for the qualitative rating scale was assessed by Intraclass Correlation Coefficient.



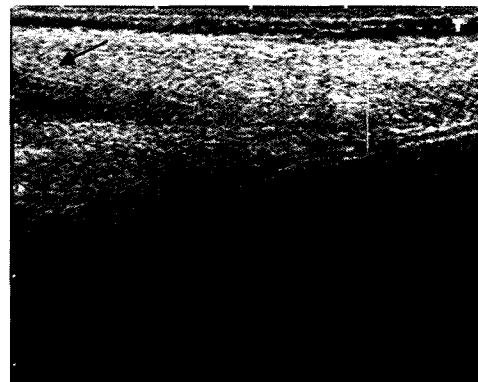
A - Control



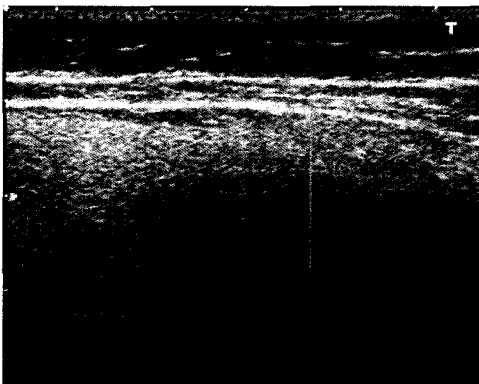
B - DMD



C - DMD



D - DMD



E - DMD

Figure 4.5. Ultrasound scans of MG showing progression of disease. A) Note the incomplete fiber pattern with dark patches in the background (control). B) & C) Increasing prominence of the fiber pattern from B to C. This is due to fat and connective tissue infiltration. These images are rated 'mild' and 'moderate'. D) This scan is rated 'severe'. The image is almost completely echogenic with only a few fibers visible (red arrows). E) This DMD image has no discernible fiber pattern and a marked increase in echogenicity. This scan is rated 'obliterated'.

Chapter 5: Results

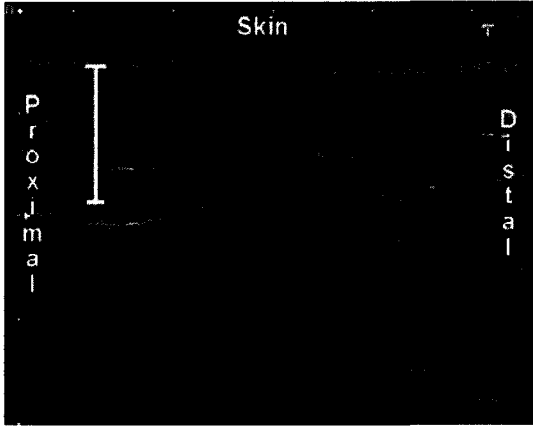
The FBL, PA and MT from the quantifiable US scans are presented for the control and DMD groups. This is followed by a comparison of the results between the two groups. In the final section, qualitative findings of unmeasurable scans for the DMD group are summarized. Appendix C summarizes age-related data.

5.1 Control group

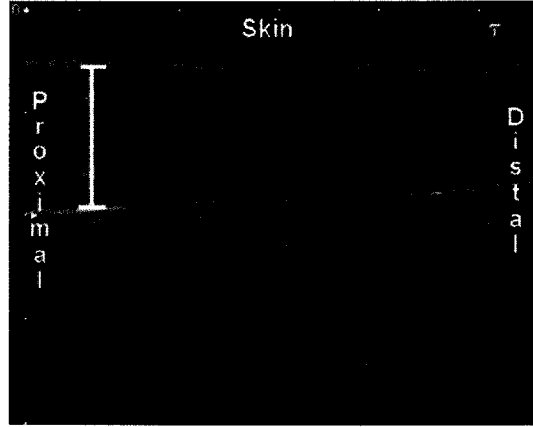
The fiber bundle length, angle of pennation, and muscle thickness of MG, LG, and PS were quantified using the US scans. An example of these scans is presented in Figure 5.1. The mean height, weight, and leg length of the control group were 136cm, 40kg, and 75cm respectively. No significant correlations were found between these physical characteristics and the architectural parameters, except between height, weight, and muscle thickness. This is in line with the findings of Maurits et al. (2004). Age distribution for the control group is as follows: 6yr: n = 1, 7yr: n = 1, 8yr: n = 3, 9yr: n = 1, 10yr: n = 5, 11yr: n = 3, 12yr: n = 2, 14yr: n = 1, 15yr: n = 1. There were some scans where the plane of the fiber bundles could not be imaged. For the relaxed condition, 20 of a total of 108 scans in the 18 subjects could not be measured (2 MG, 10 LG, and 8 PS). In the contracted state, 25 of the 108 scans were unmeasurable (5MG, 4 LG, 16 PS).

5.1.1 Fiber Bundle Length

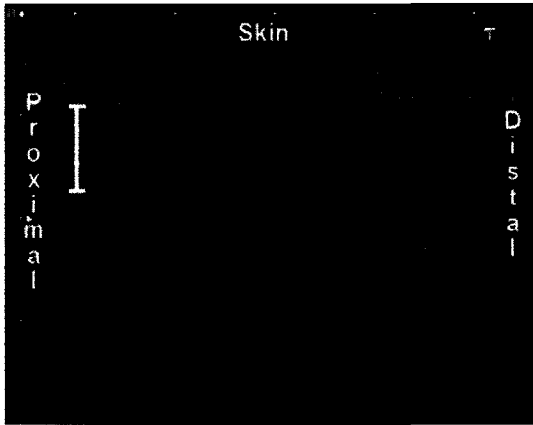
Mean FBL, relaxed and contracted, for MG, LG, and PS are summarized in Table 5.1. The mean FBL of MG in the relaxed state was significantly shorter than in the contracted state ($p < 0.05$). This was also the case for LG and PS.



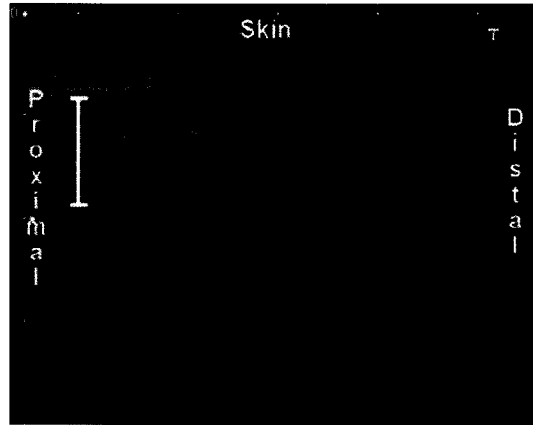
A. MG relaxed



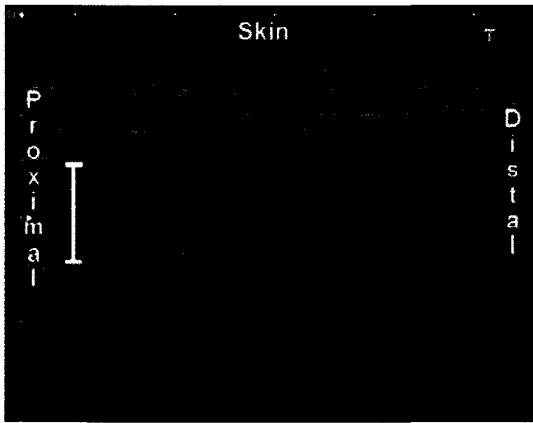
B. MG contracted



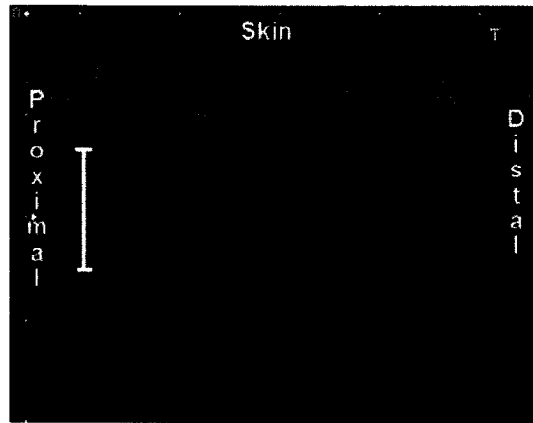
C. LG relaxed



D. LG contracted



E. PS relaxed



F. PS contracted

Figure 5.1. Ultrasound scans from one control subject. The white lines demarcate the position of each respective muscle.

In the relaxed state, the FBL of MG, LG, and PS were all significantly different from each other ($p < 0.05$). LG had the longest mean FBL (6.4 ± 0.8 cm) followed by MG (5.8 ± 0.9 cm); PS had the shortest mean FBL (4.3 ± 1.0 cm). In the contracted state, the mean FBL of MG (3.9 ± 1.1 cm), PS (3.8 ± 1.4 cm), and LG (4.5 ± 1.0 cm) were not significantly different. Upon contraction, the fiber bundles of PS shortened by 25.2%, LG by 29.7% and MG by 32.8%.

Muscle (n)	Mean FBL (cm \pm SD)	Difference on contraction (cm %)	Range (cm)
MG Relaxed (34) Contracted (31)	$5.8 \pm 0.9^{a,1}$ $3.9 \pm 1.1^{a,2}$	1.9cm 32.8%	4.1 – 7.6 2.2 – 6.8
LG Relaxed (24) Contracted (32)	$6.4 \pm 0.8^{b,3}$ $4.5 \pm 1.0^{a,4}$	1.9cm 29.7%	5.2 – 7.8 2.5 – 6.4
PS Relaxed (28) Contracted (20)	$4.3 \pm 1.0^{c,5}$ $3.8 \pm 1.4^{a,6}$	0.5cm 25.2%	2.2 – 6.0 1.9 – 6.9

Table 5.1. Mean fiber bundle lengths (FBL) for the control group. Groups with different superscripts are significantly different ($p < 0.05$) from each other. Letter superscripts (a – c) compare different muscles while number superscripts (1 – 6) compare relaxed and contracted conditions within each muscle. SD = Standard deviation.

5.1.2 Angles of Pennation

Posterior and anterior PA of MG, LG, and PS are summarized in Table 5.2. For both relaxed and contracted conditions, LG had the smallest mean posterior and anterior PA while PS had the largest.

5.1.2.1 Posterior PA

The mean relaxed posterior PA of LG ($5.6^\circ \pm 1.5^\circ$) was significantly smaller ($p < 0.05$) than MG ($10.9^\circ \pm 2.5^\circ$) and PS ($16.2^\circ \pm 5.5^\circ$). The difference between the mean

relaxed posterior PA of MG and PS was also significant ($p < 0.05$). Mean relaxed posterior PA of LG was 5.2° less than MG and 9.4° less than PS, whereas mean relaxed posterior PA of MG was 4.2° less than PS.

Mean contracted posterior PA of LG ($10.3^\circ \pm 4.5^\circ$) was significantly smaller ($p < 0.05$) than MG ($19.5^\circ \pm 7.5^\circ$) and PS ($22.7^\circ \pm 10.1^\circ$); the contracted posterior PA of MG was not significantly different ($p < 0.05$) than PS.

5.1.2.2 Anterior PA

The mean relaxed anterior PA of LG ($13.5^\circ \pm 1.1$) was significantly smaller ($p < 0.05$) than MG ($16.3^\circ \pm 3.0^\circ$), but not PS ($15.1^\circ \pm 4.7^\circ$). There was no significant difference between the mean relaxed anterior PAs of MG and PS.

Muscle (n)	Mean Ant PA (deg \pm SD) [Range]	Difference on contraction (deg %)	Mean Post PA (deg \pm SD) [Range]	Difference on contraction (deg %)
MG				
Relaxed (34)	$16.1 \pm 3.1^{a,1}$ [10.1-24.0]	7.3° 45.3%	$10.9 \pm 2.5^{a,1}$ [6.8-19.9]	8.6° 78.9%
Contracted (31)	$23.4 \pm 6.9^{a,2}$ [13.2-42.0]		$19.5 \pm 7.5^{a,2}$ [7.3-38.2]	
LG				
Relaxed (24)	$13.7 \pm 1.3^{b,3}$ [11.5-17.8]	6.5° 47.4%	$5.6 \pm 1.5^{b,3}$ [2.9-10.6]	4.7° 83.9%
Contracted (32)	$20.2 \pm 4.3^{a,4}$ [12.7-31.1]		$10.3 \pm 4.5^{b,4}$ [3.5-20.8]	
PS				
Relaxed (28)	$15.2 \pm 5.1^{ab,5}$ [8.2-27.3]	6.5° 42.8%	$16.2 \pm 5.5^{c,5}$ [7.0-28.1]	6.5° 40.1%
Contracted (20)	$21.7 \pm 8.3^{a,6}$ [12.0-41.7]		$22.7 \pm 10.1^{a,6}$ [12.0-46.3]	

Table 5.2. Mean anterior (Ant) and posterior (Post) pennation angles (PA) for the control group. Groups with different superscripts are significantly different ($p < 0.05$) from each other. Letter superscripts (a – c) compare different muscles while number superscripts (1 – 6) compare relaxed and contracted conditions within each muscle. deg = degrees, SD = Standard deviation.

The mean contracted anterior PA of MG ($23.5^{\circ} \pm 6.8^{\circ}$), LG ($20.5^{\circ} \pm 4.4^{\circ}$), and PS ($22.1^{\circ} \pm 8.3^{\circ}$) were not significantly different (Table 5.2).

5.1.2.3 Change in PA on contraction

The amount of change in PA, from relaxed to contracted, was calculated in degrees. MG had the greatest change of anterior PA on contraction (7.3°) compared to LG (6.5°) and PS (6.5°). The posterior PA of MG increased 8.6° on contraction whereas PS increased 6.5° and LG increased 4.7° . The relaxed and contracted conditions for each of MG, LG, and PS were significantly ($p < 0.05$) different (e.g., mean relaxed anterior PA of MG was significantly different than its mean contracted anterior PA).

5.1.4 Muscle Thickness

Muscle Thickness in relaxed and contracted conditions of MG, LG, and PS are presented in Table 5.3. In the relaxed condition, LG had the smallest mean MT ($0.76\text{cm} \pm 0.1\text{cm}$) of the three muscles, while MG ($1.1\text{cm} \pm 0.2$) and PS ($1.1\text{cm} \pm 0.3\text{cm}$) had

Muscle (n)	Mean MT (cm \pm SD)	Difference on contraction (cm %)	Range (cm)
MG Relaxed (36) Contracted (35)	$1.1 \pm 0.2^{\text{a},1}$ $1.2 \pm 0.2^{\text{a},2}$	0.1cm 9.1%	0.8 – 1.5 0.9 – 1.7
LG Relaxed (35) Contracted (36)	$0.76 \pm 0.1^{\text{b},3}$ $0.83 \pm 0.2^{\text{b},4}$	0.07cm 9.2%	0.6 – 1.0 0.5 – 1.2
PS Relaxed (35) Contracted (33)	$1.1 \pm 0.3^{\text{a},5}$ $1.2 \pm 0.3^{\text{a},6}$	0.1cm 9.1%	0.6 – 1.6 0.7 – 1.9

Table 5.3. Mean muscle thicknesses (MT) for the control group. Groups with different superscripts are significantly different ($p < 0.05$) from each other. Letter superscripts (a – b) compare different muscles while number superscripts (1 – 6) compare relaxed and contracted conditions within each muscle. SD = Standard deviation.

identical mean thicknesses. The mean relaxed MT of LG was significantly different ($p<0.05$) from MG and PS.

Similar to the relaxed condition, LG had the smallest mean contracted MT ($0.83\text{cm}\pm 0.2\text{cm}$) compared to MG ($1.2\text{cm}\pm 0.2\text{cm}$) and PS ($1.2\text{cm}\pm 0.3\text{cm}$). The contracted MT of LG was significantly smaller than MG and PS ($p<0.05$). The relaxed and contracted means for each of MG, LG, and PS were significantly different ($p<0.05$).

5.2 DMD group

The FBL, PA, and MT of MG, LG, and PS for the DMD group ($n = 36$) were quantified using the US scans. An example of these scans is presented in Figure 5.2. The mean height, weight, and leg length of the DMD group were 131cm, 38kg, and 63cm respectively. No significant correlations were found between these physical characteristics and the architectural parameters. Age distribution of subjects is as follows: 5yr = 1; 6yr = 1; 7yr = 2; 8yr = 1; 9yr = 5; 10yr = 1; 11yr = 2; 13yr = 3; 14yr = 1; 15yr = 1. However, 145 of a total of 216 images for the DMD group had abnormal infiltration of fat and connective tissue, so the qualitative rating scale was used to compare these scans. In the relaxed condition, 67 of a total of 108 scans for the 18 subjects (19 MG, 25 LG, 23 PS) were unmeasurable. In the contracted condition, 75 of the 108 scans were unmeasurable and therefore were qualitatively assessed (20 MG, 22 LG, 31 PS).

For both relaxed and contracted conditions of FBL and Ant and Post PA, the number of measurable scans decreased after the age of 9, with no quantifiable scans at ages 10, 12, and 14. MG was the only muscle that was measurable at age 15. For PS, no scans were measurable after age 11; for LG, none were measurable after age 13. In the

contracted condition, PS scans at ages 5, 6, and 8 which were previously quantifiable when relaxed became unmeasurable, whereas this trend was not observed for MG and LG. For MT, LG was the most quantifiable in the older subjects age 10 – 15. In the contracted condition, no quantifiable scans for MT were available for the ages of 12 and 14.

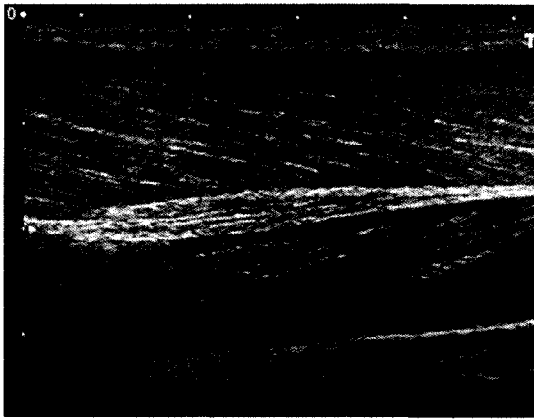
5.2.1 Fiber Bundle Length (DMD)

Mean relaxed and contracted FBL for MG, LG, and PS are summarized in Table 5.5. MG had the longest mean relaxed FBL ($5.7 \pm 0.8\text{cm}$) while PS had the shortest ($5.0 \pm 1.3\text{cm}$). The mean relaxed FBL of LG was 5.6 ± 1.2 . There was no significant difference in relaxed FBL between the muscles.

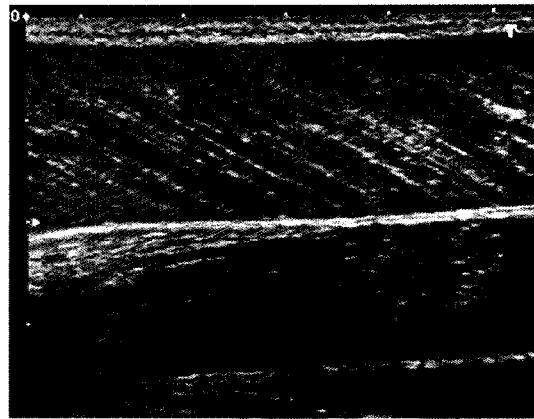
On contraction, LG had the longest mean FBL ($4.5 \pm 1.3\text{cm}$) and PS was the shortest ($3.3 \pm 0.8\text{cm}$). LG had the smallest percentage change in FBL on contraction (19.6% / 1.1cm) and PS had the largest percentage change (34% / 1.7cm); the change on

Muscle (n)	Mean FBL (cm \pm SD)	Difference on contraction (cm %)	Range (cm)
MG Relaxed (16) Contracted (16)	$5.7 \pm 0.8^{a,1}$ $4.2 \pm 1.2^{a,2}$	1.5cm 24.6%	4.3 – 6.8 2.7 – 6.6
LG Relaxed (10) Contracted (14)	$5.6 \pm 1.2^{a,3}$ $4.5 \pm 1.3^{a,4}$	1.1cm 19.6%	4.0 – 7.4 2.7 – 6.6
PS Relaxed (12) Contracted (5)	$5.0 \pm 1.3^{a,5}$ $3.3 \pm 0.8^{a,5}$	1.7cm 34.0%	3.1 – 7.7 2.3 – 4.2

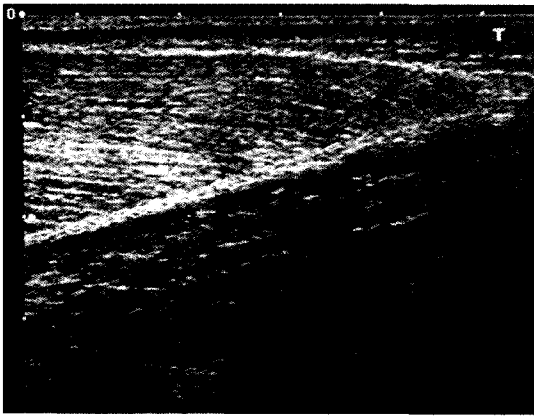
Table 5.4. Mean fiber bundle lengths (FBL) for the DMD group. Groups with different superscripts are significantly different ($p < 0.05$) from each other. Letter superscripts (a, b) compare different muscles while number superscripts (1 – 6) compare relaxed and contracted conditions within each muscle. SD = Standard deviation.



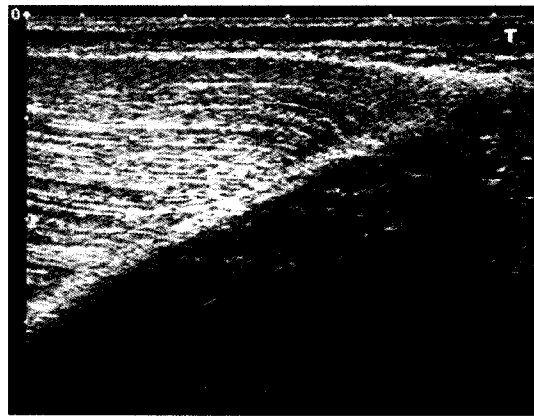
A.



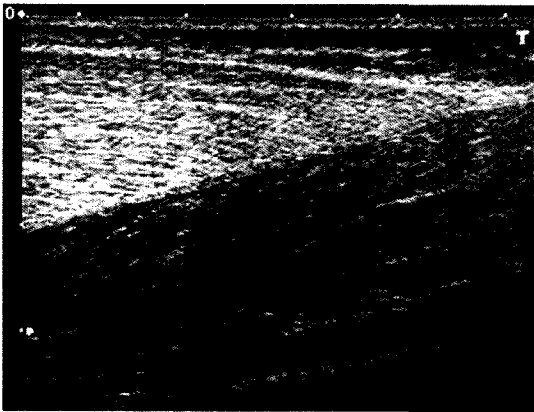
B.



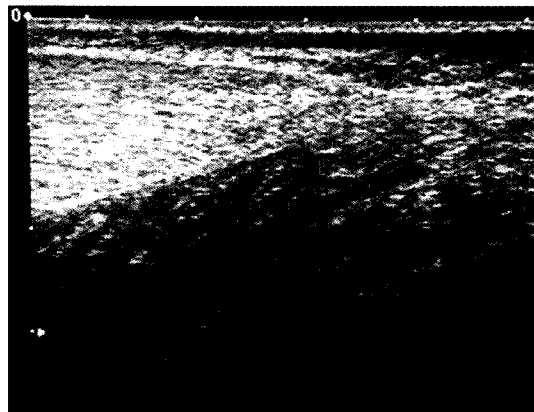
C.



D.



E.



F.

Figure 5.2. Ultrasound scans of one DMD subject. A. MG relaxed B. MG contracted C. LG relaxed D. LG contracted E. PS relaxed F. PS contracted.

contraction for MG was 24.6% (1.4cm). The relaxed and contracted conditions for each of MG, LG, and PS were significantly ($p<0.05$) different (e.g., mean relaxed FBL of MG was significantly different than its mean contracted FBL).

5.2.2 Angles of Pennation (DMD)

Mean relaxed and contracted PA for MG, LG, and PS are presented in Table 5.5. The mean relaxed posterior PA of MG and LG were significantly smaller ($p<0.05$) than PS, but MG and LG were not significantly different from each other. There was no significant difference in relaxed anterior PA of MG, LG, and PS. In the contracted condition, the posterior PA of MG and PS was significantly larger ($p<0.05$) than LG, but MG and PS were not different from each other. No significant difference was found between the contracted anterior PA of MG, LG, and PS.

5.2.2.1 Posterior PA

LG had the smallest mean relaxed ($8.7^{\circ}\pm 5.1^{\circ}$) and contracted ($12.1^{\circ}\pm 4.8^{\circ}$) posterior PA, while PS had the largest in both conditions ($17.0^{\circ}\pm 4.4^{\circ}$, relaxed; $27.6^{\circ}\pm 2.7^{\circ}$, contracted). The mean relaxed posterior PA of PS was 5.0° larger than that of MG and 8.3° larger than that of LG, whereas the mean relaxed posterior PA of MG was 3.3° larger than LG. The mean contracted posterior PA of PS was 3.2° larger than the mean of MG and 15.5° larger than LG; MG was 12.3° larger than LG.

5.2.2.2 Anterior PA

In the relaxed condition, the mean anterior PA of PS ($15.9^{\circ}\pm 5.0^{\circ}$) was the smallest and the mean of MG ($18.6^{\circ}\pm 3.5^{\circ}$) was the largest (Table 5.5). The mean relaxed anterior PA of MG was 2.7° larger than PS, but only 0.6° larger than LG. For the

contracted condition, the mean anterior PA of PS ($27.1^{\circ} \pm 2.4^{\circ}$) was similar to that of MG ($28.5^{\circ} \pm 8.3$), while the mean of LG ($26.1^{\circ} \pm 7.2^{\circ}$) was the smallest.

Muscle (n)	Mean Ant PA (deg \pm SD) [range]	Difference on contraction (deg %)	Mean Post PA (deg \pm SD) [range]	Difference on contraction (deg %)
MG Relaxed (16)	$18.6 \pm 3.5^{a,1}$ [11.6 – 23.5]	9.9° 53.2%	$12.0 \pm 1.8^{a,1}$ [10.1 – 17.1]	12.4° 103%
Contracted(16)	$28.5 \pm 8.3^{a,2}$ [13.5 – 43.5]		$24.4 \pm 8.7^{a,2}$ [13.0 – 44.4]	
LG Relaxed (10)	$18.0 \pm 3.7^{a,3}$ [11.7 – 23.1]	8.1° 45.0%	$8.7 \pm 5.1^{a,3}$ [5.1 – 22.9]	3.4° 39.1%
Contracted (14)	$26.1 \pm 7.2^{a,4}$ [14.9 – 38.1]		$12.1 \pm 4.8^{b,4}$ [4.0 – 20.2]	
PS Relaxed (12)	$15.9 \pm 5.0^{a,5}$ [9.5 – 24.6]	11.2° 70.4%	$17.0 \pm 4.4^{b,5}$ 9.8 – 25.8	10.6° 62.4%
Contracted (5)	$27.1 \pm 2.4^{a,5}$ [24.4 – 30.6]		$27.6 \pm 2.7^{a,5}$ 23.6 – 30.2	

Table 5.5. Mean anterior (Ant) and posterior (Post) pennation angles (PA) for the DMD group. Groups with different superscripts are significantly different ($p < 0.05$) from each other. Letter superscripts (a – c) compare different muscles while number superscripts (1 – 6) compare relaxed and contracted conditions within each muscle. deg = degrees, SD = Standard deviation.

5.2.2.3 Change in PA on contraction

PS had the largest change in anterior PA on contraction (11.2°) compared to MG (9.9°) and LG (8.1°). The posterior PA of MG increased by 12.4° on contraction; the PS increased by 10.6° , and the LG by 3.4° . The relaxed and contracted conditions for each of MG, LG, and PS were significantly ($p < 0.05$) different (e.g., mean relaxed anterior PA of MG was significantly different than its mean contracted anterior PA).

5.2.3 Muscle Thickness (DMD)

Relaxed and contracted mean MT for MG, LG, and PS are presented in Table 5.6. MG had the largest mean relaxed ($1.4\text{cm}\pm 0.4\text{cm}$) and contracted ($1.6\text{cm}\pm 0.3\text{cm}$) MT, and LG had the smallest mean MT for both muscle conditions ($1.06\text{cm}\pm 0.3\text{cm}$, relaxed; $1.11\text{cm}\pm 0.4\text{cm}$, contracted).

Muscle (n)	Mean MT (cm \pm SD)	Difference on contraction (cm %)	Range (cm)
MG Relaxed (28) Contracted (24)	$1.4 \pm 0.4^{a,1}$ $1.6 \pm 0.4^{a,2}$	0.2cm 14.3%	0.8 – 2.7 0.9 – 2.6
LG Relaxed (24) Contracted (28)	$1.06 \pm 0.3^{b,3}$ $1.11 \pm 0.4^{b,3}$	0.05cm 4.7%	0.7 – 2.1 0.7 – 2.0
PS Relaxed (19) Contracted (17)	$1.3 \pm 0.3^{ab,4}$ $1.4 \pm 0.3^{a,5}$	0.1cm 7.7%	0.9 – 1.9 1.1 – 2.0

Table 5.6. Mean muscle thickness (MT) for the DMD group. Groups with different superscripts are significantly different ($p<0.05$) from each other. Letter superscripts (a – c) compare different muscles while number superscripts (1 – 5) compare relaxed and contracted conditions within each muscle. SD = Standard deviation.

The mean relaxed MTs of MG was significantly larger ($p<0.05$) than LG, but not PS ($1.3\text{cm}\pm 0.2\text{cm}$). For the contracted condition, mean MT of LG was significantly smaller ($p<0.05$) than MG and PS; mean MTs of MG and PS were not different from each other.

On contraction, MG had the largest percentage change in MT (14.3%) compared to PS (7.6%). As in the control group, identical means were found for relaxed and contracted MT of LG. This may be due to the high degree of tapering in the distal portion of the muscle, which may not reflect the change in muscle thickness upon contraction.

5.2.4 Correlation between muscle architectural parameters

The relationships between FBL, anterior PA, posterior PA, and MT were explored using Pearson's Correlation. For the DMD group, there were significant correlations between MT and posterior PA for MG and LG, and between MT and anterior PA for PS (Table 5.7). Correlations between FBL and PA only showed a significance for PS ($r = -0.738$), and none of the r -values for the FBL-MT association were significant. Only the r -values for PA-MT are shown.

	Anterior PA	Posterior PA
MG MT	0.251	0.589*
LG MT	0.450	0.930*
PS MT	0.596*	-0.111

Table 5.7. Pearson's correlation values between pennation angle and muscle thickness in the relaxed condition for the DMD group.

For the control group, significant correlations were found between MT and posterior PA of MG and between MT and both PAs for PS (Table 5.8). Significant correlations ($p < 0.05$) were also found between the MTs of all three muscles (unpublished data).

	Anterior PA	Posterior PA
MG MT	0.318	0.396*
LG MT	0.239	0.269
PS MT	0.660*	0.546*

Table 5.8. Pearson's correlation values between pennation angle and muscle thickness in the relaxed condition for the Control group.

5.3 Control group vs. DMD group

5.3.1 Fiber Bundle Length

Mean relaxed and contracted FBL for the control and DMD groups are summarized in Table 5.9 and graphically in Figure 5.3. The relaxed FBL of PS for DMD subjects ($5.0\text{cm}\pm 1.3$) was longer than the FBL of controls ($4.3\text{cm}\pm 1.0$). In contrast, the contracted FBL of PS for control subjects ($3.8\text{cm}\pm 1.4$) was longer than those of DMD subjects ($3.3\text{cm}\pm 0.8$). For MG and LG, control subjects had longer relaxed FBL ($5.8\text{cm}\pm 0.9$ and $6.4\text{cm}\pm 0.8$) than DMD subjects ($5.7\text{cm}\pm 0.8$ and $5.6\text{cm}\pm 1.2$). In the contracted condition, control subjects had shorter FBL for MG ($3.9\text{cm}\pm 1.1$) compared to DMD subjects ($4.2\text{cm}\pm 1.3$). The means for contracted FBL of LG were identical. These differences in FBL were not statistically significant ($p<0.05$).

Muscle	Control FBL (cm ± SD)	Change on contraction (cm)	DMD FBL (cm ± SD)	Change on contraction (cm)	% diff. between control and DMD (Relaxed)	% difference between change on contraction
MG						
Rel	5.8 ± 0.9^a	1.9^1	5.7 ± 0.8^a	1.5^1	2%↓	21%↓
Con	3.9 ± 1.1^b		4.2 ± 1.2^b			
LG						
Rel	6.4 ± 0.8^c	1.9^2	5.6 ± 1.2^c	1.1^3	13%↓	42%↓*
Con	4.5 ± 1.0^d		4.5 ± 1.3^d			
PS						
Rel	4.3 ± 1.0^e	0.5^4	5.0 ± 1.3^e	1.7^5	16%↑	240%↑*
Con	3.8 ± 1.4^f		3.3 ± 0.8^f			

Table 5.9. Mean fiber bundle lengths for control vs DMD groups. Different letter superscripts indicate statistical significance ($p<0.05$) between the two groups for the same muscle condition. Number superscripts indicate statistical significance ($p<0.05$) of the difference between relaxed and contracted means for the two groups. SD = Standard deviation, diff. = difference, ↑ = more than control, ↓ = less than control. * = statistically significant ($p<0.05$).

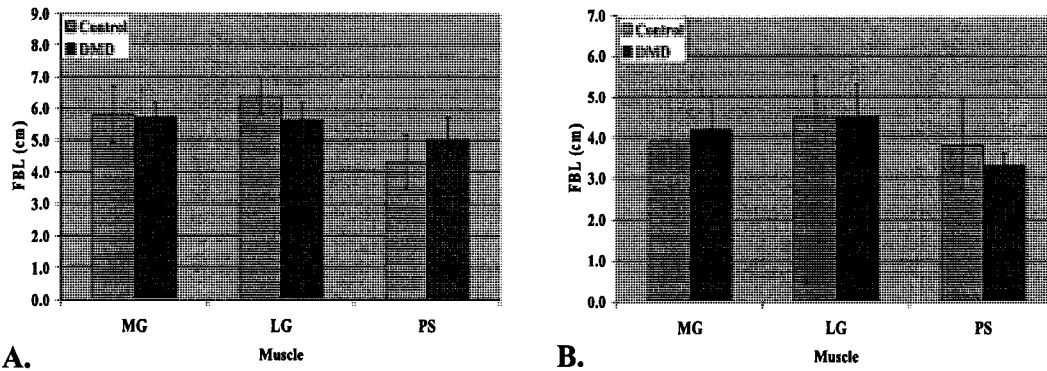


Figure 5.3. Bar graphs of mean fiber bundle lengths for control vs. DMD groups. A. Relaxed. B. Contracted PA. Note that the y-axes are scaled differently in graph A and B to enable better visualization of data.

The FBL of PS in the DMD group shortened more on contraction than the FBL of the control group (Table 5.9). In contrast, the FBL of MG and LG in the DMD group shortened less than the control group. The change in FBL was significantly different ($p < 0.05$) between DMD and control groups for LG and PS, but not for MG.

5.3.2 Angles of Pennation

5.3.2.1 Posterior PA

Mean relaxed and contracted posterior PA for control and DMD groups are summarized in Table 5.10 and graphically displayed in Figure 5.4. The posterior PA of DMD subjects for all three muscles in relaxed and contracted conditions were larger than the control group. However, only relaxed LG showed a statistical significance ($p < 0.05$) in the difference of posterior PAs ($8.7^\circ \pm 5.1$ for DMD, $5.6^\circ \pm 1.7$ for control).

For MG and PS, the DMD group had significantly ($p < 0.05$) greater change in posterior PA on contraction than the control group (Table 5.10). However, for LG the

control group had greater change of posterior PA on contraction than DMD subjects, although the difference was not significant.

Muscle	Control Post PA (deg ± SD)	Change on contraction (degrees)	DMD Post PA (deg ± SD)	Change on contraction (degrees)	% diff. between control and DMD (Relaxed)	% difference between change on contraction
MG Rel Con	10.9 ± 2.5 ^a 19.5 ± 7.5 ^b	8.6 ¹	12.0 ± 1.8 ^a 24.4 ± 8.7 ^b	12.4 ²	10%↑	44%↑*
LG Rel Con	5.6 ± 1.5 ^c 10.3 ± 4.5 ^e	4.7 ³	8.7 ± 5.1 ^d 12.1 ± 4.8 ^e	3.4 ³	55%↑*	28%↓
PS Rel Con	16.2 ± 5.5 ^f 22.7 ± 10.1 ^g	6.5 ⁴	17.0 ± 4.4 ^f 27.6 ± 2.7 ^g	10.6 ⁵	5%↑	63%↑*

Table 5.10. Mean posterior pennation angles (Post PA) for control and DMD groups. Different letter superscripts indicate statistical significance ($p < 0.05$) between the two groups for the same muscle condition. Number superscripts indicate statistical significance ($p < 0.05$) of the difference between relaxed and contracted means for the two groups. SD = Standard deviation, diff. = difference, ↑ = more than control, ↓ = less than control. * = statistically significant ($p < 0.05$).

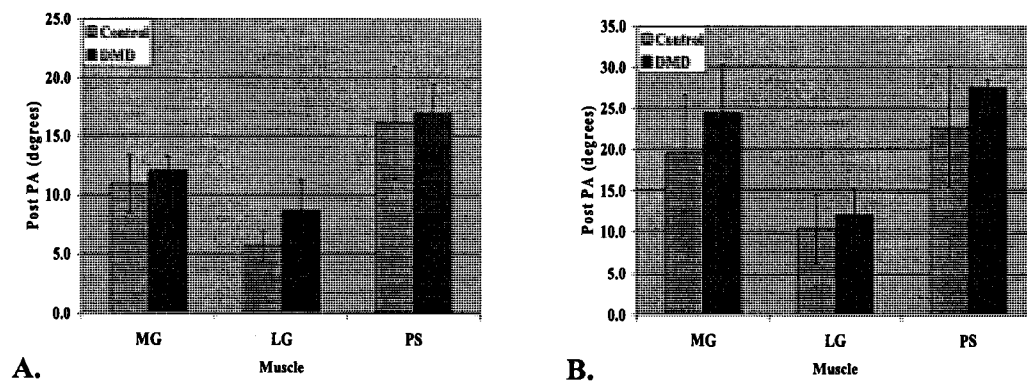


Figure 5.4. Bar graphs of mean posterior pennation angles (Post PA) for control vs. DMD groups. A. Relaxed B. Contracted PA. Note that the y-axes are scaled differently in graph A and B to enable better visualization of data.

5.3.2.2 Anterior PA

Mean relaxed and contracted anterior PA for control and DMD groups are summarized in Table 5.11 and graphically displayed in Figure 5.5. Both MG (relaxed)

Muscle	Control Ant PA (deg ± SD)	Change on contraction (degrees)	DMD Ant PA (deg ± SD)	Change on contraction (degrees)	% diff. between control and DMD (Relaxed)	% difference between change on contraction
MG						
Rel	16.1 ± 3.1 ^a	7.3 ¹	18.6 ± 3.5 ^b	9.9 ¹	16%↑*	36%↑
Con	23.4 ± 6.9 ^c		28.5 ± 8.3 ^c			
LG						
Rel	13.7 ± 1.3 ^d	6.5 ²	18.0 ± 3.7 ^e	8.1 ²	31%↑*	25%↑
Con	20.2 ± 4.3 ^f		26.1 ± 7.2 ^g			
PS						
Rel	15.2 ± 5.1 ^h	6.5 ³	15.9 ± 5.0 ^h	11.2 ⁴	5%↑	72%↑*
Con	21.7 ± 8.3 ⁱ		27.1 ± 2.4 ⁱ			

Table 5.11. Mean anterior pennation angles (Ant PA) for control and DMD groups. Different letter superscripts indicate statistical significance (p<0.05) between the two groups for the same muscle condition. Number superscripts indicate statistical significance (p<0.05) of the difference between relaxed and contracted means for the two groups. SD = Standard deviation, diff. = difference, ↑ = more than control, ↓ = less than control. * = statistically significant (p<0.05).

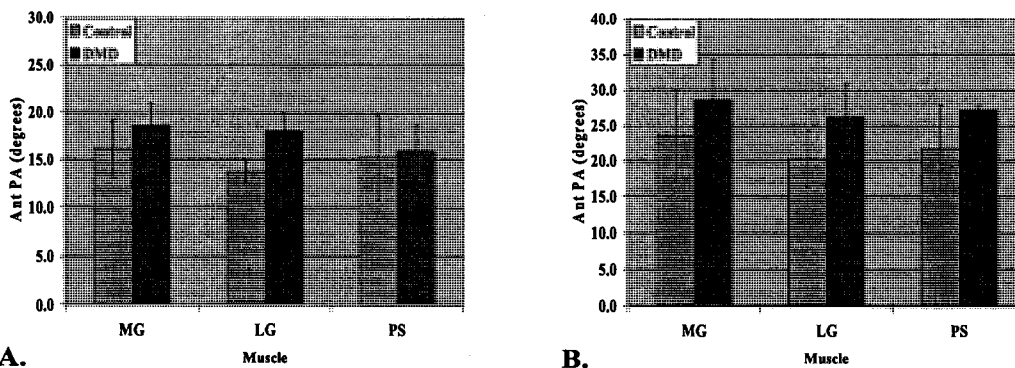


Figure 5.5. Bar graphs of mean anterior pennation angles (Ant PA) for control and DMD groups. A. Relaxed B. Contracted. Note that the y-axes are scaled differently in graph A and B to enable better visualization of data.

and LG (relaxed and contracted) of the DMD subjects had significantly ($p<0.05$) larger anterior PA than control subjects. The anterior PA of PS in relaxed and contracted conditions were also larger than control subjects but these differences were not statistically significant (Table 5.11).

5.3.3 Muscle Thickness

Mean relaxed and contracted MT for the control and DMD groups are summarized in Table 5.12 and graphically in Figure 5.6. The mean MT for all three muscles of the DMD subjects were significantly larger ($p<0.05$) than the mean MTs of the control subjects for both relaxed and contracted conditions. The change in MT on contraction was not significant between the two groups for all three muscles (Table 5.12).

Muscle	Control MT (cm \pm SD)	Change on contraction (cm)	DMD MT (cm \pm SD)	Change on contraction (cm)	% diff. between control and DMD (Relaxed)	% difference between change on contraction
MG						
Rel	1.1 \pm 0.2 ^a	0.1 ¹	1.4 \pm 0.4 ^b	0.2 ¹	27% \uparrow *	100% \uparrow
Con	1.2 \pm 0.2 ^c		1.6 \pm 0.4 ^d			
LG						
Rel	0.76 \pm 0.1 ^e	0.07 ²	1.06 \pm 0.3 ^f	0.05 ²	40% \uparrow *	29% \downarrow
Con	0.83 \pm 0.2 ^g		1.11 \pm 0.4 ^h			
PS						
Rel	1.1 \pm 0.3 ⁱ	0.1 ³	1.3 \pm 0.3 ^j	0.1 ³	18% \uparrow *	n/d
Con	1.2 \pm 0.3 ^k		1.4 \pm 0.3 ^l			

Table 5.12. Mean muscle thicknesses (MT) for control and DMD groups. Different letter superscripts indicate statistical significance ($p<0.05$) between the two groups for the same muscle condition. Number superscripts indicate statistical significance ($p<0.05$) of the difference between relaxed and contracted means for the two groups. SD = Standard deviation, diff. = difference, \uparrow = more than control, \downarrow = less than control. * = statistically significant ($p<0.05$).

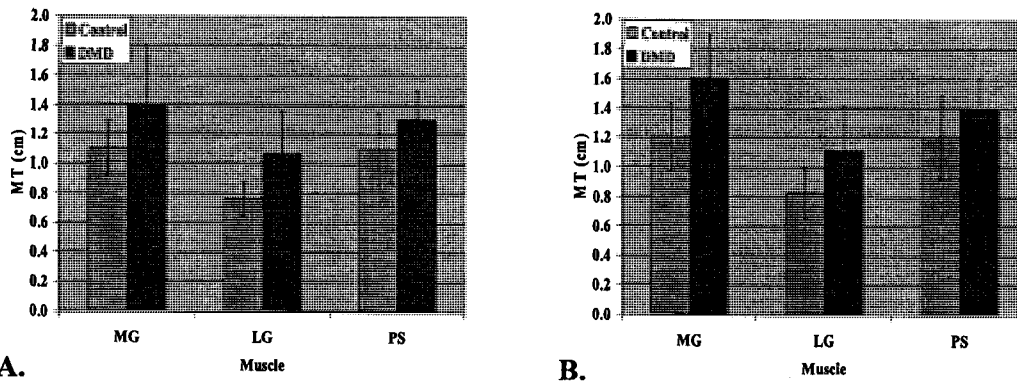


Figure 5.6. Bar graphs of mean muscle thicknesses (MT) for control and DMD and groups. A. Relaxed. B. Contracted.

5.4 Qualitative Rating

5.4.1 Overview

Qualitative rating of US images was carried out for all scans, with a focus on relaxed scans of DMD and control subjects that could not be quantified. All DMD subjects had at least one unmeasurable US scan, and sixteen of the eighteen DMD subjects had at least one scan rated ‘severe’ or ‘obliterated’. Furthermore, out of the eighteen DMD subjects, 12 had three or more scans that were unmeasurable while the remaining six subjects had 1-2 unquantifiable scans (Table 5.13). Three control subjects each had 1 image rated ‘mild’. None of the controls had scans rated ‘moderate’, ‘severe’ or ‘obliterated’. For the DMD scans, interrater reliability between the three raters was excellent with $R = 0.931$ (average measure; 95% confidence interval: 0.798, 0.981).

5.4.2 Age distribution of scans

DMD subjects with 1-2 unquantifiable scans had an average age of 7.1 ± 1.5 years, whereas subjects with three or more unquantifiable scans had an average age of 11.3 ± 2.2

years. The average age of control subjects with 1-2 unquantifiable scans was 10.0 ± 2.1 years, while the average age in the group with 3-4 unquantifiable scans was 10.4 ± 1.3 years.

Subject (DMD)	Age (Year, Month)	MG		LG		PS		# of unquantifiable scans		
		Left	Right	Left	Right	Left	Right	Left	Right	Total
1	10y 5m	X	X	X	X	X	X	3	3	6
2	15y 2m	✓	✓	X	X	X	X	2	2	4
3	9y 6m	✓	X	X	X	✓	✓	1	2	3
4	12y 11m	X	X	X	X	X	X	3	3	6
5	11y 0m	✓	X	X	✓	X	X	2	2	4
6	6y 10m	✓	✓	X	✓	✓	✓	1	0	1
7	7y 6m	✓	✓	✓	✓	✓	X	0	1	1
8	5y 7m	✓	X	✓	X	✓	✓	0	2	2
9	13y 6m	X	X	X	X	X	X	3	3	6
10	13y 11m	X	X	X	X	X	X	3	3	6
11	8y 8m	X	X	X	X	X	X	3	3	6
12	9y 5m	X	X	X	X	X	X	3	3	6
13	11y 7m	✓	X	X	X	X	✓	2	2	4
14	9y 4m	✓	X	X	X	✓	✓	1	2	3
15	13y 2m	✓	n/a	✓	n/a	X	n/a	1	n/a	1
16	9y 5m	✓	✓	✓	✓	X	X	1	1	2
17	8y 5m	X	X	X	X	X	✓	3	2	5
18	6y 3m	✓	✓	✓	✓	X	✓	1	0	1

Table 5.13. Distribution of quantifiable images in the relaxed state for the DMD group. “X” represents a scan with no quantifiable parameters and “✓” represents a scan that was quantifiable. The last column marks the total number of unquantifiable scans for each subject.

5.4.3 Rating scores

5.4.3.1 Comparison by Age

Both the DMD and control group had eleven boys ≤ 10 years, and seven boys ≥ 11 years. For the DMD subjects, the younger group (i.e., 10 years and under) had 58% of images rated “obliterated”, 31% rated “severe”, and 11% rated “moderate”. The older

DMD boys had 76% rated “obliterated”, 19% “severe”, and 5% “moderate”. None of the DMD boys had normal or mild ratings in any scan (Table 5.14).

In the control group, a majority of unquantifiable scans (17 out of 22 scans) were determined to be “out of plane” as the muscle fibers could not be visualized on the scans, but were visible on exploratory scans (Fig. 5.7).

Muscle	10 years & under				11 years & over			
	Mild	Mod	Severe	Obliterated	Mild	Mod	Severe	Obliterated
MG	0	2	2	5	0	1	3	6
LG	0	1	6	5	0	1	3	9
PS	0	0	0	5	0	0	1	13
Subtotal	0	3	8	15	0	2	7	28
Total	26				37			

Table 5.14. Distribution of qualitative ratings in the DMD group by age and muscle. Both relaxed and contracted scans are included. Four PS scans from the ≤ 10 years group were “out of plane” so they were not rated.

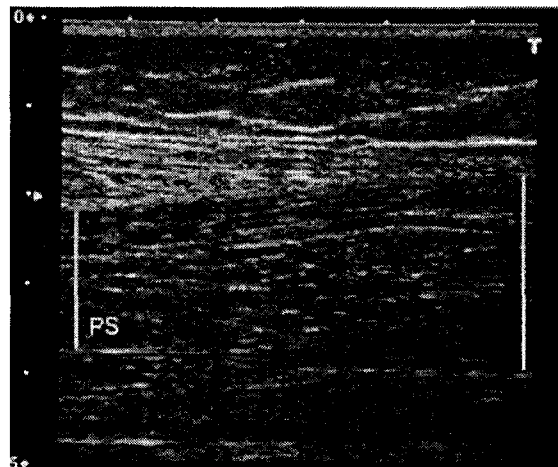


Figure 5.7. Ultrasound scan of posterior soleus rated “out of plane”. Connective tissue is visible in the image but no measurable fiber bundle is present.

5.4.3.2 Comparison of qualitative rating scale with Timed Function Tests

The timed function test (TFT) results for the DMD children are listed in tables 5.15 to 5.18. Qualitative rating scores were significantly correlated ($p < 0.05$) to subjects' age ($\rho = 0.530$) and TFT results for walking ($\rho = 0.670$) and stairs ($\rho = 0.816$). Non-ambulatory children (5 out of 18 subjects) were not assessed with TFT. DMD boys with 'severe' to 'obliterated' ratings took an average of 8.8sec to complete the walk portion of the TFT test and 6.7sec on stairs compared to 4.95sec (walk) and 2.78sec (stairs) for those with scans rated 'mild' to 'moderate' (Table 5.15).

For boys ≤ 10 years of age, qualitative rating scores were significantly correlated ($p < 0.05$) to their age ($\rho = 0.633$) and TFT results for walking ($\rho = 0.679$). Although not statistically significant, the correlation of rating scores to TFT results for stairs was $\rho = 0.525$ (Table 5.16). For boys ≥ 11 years of age, qualitative rating scores were significantly correlated ($p < 0.05$) to TFT results for stairs ($\rho = 1.00$). The correlation of rating scores to TFT results for walking was $\rho = 0.500$, but this was not statistically significant. However, the significance values in the older group may be affected by the small number of subjects who were able to complete the TFTs. Older boys also tended to have poorer qualitative ratings compared to the younger group (Tables 5.17 and 5.18).

Comparing the younger boys to the older boys, there was a significant difference between the TFT results, both walking and stairs, and the qualitative ratings of the two groups ($p < 0.05$). Furthermore, the muscle preserving effects of steroids are clearly reflected in the TFT scores of boys on the drug and boys who are not. Older subjects on steroids had similar or better TFT scores than younger subjects not on steroids. Finally, a

comparison between ambulatory and non-ambulatory boys also yielded a significant difference in the qualitative rating scores of the two groups ($p < 0.05$).

Rating	TFT – Walk (sec)	TFT – Stairs (sec)
Mild – Moderate	4.95	2.78
Moderate – Severe	4.97	4.00
Severe – Obliterated	8.80	6.70

Table 5.15. Mean results on timed function tests (TFT). Performance times are listed beside the corresponding qualitative rating levels of the DMD subject scans.

	Whole Group	Young (≤ 10)	Old (≥ 11)
Age	0.607*	0.700*	0.442
TFT (walk)	0.705*	0.698*	0.885
TFT (stairs)	0.797	0.525	1.00*

Table 5.16. Pearson's correlation (r values) between qualitative rating scores and age, TFT (walk), and TFT (stairs). separated into whole group, young boys, and older boys. * denotes statistical significance ($p < 0.05$).

Subject	Age	Qualitative Rating						Ambulatory	TFT – Walk (sec)	TFT – Stairs (sec)
		MG		LG		PS				
		L	R	L	R	L	R			
1	*5y 7m	1	2	2	3	1	1	Yes	4.8	3.6
2	6y 10m	1	2	3	2	1	1	Yes	4.0	1.8
3	*9y 5m	2	2	2	2	5	5	Yes	5.0	2.2
4	*6y 3m	2	2	3	2	5	2	Yes	6.0	3.5
5	*7y 6m	2	2	3	2	3	5	Yes	5.8	5.4
6	9y 4m	2	3	3	2	2	1	Yes	4.5	3.8
7	9y 6m	2	3	3	3	2	1	Yes	4.6	2.8
8	8y 5m	4	2	4	3	4	2	Yes	5.6	4.8
9	8y 8m	4	4	4	4	4	4	Yes	7.0	7.0
10	9y 5m	4	4	4	4	4	4	Yes	8.0	6.0
11	10y 5m	4	3	4	4	4	4	No	X	X

Table 5.17. Comparison of qualitative data to timed function tests (TFT) for younger DMD children (≤ 10 years). Subjects not on steroids at the time of the US scan are marked by *. Unavailable data are marked with an X.

Subject	Age	Qualitative Rating						Ambulatory	TFT – Walk (sec)	TFT – Stairs (sec)
		MG		LG		PS				
		L	R	L	R	L	R			
1	11y 7m	2	2	3	2	3	1	Yes	8.2	5.1
2	*11y 0m	3	4	4	2	4	4	No	X	X
3	13y 2m	2	X	3	X	4	X	No	X	X
4	13y 6m	3	4	4	3	4	4	Partial	13.0	X
5	15y 2m	3	3	4	3	4	4	No	X	X
6	12y 11m	4	3	4	4	4	4	Yes	11.0	10.6
7	13y 11m	4	4	4	4	4	4	No	X	X

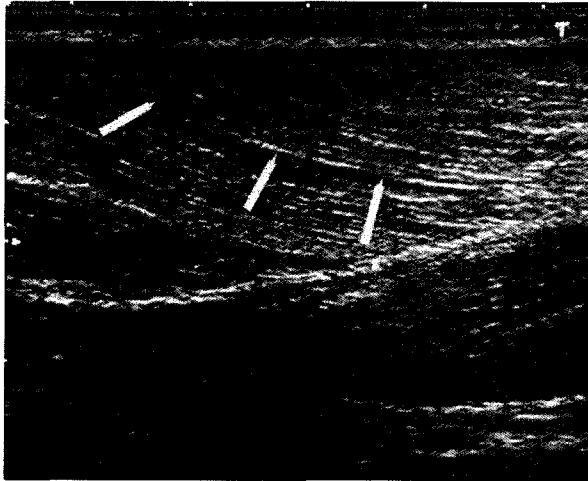
Table 5.18. Comparison of qualitative data to timed function tests (TFT) for older DMD children (≥ 11 years). Subjects not on steroids at the time of the US scan are marked by *. Unavailable data are marked with an X.

5.4.3.3 Fiber bundle curvature

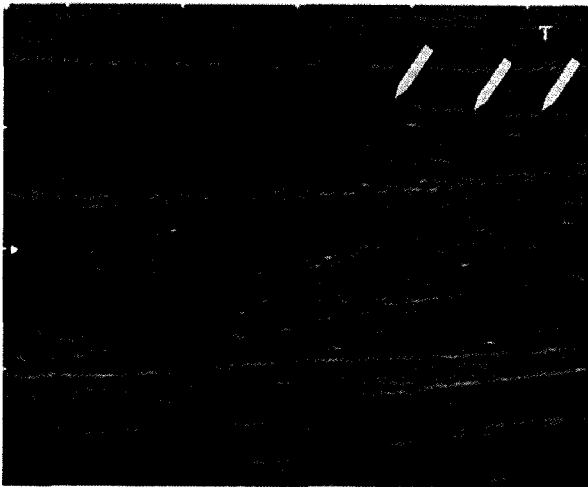
In addition to the increase in echogenicity and changes to the fiber pattern observed in DMD subjects, excessive fiber bundle curvature may also be observed in DMD muscle that is not seen in control subjects (Fig. 5.8A). Although a very small degree of curvature was seen in one control subject from this study (Fig. 5.8B), the curvature observed in DMD subjects far exceeds that seen in the control subject.

5.4.3.4 Deformity of aponeurosis

Abnormal appearance of aponeuroses in DMD muscles is shown in figure 5.9. Besides excessive curvature compared to controls (Fig. 5.9A & B), figure 5.9C shows a deformity in the MG aponeurosis of a DMD subject. This phenomenon was not seen in any of the control subject scans (Fig. 5.9D).



A – DMD



B – Control

Figure 5.8. Excessive curvature of DMD muscle fibers. A) US scan of MG fiber bundles in a child with DMD. B) US scan of MG in a control subject.

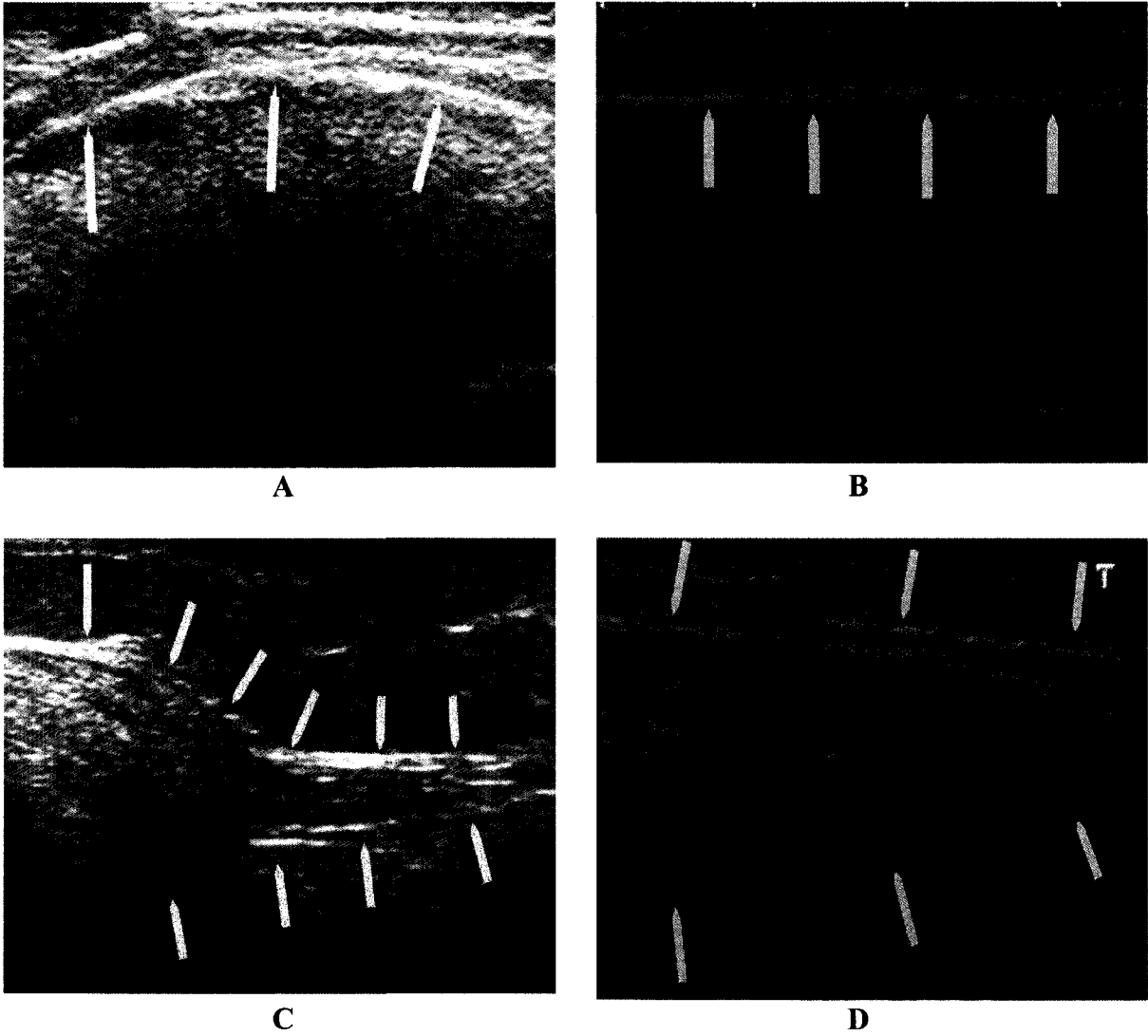


Figure 5.9. Deformity of DMD aponeurosis. A) US scan demonstrating abnormal curvature of aponeurosis of MG in a DMD boy B) Normal curvature in MG aponeurosis of a control boy. C) Scan showing deformity in MG aponeurosis in DMD boy. D) MG aponeurosis in control subject.

Chapter 6: Discussion

This ultrasound study of gastrocnemius and soleus muscles in healthy children and children with DMD is the first of its kind to comprehensively quantify muscle architectural parameters for both groups. Earlier ultrasound studies of gastrocnemius and soleus architecture have focused primarily on healthy adults, while studies involving healthy children are scarce; four studies that included healthy children were found in the literature – Morse et al. (2008), Binzoni et al. (2001), Kearns et al. (2001), and Fischer et al. (1988). The first three are quantitative studies and the last is qualitative. It should be noted that Morse et al. (2008) is the only study to report quantitative FBL and PA data of LG for children. Kearns et al. (2001) reported data for healthy adolescents, but only included a single mean for MT of MG, and the data from Binzoni et al. (2001) was an amalgamation of measurements of MG from children and adults. An extensive literature search for studies of gastrocnemius and soleus architecture in children with DMD yielded no results.

6.1 Quantitative muscle architecture of control group

This thesis is the first to quantify FBL, PA, and MT in healthy boys aged 5-15 years for MG, LG, and PS in one study. The findings for LG from this study were similar to those reported by Morse et al. (2008); both results were within one standard deviation of each other. See Table 6.1 for a summary of data.

Binzoni et al. (2001) used scatterplots to summarize their numerical data (Post PA and MT for MG) by age. The data extracted from the scatterplots for subjects aged 5- 15 is presented in Table 6.1. The mean relaxed MT found in this study is similar to that

reported by Binzoni et al. (2001), but the mean relaxed posterior PA varies by 3 degrees, although this is still within one standard deviation of the current mean. Binzoni and colleagues observed that the relaxed posterior PA of MG tended to increase from newborn to adolescence, after which the pennation angle leveled off to reach a plateau. This general trend was not observed in the 5- 15 year old age group in the present study, but this may be due to the much younger age cut-off compared to Binzoni et al. (2001).

MG	Binzoni et al. (2001)	Current Study
Post PA		
Rel	13.9±3.0°	10.9±2.5°
Con	n/a	n/a
MT		
Rel	1.2±0.2cm	1.1±0.2cm
Con	n/a	n/a
MG	Kearns et al. (2001)	Current Study
MT		
Rel	2.05±0.24cm	1.1±0.2cm
Con	n/a	n/a
LG	Morse et al. (2008)	Current study
Ant PA		
Rel	10.8±2.5°	13.7±1.3°
Con	16.6±4.6°	20.2±4.3°
FBL		
Rel	7.0±0.8cm	6.4±0.8cm
Con	4.2±0.8cm	4.5±1.0cm

Table 6.1. Comparison of mean architectural parameters of MG and LG between studies. Previous studies by Binzoni et al. (2001), Kearns et al., (2001), Morse et al. (2008) are listed along with the current study.

For subjects aged 5 to 10 years, the mean relaxed posterior PA from Binzoni et al. (2001) was estimated to be 12.4±3.2°, which is within range of the mean from the current study (10.6±2.1°). On the other hand, the estimated mean for older subjects aged 11 to 15 years was 15.4±2.8° from Binzoni et al. (2001), and this is nearly two standard deviations greater than the 10.9±2.0 degrees reported in this study. As expected, muscle

thickness was found to increase in the older age group in both studies. Mean relaxed muscle thickness documented in this study for the subjects aged 5-10 years was 1.0 ± 0.1 cm, which increased slightly to 1.2 ± 0.2 cm for the older subjects aged 11-15 years. Binzoni et al. (2001) found the same trend in their relaxed mean MT; subjects aged 5-10 years had a mean MT of 1.1 ± 0.3 cm and subjects aged 11-15 years had a mean of 1.3 ± 0.2 cm.

The mean MT reported by Kearns et al. (2001) was nearly double the 1.1 cm found in the present study. This difference may be explained by the fact that the control subjects of Kearns et al.'s study (2001) were older than the subjects from in the current study (mean age of 18.3 ± 0.6 years compared to 10.1 ± 2.1 years), and the protocols for measuring MT were different. Kearns et al. (2001) imaged their subjects in a standing position, which may cause at least some degree of contraction in the MG and therefore influence the MT results.

6.2 Quantitative muscle architecture of DMD group

In this section, only the results from this study will be discussed, as there are no other studies to compare with.

The length of a muscle fiber influences the force and velocity of a muscle contraction; longer fibers have faster contraction speeds and broader peaks in their L-T curves (Narici, 1999). Although the relaxed FBL of DMD was not significantly different from that of controls, there was a trend towards shorter FBL in MG and LG of DMD subjects. The finding of shorter FBL with greater MT in DMD subjects is in contrast to Kearns et al. (2001), who reported a positive correlation between FBL and MT. However, the subjects in Kearns et al. (2001) were athletes (16.5 ± 0.5 years) so the comparison is not

entirely analogous. Even so, FBL of PS in the DMD group did tend to be longer than that of controls, so the positive FBL-MT correlation held true for PS (Table 5.7).

Despite the non-significant differences in FBL between DMD and controls, the difference in the amount of change (Table 5.9) in FBL on contraction between the two groups was statistically significant ($p < 0.05$) for LG (DMD < control) and PS (DMD > control). For MG of DMD, even though it was not significant, there was 21% less change on contraction in FBL than in controls. When relaxed FBL is altered, as in the DMD group, the muscle may become mechanically disadvantaged because the fibre bundles are moving at a weaker portion of the length-tension curve.

The larger resting PA and MT seen in DMD subjects may be a result of pseudohypertrophy of the calves due to fat and fibrous tissue infiltration. These increases are consistent with prior reports of changes to PA due to muscle hypertrophy (i.e., greater MT). Earlier studies have shown a high correlation between MT and PA following strength training in adults (Kawakami et al.; 1993, 1995) and in athletes (Ichinose et al., 1998; Ikegawa et al., 2008). Subjects with DMD from the current study also showed significant correlations between PA and MT (Table 5.7). However, since pseudohypertrophy of muscles is not accompanied by an increase in strength, the larger resting PA will further place the muscle at a mechanical disadvantage because the fibers are positioned at a greater angle to the axis of force (Lieber and Friden, 2000).

These differences in FBL and PA observed in dystrophic muscle illustrate the complex nature of muscle adaptations. Even for healthy adult muscle, previous studies documenting architectural changes as a result of training (Kawakami et al., 1995; Seynnes et al., 2007) or its opposite, deconditioning, can be contradictory (Kawakami,

Akima et al., 2001; de Boer et al., 2007). When muscle adaptation is further modified by a disease process with an unclear pathogenesis, the challenge to elucidate the changes is greatly multiplied.

One longstanding puzzle of the DMD disease process is that it does not affect all skeletal muscles uniformly. Generally, the function of the ankle plantar flexors tend to be preserved longer than the dorsiflexors, but individual changes within MG, LG, and PS are not known. The current study found that out of the three muscles, LG of DMD subjects differed the most from healthy muscle for anterior PA, posterior PA, and MT in the relaxed state followed by MG, while changes in PS for these parameters were less (Table 6.2). On the other hand, PS had the largest amount of change on contraction in FBL, anterior PA, and posterior PA (Table 6.3). These results appear to indicate that the architecture of the MG/LG, specifically its PA, is changing faster than that of the soleus in DMD subjects. The increased PA will weaken MG/LG due to the increased angle of pull for its fiber bundles, and may partially explain the decreased amount of contraction (i.e., amount of change in FBL) seen in MG/LG. Consequently, the large amount of change on contraction of PS architecture may be an adaptation, structurally or in terms of muscle recruitment, to compensate for decreased MG/LG activity.

	Relaxed state			
	FBL	Ant PA	Post PA	MT
DMD MG	2%↓	16%↑*	10%↑	27%↑*
DMD LG	13%↓	31%↑*	55%↑*	40%↑*
DMD PS	16%↑	5%↑	5%↑	18%↑*

Table 6.2. Percentage difference of architectural parameters between DMD and control subjects in the relaxed state. ↑ = more than control, ↓ = less than control, * = statistically significant (p<0.05).

Amount of change on contraction				
	FBL	Ant PA	Post PA	MT
DMD MG	21%↓	36%↑	44%↑*	100%↑
DMD LG	42%↓*	25%↑	28%↓	29%↓
DMD PS	240%↑*	72%↑*	63%↑*	n/d

Table 6.3. Percentage difference between DMD and control subjects in the amount of change in architectural parameters on contraction. ↑ = more than control, ↓ = less than control, n/d = no difference, * = statistically significant (p<0.05).

These potential adaptations, although speculative, are not without precedent. Studies involving atrophy models in adults (Riley et al., 1998; Widrick et al., 1999, 2001) and post-operative histological changes in children with DMD (Wang et al., 1999) have provided indirect insight for this process. Wang et al. (1999) investigated the morphometric alterations of muscle fiber type in children with DMD, and found a severe reduction in Type II fibers and concomitant increase in Type I fibers. Riley et al., (1998) and Widrick et al. (1999) showed that the speed of soleus Type I fibers can increase, without fiber type switching, to compensate for an atrophy in muscle subsequent to bed rest and space flight. Furthermore, Widrick (2001) hypothesized that there may be a shift in recruitment of plantar flexors during space flight, which increases activation of gastrocnemius and leaves soleus less active. Hypothetically, if this process were also to occur in DMD, the shift to the gastrocnemius will place earlier strain on it, thereby causing it to degenerate first. As the muscle weakens, the soleus will have to increase its activation and contraction to compensate. This could explain the findings in the present study of increased soleus contraction, decreased gastrocnemius contraction, and greater muscle thickness in MG/LG compared to PS. Further investigations will be required to fully explore the muscle recruitment patterns of the plantar flexors in children with DMD.

6.2.1 Quantitative results and Timed Function Tests

When comparing the young (≤ 10 years) and older (≥ 11 years) boys with DMD, the time to complete the stair climb and the walking timed function tests increased for the older group. Mean TFT times in the young group were 4.1secs (stairs) and 5.5secs (walk) compared to 7.9secs (stairs) and 10.7secs (walk) for the older group. The younger group of boys also had larger amounts of change in FBL and PA for all the muscles except posterior PA of LG (Table 6.4). The change in the FBL of the older group is very small – actually none for LG – and the FBL of PS even lengthened on contraction. Similarly, the PA of the older group changed little in comparison to the younger group, and both PAs of LG became smaller on contraction. The older group did, however, have greater muscle thickness for MG/LG, which may be an indication of increased fatty infiltration compared to the PS (Table 6.4).

There is a clear trend that emerges from the comparison of architectural data and TFT results as presented in Table 6.4. The older group of boys with DMD only managed small amounts of change in FBL, anterior PA, and posterior PA. In other words, the older muscles had less range in their contractions, which would translate directly to less locomotion overall. Accordingly, the TFT scores for the older group were significantly much worse than the scores of the younger group, who had greater change in their muscles on contraction.

Young (≤ 10 years)						
	FBL (cm)	Ant PA (degrees)	Post PA (degrees)	MT (cm)	TFT Stairs (secs)	TFT Walk (secs)
MG	-1.7	10.9	13.4	0.1	4.1	5.5
LG	-1.3	11.3	5.1	0.1		
PS	-2.4	12.4	11.3	0.2		
Old (≥ 10 years)						
	FBL (cm)	Ant PA (degrees)	Post PA (degrees)	MT (cm)	TFT Stairs (secs)	TFT Walk (secs)
MG	-0.5	4.2	4.9	0.3	7.9	10.7
LG	0	-3.6	-7.2	-0.2		
PS	0.5	4.4	3.3	0.1		

Table 6.4. Comparison of the amount of change on contraction of MG, LG, and PS architectural parameters to TFT scores in the young and old DMD groups. Negative signs denote change was smaller than the resting mean.

6.3 Qualitative rating of ultrasound

In the second portion of this study, the usefulness of the new subjective rating scale developed in this project for classifying DMD severity from US scans was investigated. This novel scale defines a more detailed set of criteria than previously described for staging DMD progression (Heckmatt et al., 1982). There is consensus that qualitative rating of images, from US or other imaging modalities, can be used to aid clinical decision making and is therefore a valuable part of the clinical setting (Mercuri et al., 2007). However, the radiation (CT) and costs (MRI) involved with using these other modalities as well as the degree of compliance required from young children preclude these technologies from daily use in the clinic.

Heckmatt et al. (1982) first formulated a subjective rating scale for US images of children with muscular dystrophy (Table 6.5). This simple grading system has been shown to positively correlate with the severity of changes in DMD muscle architecture seen on biopsy (Heckmatt et al., 1982). This scale has been referenced in journals as

recently as June 2008 (Pillen, Arts et al., 2008), but it has not been further developed since its inception. Other researchers have rated US images by classifying the quality of

Grade I	Normal
Grade II	Increased muscle echo, normal bone echo
Grade III	Increased muscle echo, reduced bone echo
Grade IV	Increased muscle echo, absent bone echo

Table 6.5. – Qualitative rating scale developed by Heckmatt et al. (1982) for US images of diseased muscle.

the echogenic appearance using “homogeneous” or “heterogeneous” as descriptors, and also noted the number of muscles involved by giving a rating of “focal” or “general”, depending on the number of muscle groups that were affected (Fischer, Carpenter et al., 1988). These researchers reported that the echogenicity in dystrophic muscle was typically “homogenous” with a “granular” appearance, and there was a general loss of normal architecture on the scans.

An increase in US echointensity indicates the presence of fat and/or connective tissue infiltration in the dystrophic muscle (Reimers et al., 1996). Cros et al. (1989) reported 18-38% of fat and fibrous tissue from biopsies of the gastrocnemius from DMD boys compared to healthy muscle; the control samples never exhibited more than 8% fat. Some earlier studies have quantified this brightness by using computerized gray-scale analysis of the US images (Pillen, Scholten et al., 2003). However, gray-scale analysis requires additional time and processing, which may not be practical for frequent use in clinic (Pillen, Keimpema et al., 2006).

The current scale, presented again in Table 6.6, removes computer analysis from the process and relies again on the human eye, which can detect far more than 256 shades of gray on a typical gray-scale analysis. This rating scale expands on Heckmatt's criteria of echogenicity (i.e., the brightness of the image) to include the appearance of muscle architecture (i.e., fiber bundle pattern) and the presence or absence of structural abnormalities (e.g., excessive curvature of aponeurosis). These new criteria add more detail to the subjective rating and allow for a quicker evaluation of the US images without any additional calculations.

Rating	Characteristics
0 = Normal	<ul style="list-style-type: none"> • "Random" fiber pattern • Echogenicity balanced with areas of darkness • No abnormalities of tendons or fiber bundles
1 = Mild	<ul style="list-style-type: none"> • Fiber pattern near normal • Slightly increased echogenicity • No abnormalities of tendons or fiber bundles
2 = Moderate	<ul style="list-style-type: none"> • ↑ visibility of fiber pattern • ↑ brightness • May contain abnormalities (e.g., excessive curvature of fiber bundles, disruption of aponeurosis)
3 = Severe	<ul style="list-style-type: none"> • Fiber pattern present but nearly infiltrated • Mostly echogenic tissue, but some dark areas remain • Abnormalities very apparent
4 = Obliterated	<ul style="list-style-type: none"> • No fiber pattern discernible • Entire image is echogenic • Gross abnormalities
OP = Out of plane	<ul style="list-style-type: none"> • Fibers not in plane of image

Table 6.6. New qualitative rating scale of US images for children with DMD.

The rating scale in this study is also the first to take into account structural abnormalities seen in some DMD subjects (i.e., interrupted aponeurosis, excessive fiber curvature). Narici, Binzoni et al. (1996) points out that the amount of fiber shortening during isometric MVC reported in his study, 35%, and by Griffiths (1991) on the cat MG, 28%, support the idea that the gastrocnemius tendon and aponeurosis have considerable slack at rest (i.e., increased compliance), and therefore may function as shock absorbers during high-intensity contractions. This may help to explain the interrupted aponeurosis seen in DMD muscle. As the DMD muscle becomes less able to contribute to buffering mechanical forces, the aponeuroses will likely take on additional stress and eventually show signs of strain. The increased slack at rest of the gastrocnemius musculotendinous unit proposed by Narici, Binzoni et al. (1996) may also explain the fiber curvature seen in the DMD scans.

Although not quantitatively measured in this study, the fiber curvature noted in the DMD subjects is clearly greater than in the case of healthy controls. Maganaris and Baltzopoulos (1998) concluded that if fiber curvature is present, calculations of FBL that assume the fiber is a straight line may underestimate its true length. If this is the case, curved DMD fibers will be longer than reported, and be operating in a disadvantaged portion of the L-T and F-V curves.

The present rating scale yielded a specificity of 92% and a sensitivity of 100% for subjects with DMD. Compared to previous studies using Heckmatt's criteria, Zuberi et al. (1999) achieved a specificity of 91% and a sensitivity of 78%, and Pillen, Keimpema et al. (2006) reported a specificity of 92% and a sensitivity of 71%. Both of these studies

rated US images of subjects with mixed neuromuscular diseases, which may have lowered their sensitivities.

6.3.1 Qualitative rating scores and Timed Function Tests

Timed Function Tests are currently one of the standards used in clinic to determine the extent of disease progression. A small reduction in muscle force can be translated into a large reduction in functional ability, so muscle force assessment alone will not give a complete picture of a patient's abilities (Beenakker et al., 2005).

In an earlier study, Kamala et al. (1985) reported a correlation (not given) between grade of US image, using Heckmatt's criteria, and the severity of pathologic changes on biopsy in children with progressive muscular dystrophy (type not specified). However, they did not find a correlation between the US scans and functional disability, as measured by manual muscle testing. The present study was able to show a significant correlation between TFT results and the qualitative rating scores determined by the new rating scale (walk, $r = 0.705$, $p < 0.05$; stairs, $r = 0.797$). Moreover, the rating levels of the new scale also significantly correlated with age ($r = 0.607$, $p < 0.05$). Improvements in US equipment as well as the more detailed rating scale could account for the discrepancy between Kamala et al. (1985) and the current study.

The qualitative results reported in this study are encouraging since it reintroduces the idea of using US imaging as an indicator of function, given an appropriate method of interpretation. There is an obvious need for better detection of even small changes to the DMD disease process as well as monitoring the effects of treatment and training programmes. As ultrasound imaging technology continues to improve, this modality has an excellent potential to provide the solution for this need.

Chapter 7: Conclusions

The conclusions are divided into two sections. The first section of conclusions are drawn from the quantitative portion of this study and the second section from the qualitative analysis of ultrasound images.

Conclusions related to quantitative muscle architecture:

1. This study is the most detailed documentation of MG, LG, and PS muscle architecture in children with DMD and in healthy children age 5 – 15 years to date.
2. The muscle architecture of the gastrocnemius and soleus in children with DMD differs from that of healthy controls.

Architectural differences:

- For FBL, subjects with DMD tended to have shorter lengths than controls for MG and LG, and longer lengths for PS.
 - For anterior PA, MG, LG, and PS of the DMD group have larger angles than controls, but only MG and LG were significantly different ($p < 0.05$).
 - For posterior PA, the DMD group had larger angles for all three muscles but only LG was significantly different ($p < 0.05$).
 - The DMD group had significantly thicker muscles than the control group ($p < 0.05$).
3. The differences in architecture may have negative functional consequences for the children with DMD.

Conclusions related to qualitative rating of US scans:

1. A new rating scale with expanded criteria for visual assessment of US images of dystrophic muscle was developed.
2. Scores from visual grading of US images correlate well with results from timed function tests used in clinic to monitor changes in function of children with DMD.
3. Qualitative rating of US images may be used as a viable method to monitor the progression of DMD.

Chapter 8: Future directions

- Continue documentation of DMD muscle architecture for other dystrophic muscles (e.g., gracilis, sartorius, tibialis anterior).
- Develop a method of measuring fiber bundle length that takes into account fiber curvature
- Additional studies to further validate the new qualitative rating scale.
- Implement new qualitative rating scale for other neuromuscular diseases (e.g., Spinal Muscular Atrophy).
- Implement a longitudinal study of DMD, both quantitative and qualitative, to provide a clearer picture of the progression of the disease with age.

References

- Agur, A. (2001). Architecture of the Human Soleus Muscle: Three-Dimensional Computer Modelling of Cadaveric Muscle and Ultrasonographic Documentation *In Vivo*. Institute of Medical Science. Toronto, University of Toronto. Doctor of Philosophy.
- Agur, A. and A. Dalley. (2009). Grant's Atlas of Anatomy. 12th ed. Philadelphia, Lippincott Williams & Wilkins.
- Alman, B. A., S. N. Raza, et al. (2004). "Steroid treatment and the development of scoliosis in males with duchenne muscular dystrophy." J Bone Joint Surg Am **86-A**(3): 519-24.
- Beaton, L. J., D. A. Allan, et al. (2002). "Contraction-induced muscle damage is unaffected by vitamin E supplementation." Med Sci Sports Exerc **34**(5): 798-805.
- Beenakker, E. N. M. Maurits, et al. (2005). "Functional ability and muscle force in healthy children and ambulant Duchenne muscular dystrophy patients." Eur J Paediatr Neurol **9**(6): 387-93.
- Belcastro, A. N., L. D. Shewchuk, et al. (1998). "Exercise-induced muscle injury: a calpain hypothesis." Mol Cell Biochem **179**(1-2): 135-45. 2: Belcastro AN et al. Role of calcium-activated neu...[PMID: 8905185]Related Articles, Links.
- Binzoni, T., S. Bianchi, et al. (2001). "Human gastrocnemius medialis pennation angle as a function of age: from newborn to the elderly." J Physiol Anthropol Appl Human Sci **20**(5): 293-8.
- Blake, D. J., A. Weir, et al. (2002). "Function and genetics of dystrophin and dystrophin-related proteins in muscle." Physiol Rev **82**(2): 291-329.
- Bogdanovich, S., K. J. Perkins, et al. (2004). "Therapeutics for Duchenne muscular dystrophy: current approaches and future directions." J Mol Med **82**(2): 102-15.
- Brenman, J. E., D. S. Chao, et al. (1995). "Nitric oxide synthase complexed with dystrophin and absent from skeletal muscle sarcolemma in Duchenne muscular dystrophy." Cell **82**(5): 743-52.
- Brussee, V., F. Tardif, et al. (1997). "Muscle fibers of mdx mice are more vulnerable to exercise than those of normal mice." Neuromuscul Disord **7**(8): 487-92.
- Brussock, C. M., S. M. Haley, et al. (1992). "Measurement of isometric force in children with and without Duchenne's muscular dystrophy." Phys Ther **72**(2): 105-14.
- Buetler, T. M., M. Renard, et al. (2002). "Green tea extract decreases muscle necrosis in mdx mice and protects against reactive oxygen species." Am J Clin Nutr **75**(4): 749-53.
- Buller, A. J. (1978). The contractile behaviour of mammalian skeletal muscle. Burlington, N.C., Scientific Publications Division, Carolina Biological Supply Co., 1978.
- Campbell, C. G. and P. Jacob (2003). "Deflazacort for the treatment of Duchenne Dystrophy: A systematic review." BMC Neurol **3**(1): 7.
- Carafoli, E. and M. Molinari (1998). "Calpain: a protease in search of a function?" Biochem Biophys Res Commun **247**(2): 193-203.
- Chang, W. J., S. T. Iannaccone, et al. (1996). "Neuronal nitric oxide synthase and dystrophin-deficient muscular dystrophy." Proc Natl Acad Sci U S A **93**(17): 9142-7.

- Chow, R. S., M. K. Medri, et al. (2000). "Sonographic studies of human soleus and gastrocnemius muscle architecture: gender variability." Eur J Appl Physiol **82**(3): 236-44.
- Cormack, D.H. (1984). Introduction to Histology. Philadelphia, J.B. Lippincott Company.
- Cormack, D.H. (1987). Ham's Histology. 9th ed. Philadelphia, J.B. Lippincott Company.
- Cros, D., P. Harnden, et al. (1989). "Muscle hypertrophy in Duchenne muscular dystrophy." J Neurol **236**(1): 43-47.
- Crosbie, R. H. (2001). "NO vascular control in Duchenne muscular dystrophy." Nat Med **7**(1): 27-9.
- Culligan, K. G., A. J. Mackey, et al. (1998). "Role of dystrophin isoforms and associated proteins in muscular dystrophy (review)." Int J Mol Med **2**(6): 639-48.
- de Boer, M., C. Maganaris, et al. (2007). "Time course of muscular, neural and tendinous adaptations to 23 day unilateral lower-limb suspension in young men." J Physiol **583**(Pt3): 1079-1091.
- Deval, E., D. Levitsky, et al. (2002). "Na(+)/Ca(2+) exchange in human myotubes: intracellular calcium rises in response to external sodium depletion are enhanced in DMD." Neuromuscul Disord **12**(7-8): 665.
- Disatnik, M. H., J. S. Chamberlain, et al. (2000). "Dystrophin mutations predict cellular susceptibility to oxidative stress." Muscle Nerve **23**(5): 784-92.
- Disatnik, M. H., J. Dhawan, et al. (1998). "Evidence of oxidative stress in mdx mouse muscle: studies of the pre-necrotic state." J Neurol Sci **161**(1): 77-84.
- Dorchies, O. M., S. Wagner, et al. (2006). "Green tea extract and its major polyphenol (-)-epigallocatechin gallate improve muscle function in a mouse model for Duchenne muscular dystrophy." Am J Physiol Cell Physiol **290**(2): C616-25.
- Dorland, W. A. N. (2003). Dorland's illustrated medical dictionary. Philadelphia, Saunders.
- Dubowitz, V. (1995). Muscle disorders in childhood. Philadelphia, Saunders.
- Duchenne, G.B.A. (1868). "Recherches sur la paralysie musculaire pseudohypertrophique ou paralysie myo-sclerosique." Arch Med Gen Trop **11**: 5-25.
- Enoka, R. M. (1988). "Muscle strength and its development. New perspectives." Sports Med **6**(3): 146-68.
- Fischer, A. Q., D. W. Carpenter, et al. (1988). "Muscle imaging in neuromuscular disease using computerized real-time sonography." Muscle Nerve **11**(3): 270-5.
- Fischer, A. Q. and S. Stephens (1988). "Computerized real-time neuromuscular sonography: a new application, techniques and methods." J Child Neurol **3**(1): 69-74.
- Fong, P. Y., P. R. Turner, et al. (1990). "Increased activity of calcium leak channels in myotubes of Duchenne human and mdx mouse origin." Science **250**(4981): 673-6.
- Franco, A., Jr. and J. B. Lansman (1990). "Calcium entry through stretch-inactivated ion channels in mdx myotubes." Nature **344**(6267): 670-3.
- Friederich, J. A. and R. A. Brand (1990). "Muscle fiber architecture in the human lower limb." J Biomech **23**(1): 91-5.
- Froehner, S. C. (2002). "Just say NO to muscle degeneration?" Trends Mol Med **8**(2): 51-3.

- Fukunaga, T., Y. Ichinose, et al. (1997). "Determination of fascicle length and pennation in a contracting human muscle in vivo." J Appl Physiol **82**(1): 354-8.
- Fukunaga, T., Y. Kawakami, et al. (1997). "Muscle architecture and function in humans." J Biomech **30**(5): 457-63.
- Griffiths, R. I. (1991). "Shortening of muscle fibres during stretch of the active cat medial gastrocnemius muscle: the role of tendon compliance." J Physiol **436**: 219-36.
- Grozdanic, Z. (2001). "NO message from muscle." Microsc Res Tech **55**(3): 148-53.
- Heckmatt, J., E. Rodillo, et al. (1989). "Quantitative sonography of muscle." J Child Neurol **4** **Suppl**: S101-6.
- Heckmatt, J. Z., V. Dubowitz, et al. (1980). "Detection of pathological change in dystrophic muscle with B-scan ultrasound imaging." Lancet **1**(8183): 1389-90.
- Heckmatt, J. Z., S. Leeman, et al. (1982). "Ultrasound imaging in the diagnosis of muscle disease." J Pediatr **101**(5): 656-60.
- Heckmatt, J. Z., N. Pier, et al. (1988). "Assessment of quadriceps femoris muscle atrophy and hypertrophy in neuromuscular disease in children." J Clin Ultrasound **16**(3): 177-81.
- Henry, M. D. and K. P. Campbell (1999). "Dystroglycan inside and out." Curr Opin Cell Biol **11**(5): 602-7.
- Hoffman, E. P., R. H. Brown, Jr., et al. (1987). "Dystrophin: the protein product of the Duchenne muscular dystrophy locus." Cell **51**(6): 919-28.
- Ichinose, Y., H. Kanehisa, et al. (1998). "Relationship between muscle fiber pennation and force generation capability in Olympic athletes." Int J Sports Med **19**(8): 541-6.
- Ikegawa S., K. Funato, et al. (2008). "Muscle force per cross-sectional area is inversely related with pennation angle in strength trained athletes." J Strength Cond Res **22**(1): 128-31.
- Kamala, D., S. Suresh, et al. (1985). "Real-Time Ultrasonography in Neuromuscular Problems of Children." J Clin Ultrasound **13**(7): 465-8.
- Kawakami, Y., T. Abe, et al. (1993). "Muscle-fiber pennation angles are greater in hypertrophied than in normal muscles." J Appl Physiol **74**(6): 2740-2744.
- Kawakami, Y., T. Abe, et al. (1995). "Training-induced changes in muscle architecture and specific tension." Eur J Appl Physiol Occup Physiol **72**(1-2): 37-43.
- Kawakami, Y., H. Akima, et al. (2001). "Changes in muscle size, architecture, and neural activation after 20 days of bed rest with and without resistance exercise." Eur J Appl Physiol **84**(1-2): 7-12.
- Kawakami, Y., Y. Ichinose, et al. (1998). "Architectural and functional features of human triceps surae muscles during contraction." J Appl Physiol **85**(2): 398-404.
- Kearns, C. F., M. Isokawa, et al. (2001). "Architectural characteristics of dominant leg muscles in junior soccer players." Eur J Appl Physiol **85**(3-4): 240-3.
- Kirkham, P. and I. Rahman (2006). "Oxidative stress in asthma and COPD: Antioxidants as a therapeutic strategy." Pharmacol Ther.
- Koenig, M., E. P. Hoffman, et al. (1987). "Complete cloning of the Duchenne muscular dystrophy (DMD) cDNA and preliminary genomic organization of the DMD gene in normal and affected individuals." Cell **50**(3): 509-17.

- Krag, T. O., M. Gyrd-Hansen, et al. (2001). "Harnessing the potential of dystrophin-related proteins for ameliorating Duchenne's muscular dystrophy." Acta Physiol Scand **171**(3): 349-58.
- Krotkiewski, M. and Z. Brzezinska (1996). "Lipid peroxides production after strenuous exercise and in relation to muscle morphology and capillarization." Muscle Nerve **19**(12): 1530-7.
- Kumar, A. and A. M. Boriek (2003). "Mechanical stress activates the nuclear factor-kappaB pathway in skeletal muscle fibers: a possible role in Duchenne muscular dystrophy." Faseb J **17**(3): 386-96.
- Kunkel, L. M., A. P. Monaco, et al. (1986). "Molecular genetics of Duchenne muscular dystrophy." Cold Spring Harb Symp Quant Biol **51 Pt 1**: 349-51.
- Lamminen, A., J. Jaaskelainen, et al. (1988). "High-frequency ultrasonography of skeletal muscle in children with neuromuscular disease." J Ultrasound Med **7**(9): 505-9.
- Laplace, C., O. Huet, et al. (2005). "Endothelial oxidative stress induced by serum from patients with severe trauma hemorrhage." Intensive Care Med **31**(9): 1174-80.
- Lau, K. S., R. W. Grange, et al. (1998). "Skeletal muscle contractions stimulate cGMP formation and attenuate vascular smooth muscle myosin phosphorylation via nitric oxide." FEBS Lett **431**(1): 71-4.
- Lieber, R. L. (1999). "Skeletal Muscle is a Biological Example of a Linear Electro-Active Actuator." Proceedings of SPIE's 6th Annual International Symposium on Smart Structures and Materials **3669**(03).
- Lieber, R. L. (2002). Skeletal muscle structure, function, and plasticity: the physiological basis of rehabilitation. Philadelphia, Lippincott Williams & Wilkins.
- Lieber, R. L. and C. C. Brown (1992). "Quantitative method for comparison of skeletal muscle architectural properties." J Biomech **25**(5): 557-60.
- Lieber, R. L. and J. Friden (2000). "Functional and clinical significance of skeletal muscle architecture." Muscle Nerve **23**(11): 1647-66.
- Liu, G. C., Y. J. Jong, et al. (1993). "Duchenne muscular dystrophy: MR grading system with functional correlation." Radiology **186**(2): 475-80.
- Low, J. L. and A. Reed (1996). Basic biomechanics explained. Oxford; Boston, Butterworth-Heinemann.
- Maganaris, C. N., V. Baltzopoulos, et al. (1998). "In vivo measurements of the triceps surae complex architecture in man: implications for muscle function." J Physiol **512 (Pt 2)**: 603-14.
- Maganaris, C. N. (2001). "Force-length characteristics of in vivo human skeletal muscle." Act Physiol Scand **172**(4): 279-85.
- Mallouk, N. and B. Allard (2002). "Ca(2+) influx and opening of Ca(2+)-activated K(+) channels in muscle fibers from control and mdx mice." Biophys J **82**(6): 3012-21.
- Manzur, A. Y., T. Kuntzer, et al. (2004). "Glucocorticoid corticosteroids for Duchenne muscular dystrophy." Cochrane Database Syst Rev(2): CD003725.
- Martin, D. C., M. K. Medri, et al. (2001). "Comparing human skeletal muscle architectural parameters of cadavers with in vivo ultrasonographic measurements." J Anat **199**(Pt 4): 429-34.
- Maurits, N. M., E. A. Beenakker, et al. (2004). "Muscle ultrasound in children: normal values and application to neuromuscular disorders." Ultrasound Med Biol **30**(8): 1017-27.

- McMahon, T.A. (1984). Muscles, reflexes, and locomotion. Princeton, N.J., Princeton University Press.
- Mendez, J. and A. Keys (1960). "Density and composition of mammalian muscle." Metabolism Clinical and Experimental 9: 184-188.
- Mercuri, E., A. Pichiecchio, et al. (2007). "Muscle MRI in Inherited Neuromuscular Disorders: Past, Present, and Future." J Magn Reson Imaging 25(2): 433-40.
- Moens, P., P. H. Baatsen, et al. (1993). "Increased susceptibility of EDL muscles from mdx mice to damage induced by contractions with stretch." J Muscle Res Cell Motil 14(4): 446-51.
- Moore, K. and A. Agur (2007). Essential Clinical Anatomy 3rd ed. Philadelphia, Lippincott Williams & Wilkins.
- Moore, K. and A. Dalley (1999). Clinically oriented anatomy. Philadelphia, Lippincott Williams & Wilkins.
- Morse, CI, K Tolfrey, et al. (2008) "Gastrocnemius Muscle specific force in boys and men." J Appl Physiol 104: 469-474.
- Narici, M. (1999). "Human skeletal muscle architecture studied in vivo by non-invasive imaging techniques: functional significance and applications." J Electromyogr Kinesiol 9(2): 97-103.
- Narici, M. V., T. Binzoni, et al. (1996). "In vivo human gastrocnemius architecture with changing joint angle at rest and during graded isometric contraction." J Physiol 496 (Pt 1): 287-97.
- Nicolas-Metral, V., E. Raddatz, et al. (2001). "Mdx myotubes have normal excitability but show reduced contraction-relaxation dynamics." J Muscle Res Cell Motil 22(1): 69-75.
- Pasternak, C., S. Wong, et al. (1995). "Mechanical function of dystrophin in muscle cells." J Cell Biol 128(3): 355-61.
- Petrof, B. J. (1998). "The molecular basis of activity-induced muscle injury in Duchenne muscular dystrophy." Mol Cell Biochem 179(1-2): 111-23. 3: Petrof BJ et al. Dystrophin protects the sarco...[PMID: 8475120]Related Articles, Links.
- Petrof, B. J. (2002). "Molecular pathophysiology of myofiber injury in deficiencies of the dystrophin-glycoprotein complex." Am J Phys Med Rehabil 81(11 Suppl): S162-74. 2: Petrof BJ. The molecular basis of activi...[PMID: 9543354]Related Articles, Links.
- Petrof, B. J., J. B. Shrager, et al. (1993). "Dystrophin protects the sarcolemma from stresses developed during muscle contraction." Proc Natl Acad Sci U S A 90(8): 3710-4.
- Pillen, S., I. Arts, et al. (2008). "Muscle ultrasound in neuromuscular disorders." Muscle Nerve 37(6): 679-93.
- Pillen, S., R. Scholten., et al. (2003). "Quantitative skeletal muscle ultrasonography in children with suspected neuromuscular disease." Muscle Nerve 27(6): 699-705.
- Pillen, S., M. van Keimpema, et al. (2006). "Skeletal muscle ultrasonography: visual versus quantitative evaluation." Ultrasound in Med & Biol 32(9): 1315-1321.
- Porter, G. A., G. M. Dmytrenko, et al. (1992). "Dystrophin colocalizes with beta-spectrin in distinct subsarcolemmal domains in mammalian skeletal muscle." J Cell Biol 117(5): 997-1005.

- Porter, J. D., S. Khanna, et al. (2002). "A chronic inflammatory response dominates the skeletal muscle molecular signature in dystrophin-deficient mdx mice." Hum Mol Genet **11**(3): 263-72.
- Rando, T. A. (2001). "The dystrophin-glycoprotein complex, cellular signaling, and the regulation of cell survival in the muscular dystrophies." Muscle Nerve **24**(12): 1575-94.
- Reimers, C., B. Schlotter, et al. (1996). "Calf enlargement in neuromuscular diseases: a quantitative ultrasound study in 350 patients and review of the literature." J Neurol Sci **143**(1-2): 46-56.
- Riley, D., J. Bain, et al. (1998). "Disproportionate loss of thin filaments in human soleus muscle after 17-day bed rest." Muscle Nerve **21**(10): 1280-9.
- Rodriguez, M. C. and M. A. Tarnopolsky (2003). "Patients with dystrophinopathy show evidence of increased oxidative stress." Free Radic Biol Med **34**(9): 1217-20.
- Roy, R. R. and A. Ishihara (1997). "Overview: functional implications of the design of skeletal muscles." Acta Anat (Basel) **159**(2-3): 75-7.
- Rybakova, I. N., J. R. Patel, et al. (2000). "The dystrophin complex forms a mechanically strong link between the sarcolemma and costameric actin." J Cell Biol **150**(5): 1209-14.
- Samitt, C. E. and E. Bonilla (1990). "Immunocytochemical study of dystrophin at the myotendinous junction." Muscle Nerve **13**(6): 493-500.
- Sander, M., B. Chavoshan, et al. (2000). "Functional muscle ischemia in neuronal nitric oxide synthase-deficient skeletal muscle of children with Duchenne muscular dystrophy." Proc Natl Acad Sci U S A **97**(25): 13818-23.
- Seynnes, O., M. de Boer, et al. (2007). "Early skeletal muscle hypertrophy and architectural changes in response to high-intensity resistance training." J Appl Physiol **102**(1): 368-73.
- Schedel, H., C. D. Reimers, et al. (1992). "Imaging techniques in myotonic dystrophy. A comparative study of ultrasound, computed tomography and magnetic resonance imaging of skeletal muscles." Eur J Radiol **15**(3): 230-8.
- Schottelndreier, H., B. V. Potter, et al. (2001). "Mechanisms involved in alpha6beta1-integrin-mediated Ca(2+) signalling." Cell Signal **13**(12): 895-9.
- Sherwood, L. (2001). Human physiology: from cells to systems. Pacific Grove, CA, Brooks/Cole/Thomson Learning.
- Sotgia, F., J. K. Lee, et al. (2000). "Caveolin-3 directly interacts with the C-terminal tail of beta -dystroglycan. Identification of a central WW-like domain within caveolin family members." J Biol Chem **275**(48): 38048-58.
- Spiegler, A. W., S. Schindler, et al. (1985). "Becker muscular dystrophy: carrier detection by real-time ultrasound." J Neurol **232**(5): 307-9.
- Spoor, C.W., J.L. van Leeuwen, et al. (1991). "Active force-length relationship of human lower-leg muscles estimated from morphological data: a comparison of geometric muscle models." Eur J Morphol **29**(3): 137-60.
- Thomas, G. D., M. Sander, et al. (1998). "Impaired metabolic modulation of alpha-adrenergic vasoconstriction in dystrophin-deficient skeletal muscle." Proc Natl Acad Sci U S A **95**(25): 15090-5.

- Tidball, J. G., E. Lavergne, et al. (1998). "Mechanical loading regulates NOS expression and activity in developing and adult skeletal muscle." Am J Physiol **275**(1 Pt 1): C260-6.
- Tidball, J. G. and M. J. Spencer (2000). "Calpains and muscular dystrophies." Int J Biochem Cell Biol **32**(1): 1-5.
- Turner, P. R., T. Westwood, et al. (1988). "Increased protein degradation results from elevated free calcium levels found in muscle from mdx mice." Nature **335**(6192): 735-8.
- Tyler, K. L. (2003). "Origins and early descriptions of "Duchenne muscular dystrophy"." Muscle Nerve **28**(4): 402-22.
- van Donkelaar, C. C., P. J. Willems, et al. (1999). "Skeletal muscle transverse strain during isometric contraction at different lengths." J Biomech **32**(8): 755-62.
- Vilquin, J. T., V. Brussee, et al. (1998). "Evidence of mdx mouse skeletal muscle fragility in vivo by eccentric running exercise." Muscle Nerve **21**(5): 567-76.
- Wang, J., J. Forst, et al. (1999). "Correlation of muscle fiber type measurements with clinical and molecular genetic data in Duchenne Muscular Dystrophy." Neuromuscular Disorders **9**(3): 150-8.
- Ward, S. R. and R. L. Lieber (2005). "Density and hydration of fresh and fixed human skeletal muscle." J Biomech **38**(11): 2317-20.
- Wickiewicz, T. L., R. R. Roy, et al. (1983). "Muscle architecture of the human lower limb." Clin Orthop Relat Res (179): 275-83.
- Widrick, J., S. Knuth, et al. (1999). "Effect of a 17 day spaceflight on contractile properties of human soleus muscle fibres." J Physiol **516**(3): 915-30.
- Widrick, J., J. Romatowski, et al. (2001). "Functional properties of slow and fast gastrocnemius muscle fibers after a 17-day spaceflight." J Appl Physiol **90**(6):2203-11.
- Yoshida, T., Y. Pan, et al. (1998). "Bidirectional signaling between sarcoglycans and the integrin adhesion system in cultured L6 myocytes." J Biol Chem **273**(3): 1583-90.
- Zuberi, S. M., N. Matta, et al. (1999). "Muscle ultrasound in the assessment of suspected neuromuscular disease in childhood." Neuromuscul Disord **9**(4): 203-7.

Appendix A: Sample size of DMD subjects by age

Age	N for FBL	N for Ant PA	N for Post PA	N for MT
5	1	1	1	2
6	2	2	2	2
7	4	4	4	4
8	0	0	0	2
9	4	4	4	8
10	0	0	0	0
11	2	2	2	3
12	0	0	0	0
13	1	1	1	5
14	0	0	0	0
15	2	2	2	2

Table A.1. Number of legs (MG) quantified for each architectural parameter categorized by age for DMD subjects.

Age	N for FBL	N for Ant PA	N for Post PA	N for MT
5	1	1	1	2
6	2	2	2	2
7	3	3	3	4
8	0	0	0	1
9	2	2	2	8
10	0	0	0	1
11	1	1	1	3
12	0	0	0	0
13	1	1	1	5
14	0	0	0	0
15	0	0	0	2

Table A.2. Number of legs (LG) quantified for each architectural parameter categorized by age for DMD subjects.

Age	N for FBL	N for Ant PA	N for Post PA	N for MT
5	2	2	2	2
6	1	1	1	2
7	3	3	3	3
8	1	1	1	2
9	3	3	3	7
10	0	0	0	0
11	1	1	1	2
12	0	0	0	0
13	0	0	0	1
14	0	0	0	0
15	0	0	0	0

Table A.3. Number of legs (PS) quantified for each architectural parameter categorized by age for DMD subjects.

Appendix B: Sample size of control subjects by age

Age	N for FBL	N for Ant PA	N for Post PA	N for MT
5	0	0	0	0
6	2	2	2	2
7	2	2	2	2
8	6	6	6	6
9	1	1	1	2
10	9	9	9	10
11	6	6	6	6
12	4	4	4	4
13	0	0	0	0
14	2	2	2	2
15	2	2	2	2

Table B.1. Number of legs (MG) quantified for each architectural parameter categorized by age for control subjects.

Age	N for FBL	N for Ant PA	N for Post PA	N for MT
5	0	0	0	0
6	2	2	2	2
7	2	2	2	2
8	4	4	4	6
9	0	0	0	2
10	5	5	5	10
11	6	6	6	6
12	2	2	2	4
13	0	0	0	0
14	1	1	1	2
15	2	2	2	2

Table B.2. Number of legs (LG) quantified for each architectural parameter categorized by age for control subjects.

Age	N for FBL	N for Ant PA	N for Post PA	N for MT
5	0	0	0	0
6	2	2	2	2
7	2	2	2	2
8	6	6	6	6
9	2	2	2	2
10	6	6	6	10
11	4	4	4	6
12	2	2	2	3
13	0	0	0	0
14	2	2	2	2
15	2	2	2	2

Table B.3. Number of legs (PS) quantified for each architectural parameter categorized by age for control subjects.

Appendix C: Architectural parameters by age

Control subjects

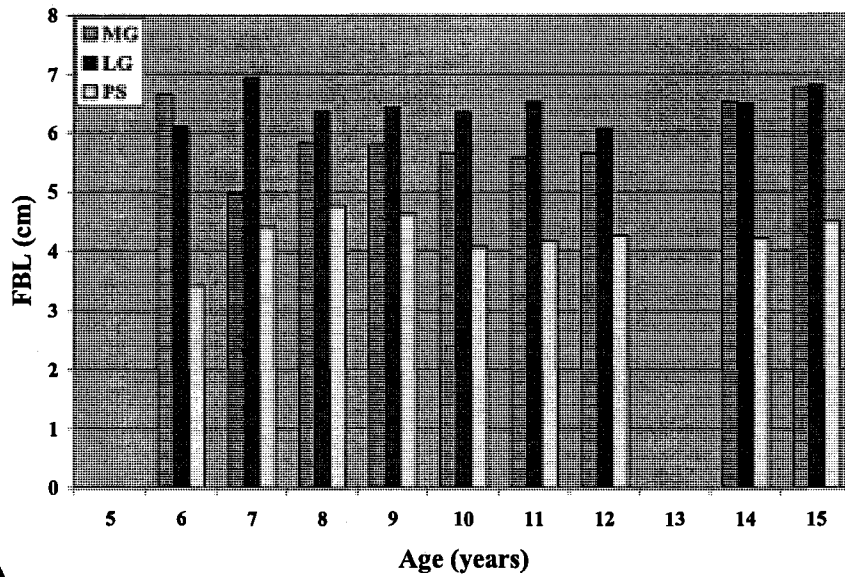
FBL by age

Mean FBL of subjects by age are summarized in Figure C.1A for the relaxed condition and Figure C.1B for the contracted condition. Mean relaxed FBL of PS was shorter than that of MG and LG in all age groups. LG had the longest mean relaxed FBL for a majority of ages. In the contracted condition, PS had the shortest FBL at most ages while LG had the longest in a majority of subjects.

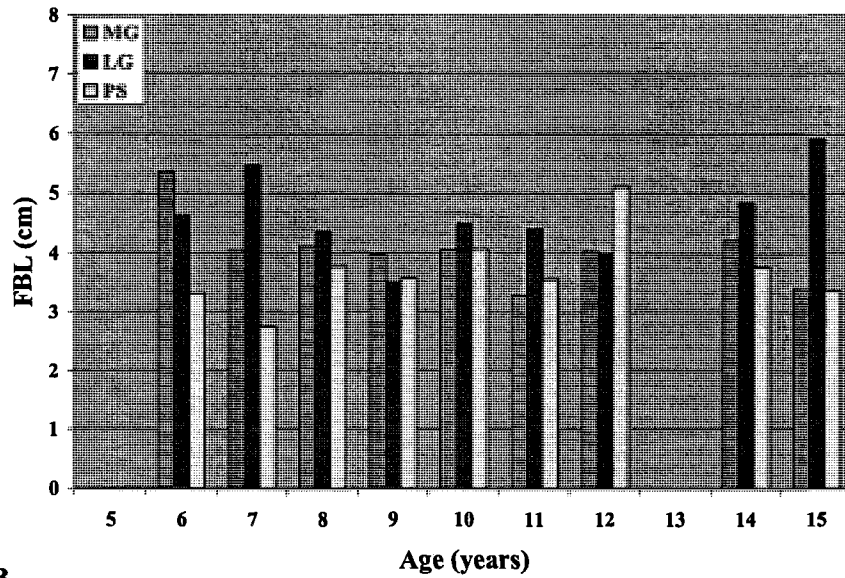
PA by age

Mean anterior PA of subjects are summarized by age in Figure C.2A for the relaxed condition and in Figure C.2B for the contracted condition. MG had the largest mean relaxed anterior PA between the ages of 8 – 11, and the smallest relaxed anterior PA at ages 6, 12, and 15. PS had the largest anterior PA in the youngest and oldest subjects at ages 6, 12, 14, and 15. In the contracted condition, the MG has the largest anterior PA between the ages of 8 – 11, and PS has the largest mean at ages 6 and 15. For relaxed and contracted conditions, the anterior PA of MG, LG, and PS were within 7° of each other in a majority of age groups.

Mean posterior PA of subjects by age are summarized in Figure C.3A for the relaxed condition and in Figure C.3B for the contracted condition. Of the three muscles, PS had the largest mean relaxed posterior PA in all but one age group (age 9), and LG had the smallest relaxed mean posterior PA at all ages. The mean contracted posterior

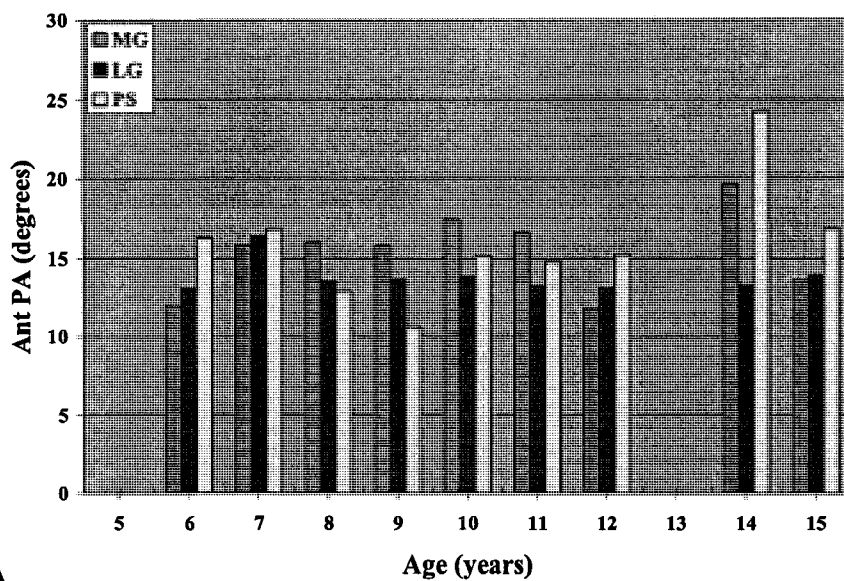


A.

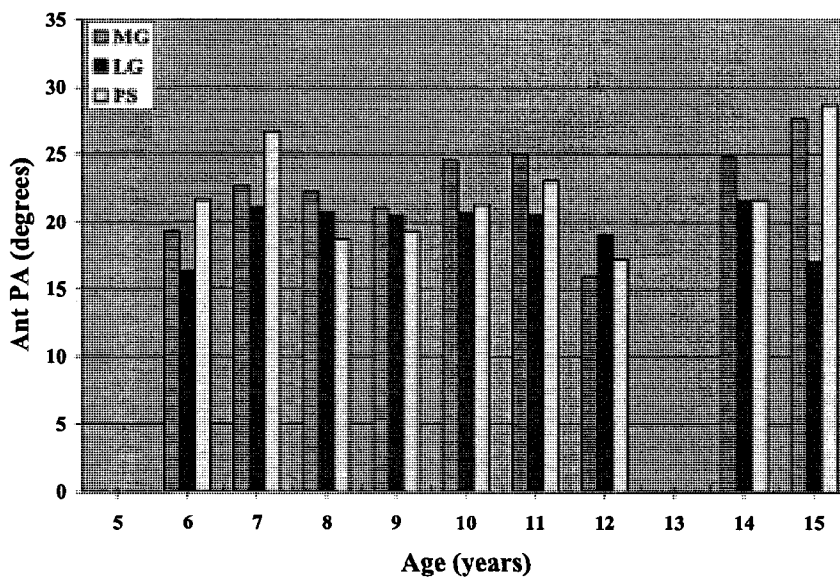


B.

Figure C.1. Bar graphs of mean fiber bundle lengths (FBL) by age for the control group. A. Relaxed. B. Contracted. See Appendix B for the number of subjects in each age group by muscle.

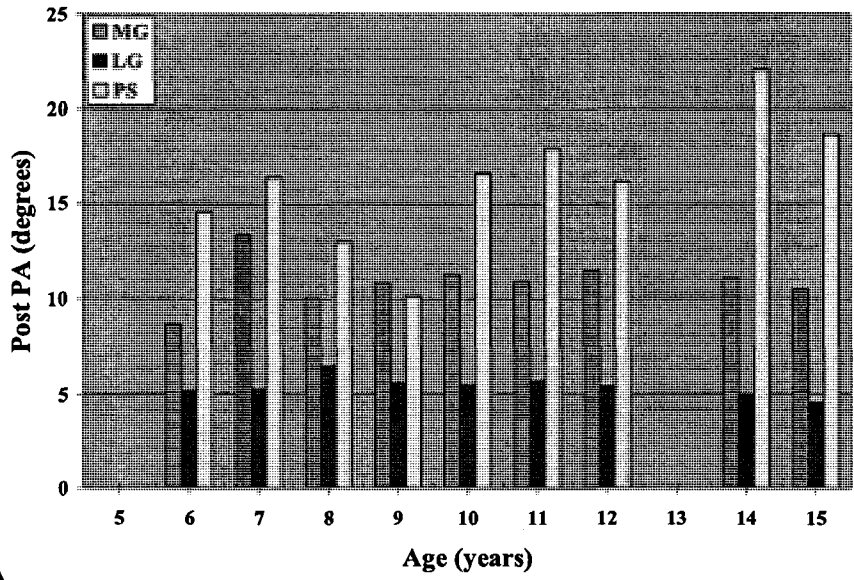


A.

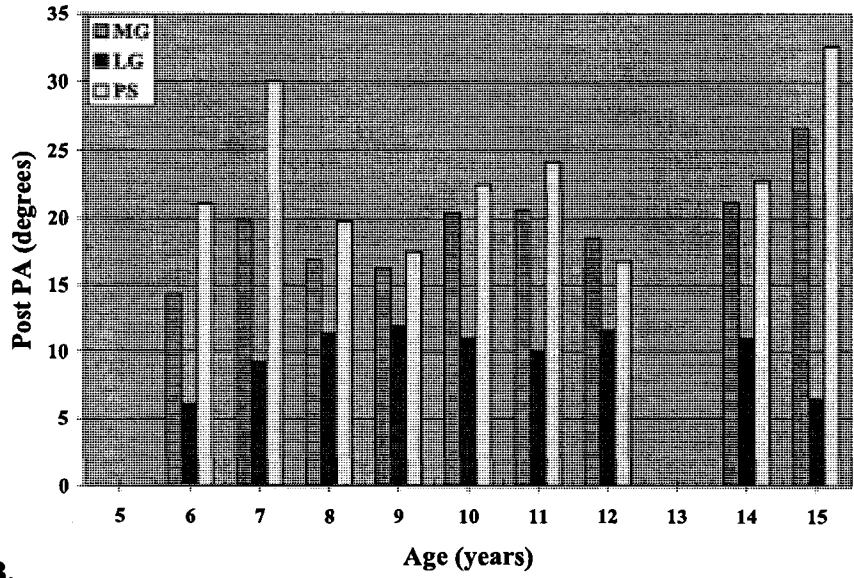


B.

Figure C.2. Bar graphs of mean anterior pennation angles (Ant PA) by age for the control group. A. Relaxed. B. Contracted. See Appendix A for the number of subjects in each age group by muscle. Note that the y-axes are scaled differently in graph A and B to enable better visualization of data.



A.



B.

Figure C.3. Bar graphs of mean posterior pennation angles (Post PA) by age for the control group. A. Relaxed. B. Contracted. See Appendix B for the number of subjects in each age group by muscle. Note that the y-axes are scaled differently in graph A and B to enable better visualization of data.

PA of PS was also larger than MG and LG except at age 12. LG had the smallest mean contracted posterior PA.

MT by age

The MT of subjects by age are summarized in Figure C.4A for the relaxed condition and Figure C.4B for the contracted condition. The relaxed and contracted MTs of MG and PS were similar at most ages, whereas LG had the smallest MT in relaxed and contracted conditions at all ages.

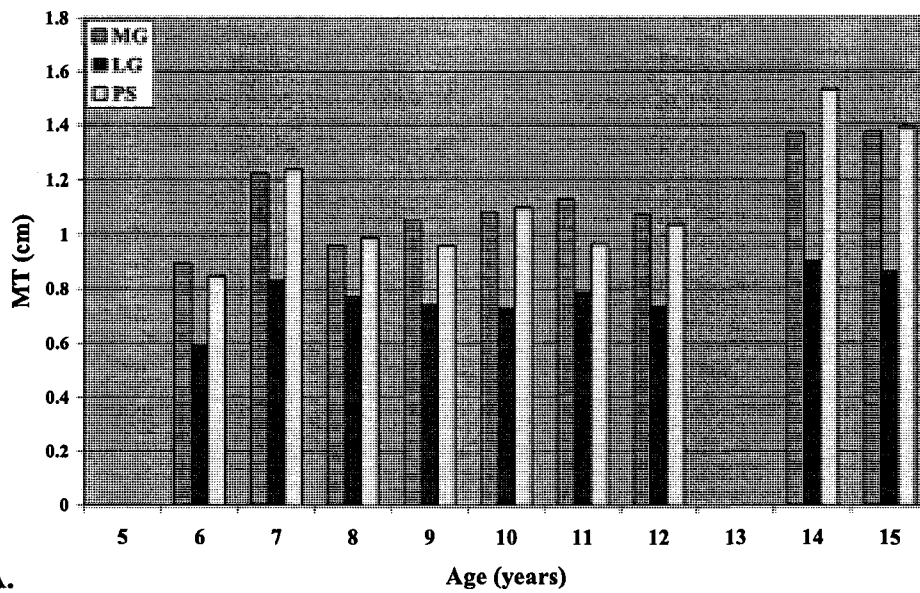
DMD subjects

FBL by age

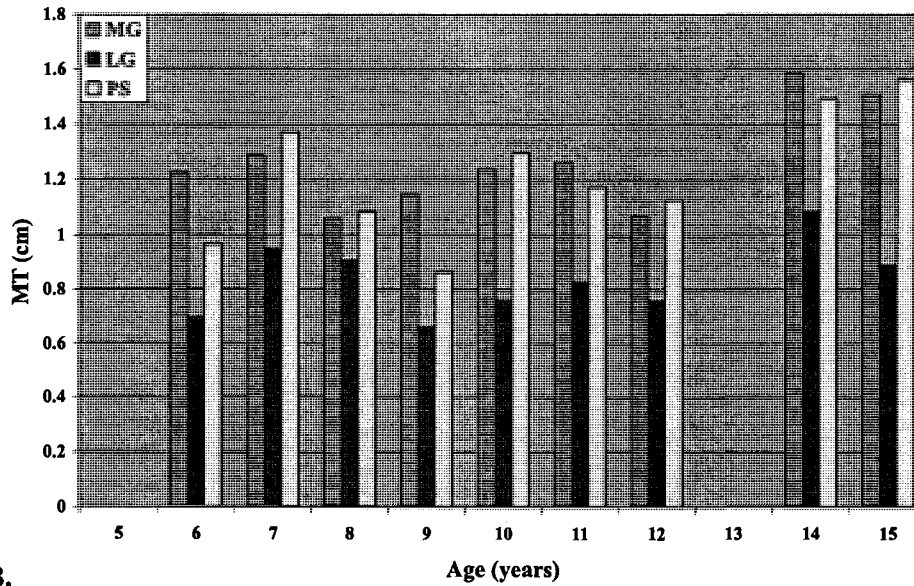
Mean FBL of the DMD subjects are summarized by age in Figure C.5A for the relaxed condition and Figure C.5B for the contracted condition. In the relaxed condition, FBL of MG was longer than LG and PS for most ages. Furthermore, MG was the only muscle that was measurable by age 15.

PA by age

Mean PA of subjects by age are summarized in Figure C.6 for anterior PA and Figure C.7 for posterior PA. Mean relaxed anterior PAs of LG and PS were mostly smaller than MG (Figure C.6A). For the contracted condition, the mean anterior PA of MG was larger than LG from age 7 onwards (Figure C.6B). Mean relaxed posterior PAs of PS were generally the largest, and the means of LG were the smallest at all ages (Figure C.7A). The mean relaxed posterior PAs of MG was between 6° – 12° for most ages. In the contracted condition, MG had the largest mean posterior PA at all ages, while LG was the

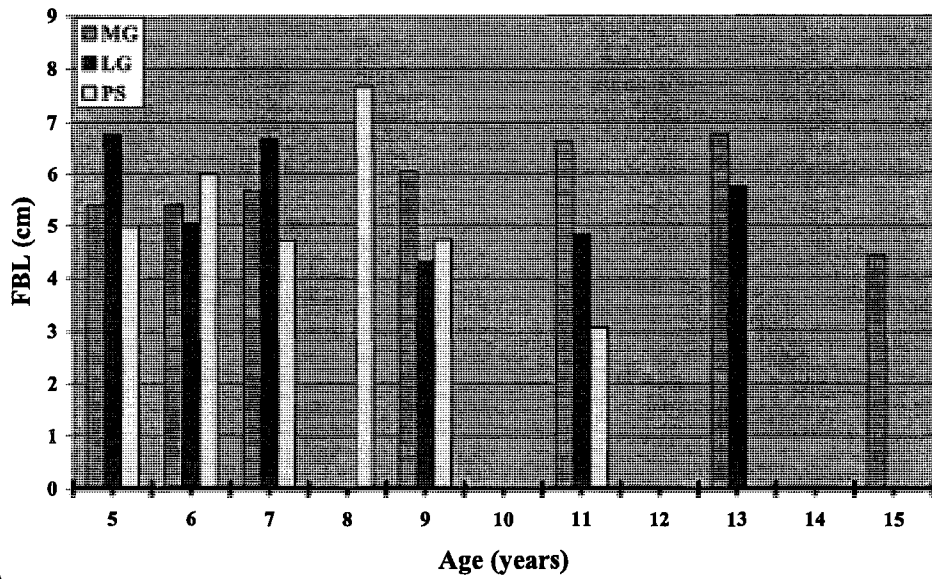


A.

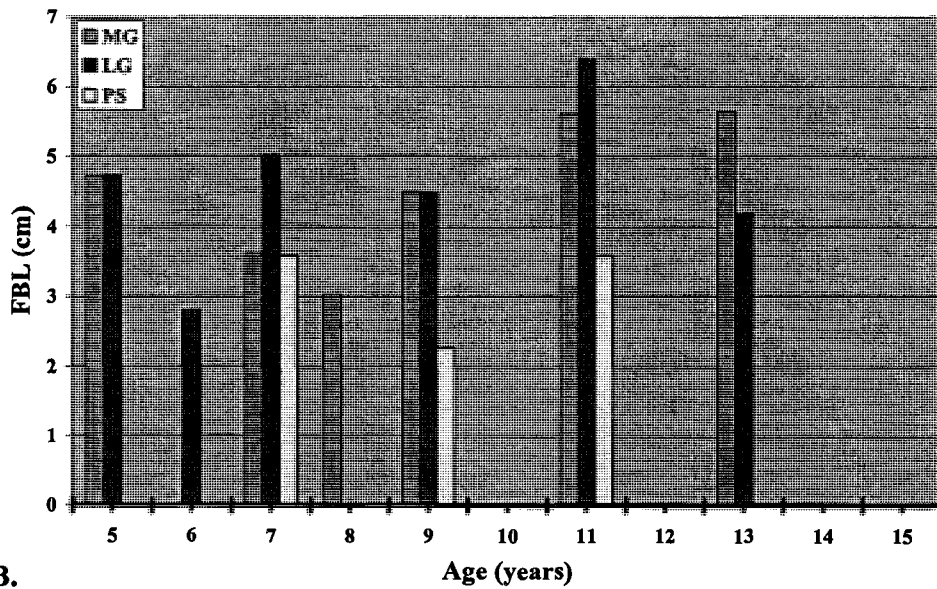


B.

Figure C.4. Bar graphs of mean muscle thicknesses (MT) by age for the control group. A. Relaxed. B. Contracted. See Appendix B for the number of subjects in each age group by muscle.

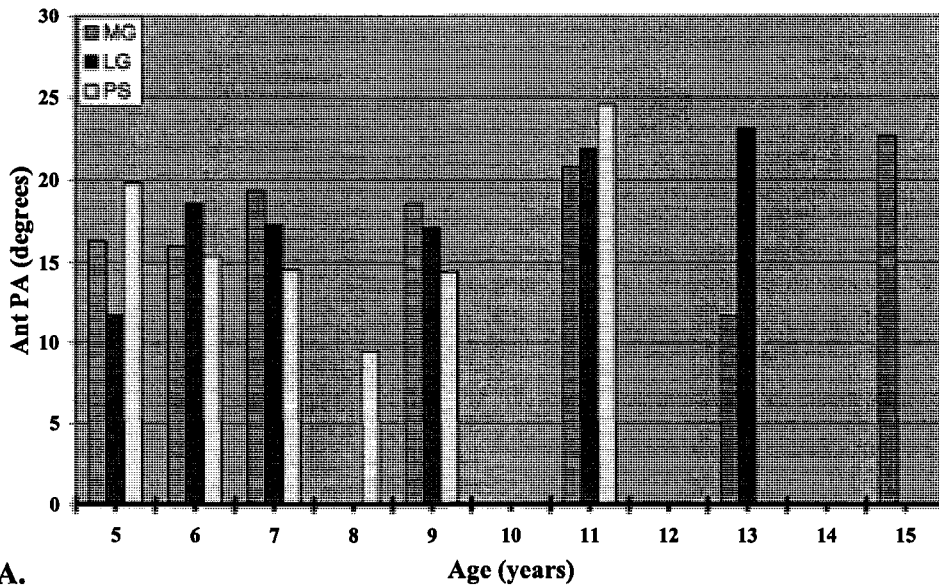


A.

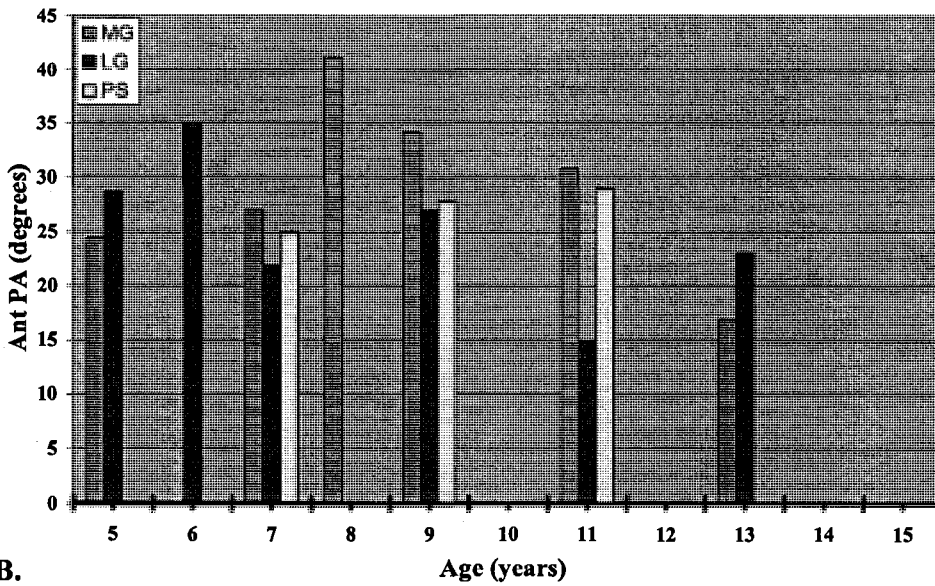


B.

Figure C.5. Bar graphs of mean fiber bundle lengths by age for the DMD group. A. Relaxed. B. Contracted. Note that the y-axes are scaled differently in graph A and B to enable better visualization of data. See Appendix A for the number of subjects in each age group by muscle.

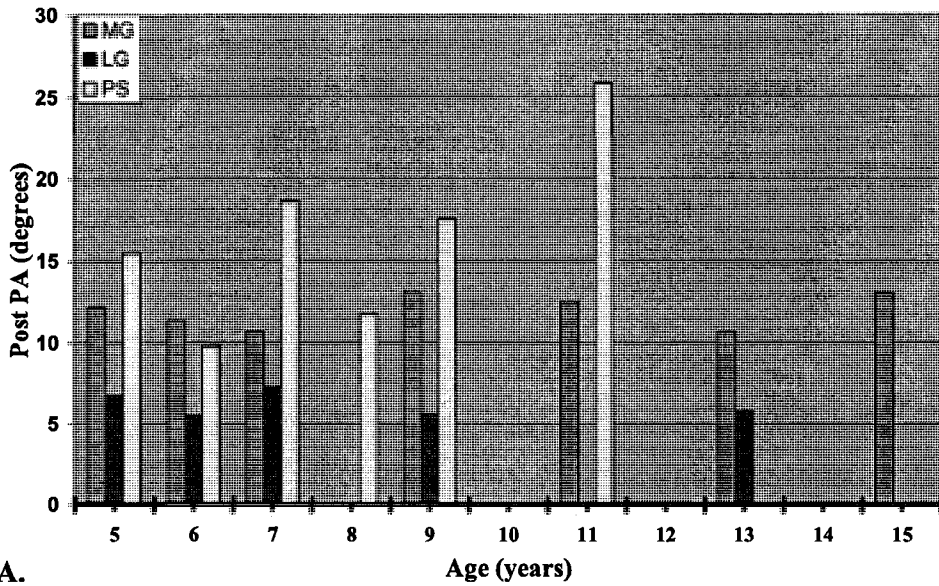


A.

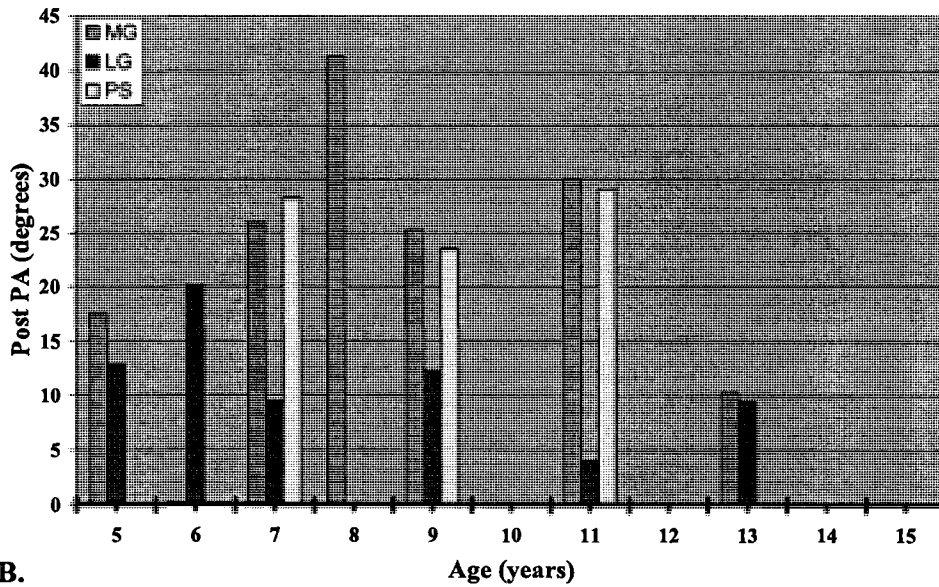


B.

Figure C.6. Bar graphs of mean anterior pennation angles (Ant PA) by age for the DMD group. A. Relaxed. B. Contracted. Note that the y-axes are scaled differently in graph A and B to enable better visualization of data. See Appendix A for the number of subjects in each age group by muscle.



A.



B.

Figure C.7. Bar graphs of mean posterior pennation angles (Post PA) by age for the DMD group. A. Relaxed. B. Contracted. Note that the y-axes are scaled differently in graph A and B to enable better visualization of data. See Appendix A for the number of subjects in each age group by muscle.

smallest for most subjects (Figure C.7B). There was a noticeable decline in the mean value of post PA after the age of 9 in the contracted condition.

MT by age

The MT of DMD subjects by age are summarized in Figure C.8A for the relaxed condition and Figure C.8B for the contracted condition. Up to age 9, the relaxed MT of MG was generally the thickest and LG was the thinnest.

Control vs. DMD comparison

FBL by age

The comparison of relaxed and contracted FBL for MG, LG, and PS between control and DMD subjects by age is presented in Figure C.9. In the relaxed condition, DMD subjects between ages 7 – 11 had longer mean relaxed FBLs of MG than control subjects (Figure C.9A). The opposite was true at age 15 when FBL of MG for controls was nearly two times longer than the FBL for DMD subjects. This difference at age 15 in relaxed FBL of MG between DMD and control subjects was the largest among all the ages tested. It should also be noted that relaxed MG was the only muscle that had a quantifiable scan for FBL at age 15 in the DMD group.

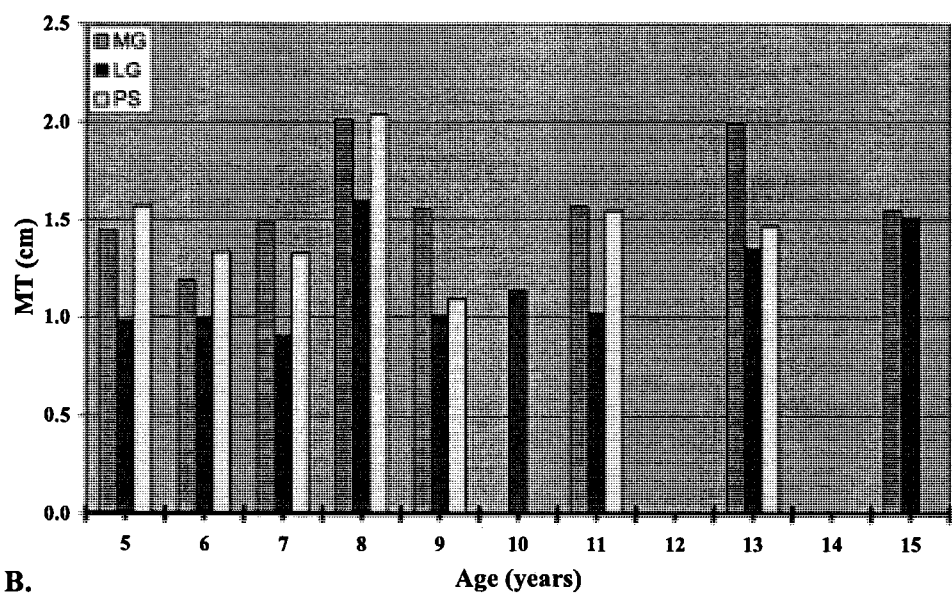
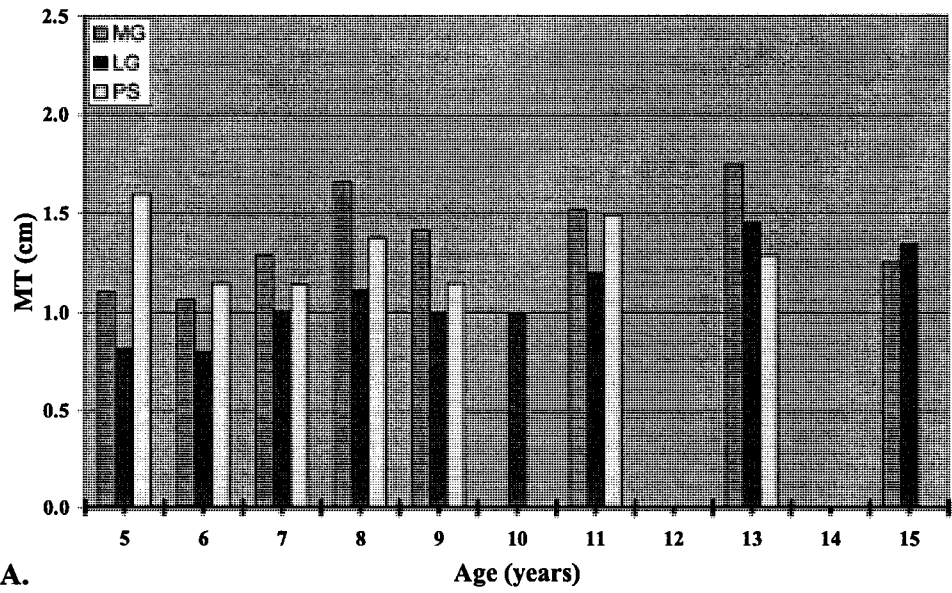


Figure C.8. Bar graphs of mean muscle thickness (MT) by age for the DMD group. A. Relaxed. B. Contracted. See Appendix A for the number of subjects in each age group by muscle.

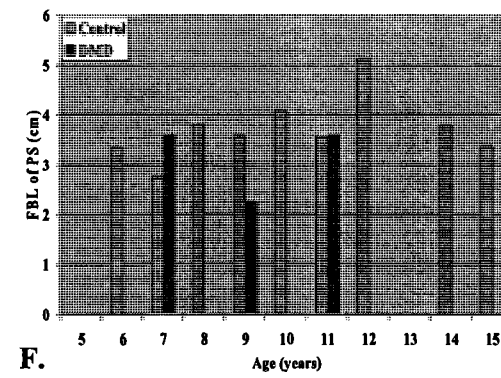
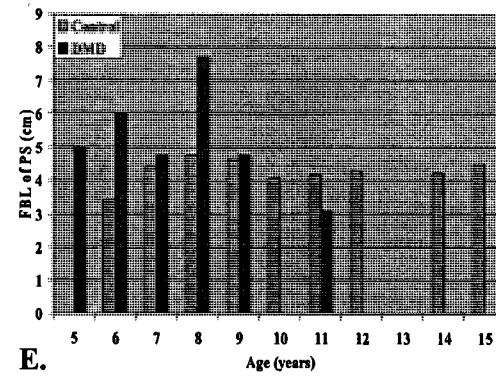
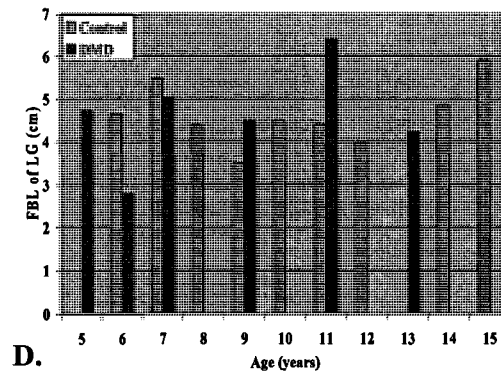
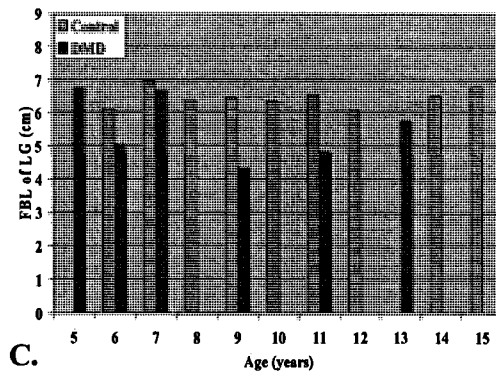
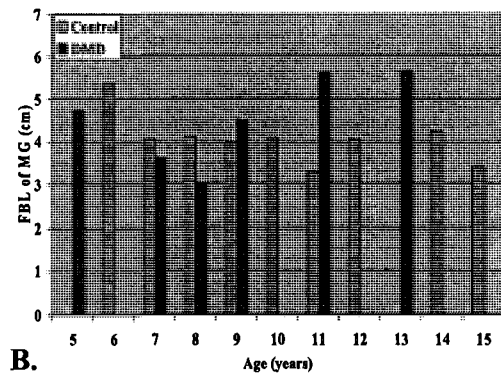
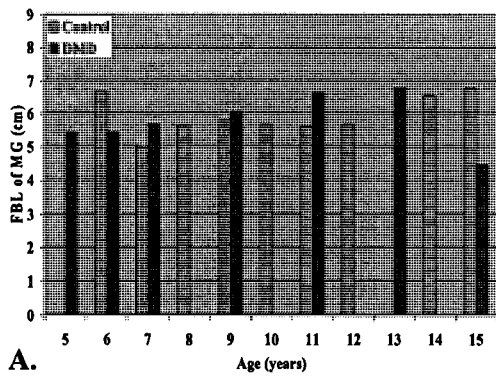


Figure C.9. Bar graphs of mean fiber bundle lengths by age for control vs. DMD groups. A. Relaxed MG B. Contracted MG C. Relaxed LG D. Contracted LG E. Relaxed PS F. Contracted PS.

There were fewer quantifiable scans for the mean relaxed FBL of LG and PS than MG in the DMD group, and the majority of the available LG and PS scans were in subjects under age 10 (Figures C.9C and C.9E). Where comparisons could be made, relaxed FBL of DMD was shorter than controls for LG, but longer than controls for PS.

For the DMD group, no quantifiable scans were available for LG and PS at ages 14 and 15; contracted PS also had the least number of quantifiable scans of the three muscles (Figures C.9D and C.9F).

PA by age (Control vs DMD)

The comparison of relaxed and contracted anterior PA for MG, LG, and PS between control and DMD subjects by age is presented in Figure C.10. MG and LG of DMD group had larger relaxed and contracted anterior PA than the control group in all age groups except at age 11 for the contracted LG.

The comparison of relaxed and contracted posterior PA for MG, LG, and PS between control and DMD subjects by age is presented in Figure C.11. MG of DMD group had larger relaxed and contracted posterior PA than the control group in a majority of age groups. LG and PS had the most unmeasurable scans in the DMD group. For example, relaxed LG (Figures C.11C) had unmeasurable scans for ages 10, 11, 14, and 15 (there were no 12 year old DMD subjects) compared to no unmeasurable scans in the control group (there were no 13 year olds in the control group).

MT by age (Control vs. DMD)

The comparison of relaxed and contracted MT for MG, LG, and PS between control and DMD subjects by age is presented in Figure C.12. In both relaxed and contracted conditions, the MT of DMD subjects was greater in a majority of age groups than controls for all three muscles. It is interesting to note that the oldest control subject (i.e., age 15) for MG had larger MT than the DMD subject, but for LG the oldest control subject had smaller MT than the DMD subject (Figure C.12A – D). The DMD scan of PS for the oldest boy was not quantifiable in relaxed or contracted conditions

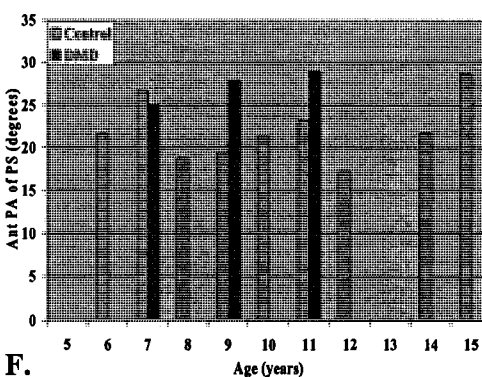
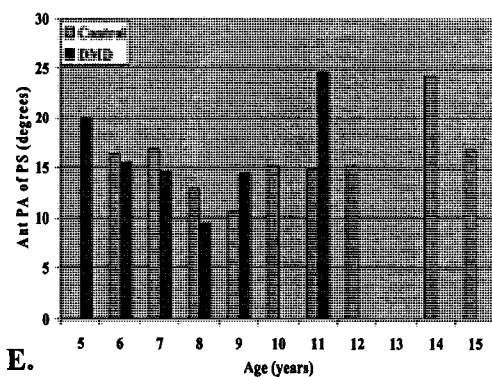
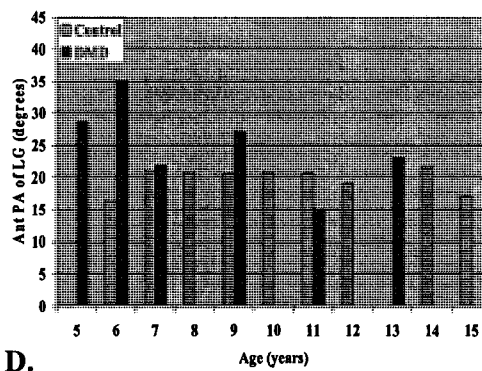
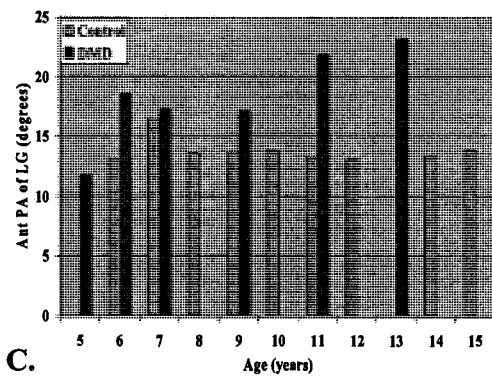
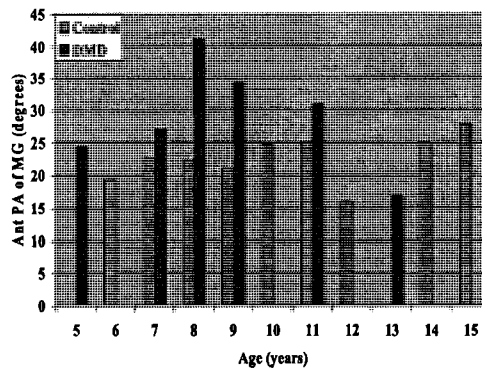
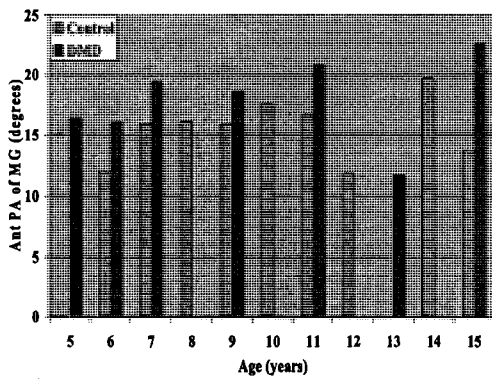


Figure C.10. Bar graphs of mean anterior pennation angles (Ant PA) by age for control and DMD groups. A. Relaxed MG B. Contracted MG C. Relaxed LG D. Contracted LG E. Relaxed PS F. Contracted PS.

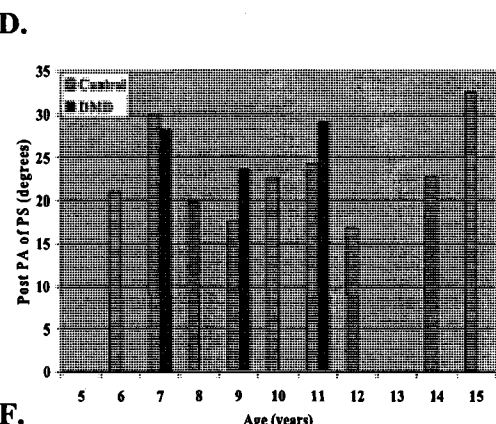
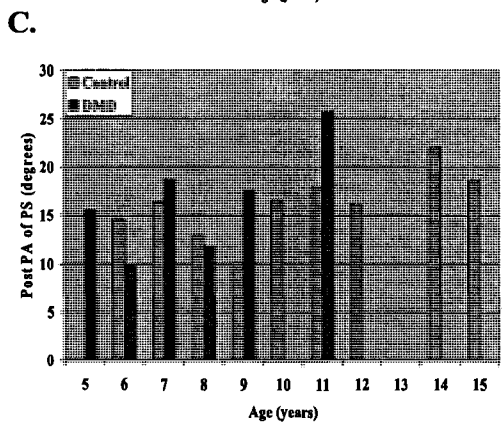
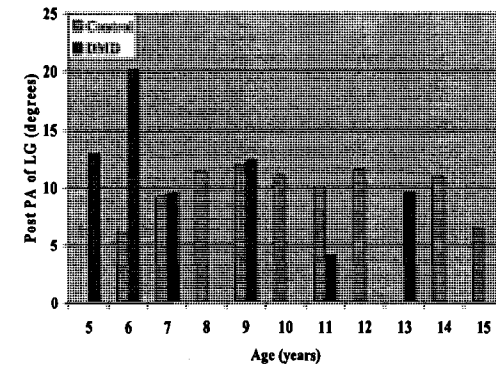
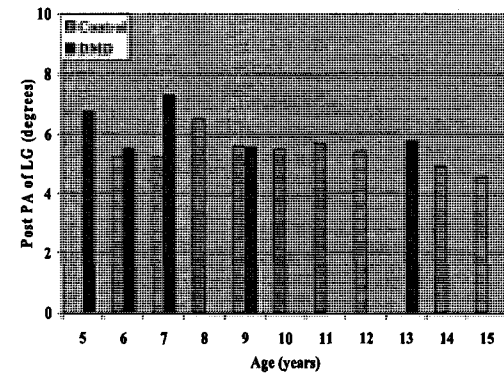
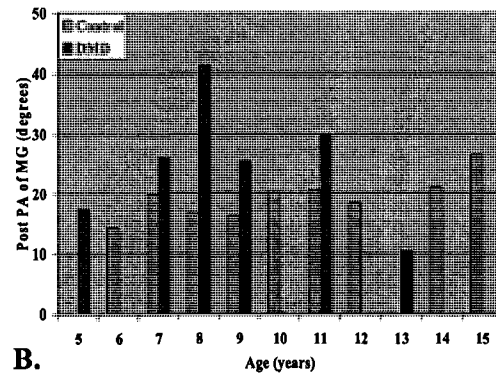
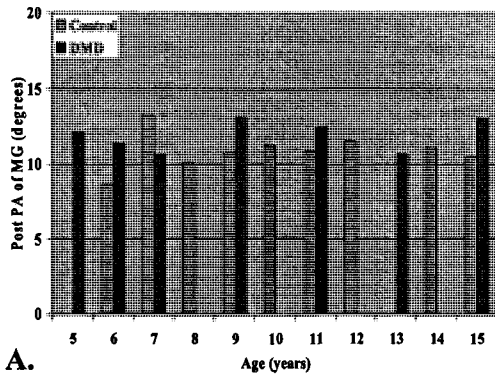


Figure C.11. Bar graphs of mean posterior pennation angles (Post PA) by age for control and DMD groups. A. Relaxed MG B. Contracted MG C. Relaxed LG D. Contracted LG E. Relaxed PS F. Contracted PS.

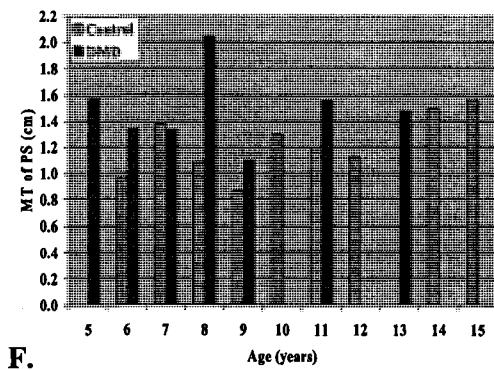
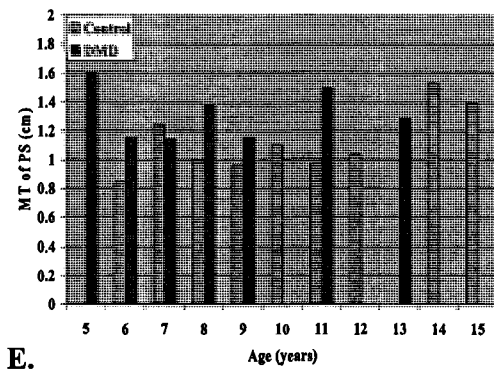
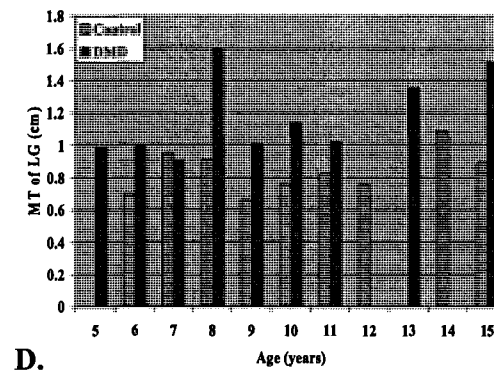
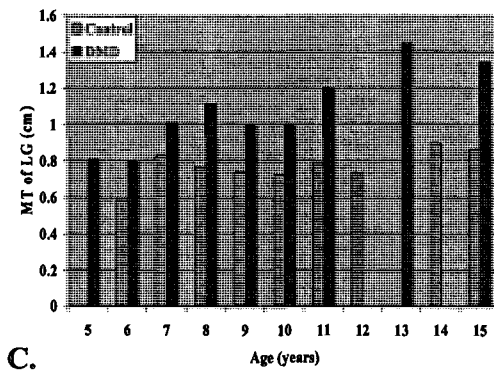
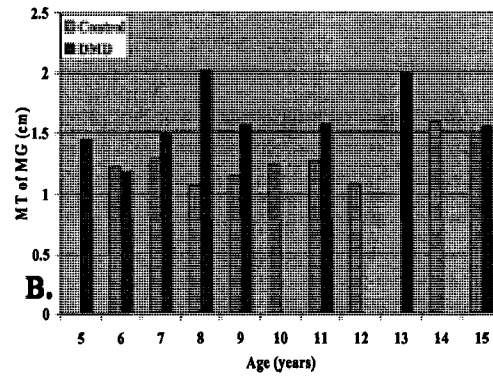
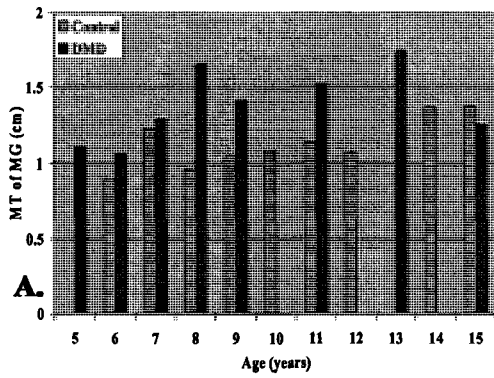


Figure C.12. Bar graphs of mean muscle thicknesses (MT) by age for control and DMD groups. A. Relaxed MG B. Contracted MG C. Relaxed LG D. Contracted LG E. Relaxed PS F. Contracted PS.

Appendix D: Calculations for Specificity and Sensitivity

Specificity and Sensitivity of the new qualitative rating scale was calculated using the formulae $d/(b+d)$ for specificity and $a/(a+c)$ for sensitivity (Table D.1).

	Subjects with DMD	Healthy controls
Qualitative rating of 1-4 (i.e., "Positive test")	108 a	9 b
Qualitative rating = 0 (i.e., "Negative test")	0 c	99 d

Table D.1. Number of legs (DMD and control) for specificity and sensitivity calculations. A qualitative rating of 1-4 is considered a "positive test" and a qualitative rating of 0 is considered a negative test).

I. Specificity calculations for new US qualitative rating scale:

$$d/(b+d)$$

$$= 99/(9+99)$$

$$= 99/108$$

$$= 91.7\%$$

II. Sensitivity calculations for new US qualitative rating scale.

$$a/(a+c)$$

$$= 108/(108+0)$$

$$= 108/108$$

$$= 100\%$$

Appendix E: Assent and Consent forms

Assent Form (boys up to 15 years)

Title of study: To see if the fibers in two of your leg muscles have changed in organization and function as a result of Duchenne muscular dystrophy.

Investigators:

Christopher Yuen, BSc(OT), MSc candidate
Department of Exercise Science, University of Toronto
(416) 978-8855

Nancy Hunt McKee, MD, FRCS(c), FACS
Department of Surgery, University of Toronto.
(416) 978-2965

Anne Agur, BSc(OT), MSc., Ph.D.
Department of Surgery, Division of Anatomy, University of Toronto.
(416) 978-8855

Doug Biggar MD, FRCP(c)
Pediatrician, Bloorview MacMillan Centre
(416) 424-3813

Joe Chan MRT(R)
Radiation Technologist, Bloorview MacMillan Center
416-425-6220 x3518

Roger Leekam MD, FRCP(c)
Radiologist (Specialist: Musculoskeletal Ultrasound)

Why are we doing this study?

It is not known how Duchenne muscular dystrophy affects muscle fiber organization. To study muscle fiber organization we look at fiber length, fiber angle and muscle thickness. We would like to find out if there are any changes in muscle fiber organization in your relaxed and working leg muscles. If we find changes in your muscles we want to see how the changes relate to your leg movements.

What will happen to me during this study?

During your visit, you will meet one of the people in charge of the study at Bloorview MacMillan Center. The study will be explained to you. You will be shown the ultrasound machine and how it works. Then we will look at two of your muscles on the back of your legs, between the knee and the ankle, with the ultrasound machine. We will look at the same muscles in both your right and left legs. To do the ultrasound study you will have to lie on a table on your stomach. Some cream will be put on the back of your leg and we will move a sensor over the surface of the skin. Sound waves will pass through your skin into the muscle. Your muscle fibers will appear on a computer screen. Pictures will be taken of many parts of each muscle first when the muscle is relaxed and then when the muscle is active. You will not feel any pain. You will also be asked what activities you do and your right and left leg length will be measured with a measuring tape.

Are there good things and bad things about the study?

As far as we know there are no bad things that happen as a result of ultrasound of muscles. You will not feel any pain and we will make you as comfortable as possible when you are on the padded table.

The good thing about the study is that we hope to learn how your muscle structure changes with Duchenne muscular dystrophy and how it may affect movement.

Who will know about what I did in this study?

Everything you tell us about yourself and all the ultrasound scans and tapes will not be given to anyone who is not a part of this study. Your name will not be printed or used in anything written or in presentations about the study.

Can I decide if I want to be in the study?

You do not have to take part in the study. No one will be mad or disappointed. If you say yes now but change your mind later, you can still say no. Your parents are reading some information about this study and they will also talk to you about it. Please ask us questions if you do not understand what you have read or what people have told you. We will answer all your questions so that we can help you understand the study.

If you give us your permission, please sign here.

I want to be in this study.	
_____	_____
Name of patient	Age of patient

Signature of patient	

Name of person who obtained assent

Signature

Date

I was present when _____ read this form and gave his/her verbal assent.

CONSENT FORM (Parent copy)

Title of the study:

Muscle architecture and function in children with Duchenne muscular dystrophy.

Investigators and collaborators:

Christopher Yuen BSc(OT), MSc candidate
Department of Exercise Science, University of Toronto
(416) 978-8855

Nancy Hunt McKee MD, FRCS(c), FACS
Department of Surgery, University of Toronto.
(416) 978-2965

Anne Agur BSc(O.T.), MSc., Ph.D.
Department of Surgery, Division of Anatomy, University of Toronto.
(416) 978-8855

Doug Biggar MD FRCP(c)
Pediatrician, Bloorview MacMillan Centre
(416) 424-3813

Joe Chan MRT(R)
Radiation Technologist, Bloorview MacMillan Center
416-425-6220 x3518

Roger Leekam MD, FRCP(c)
Radiologist (Specialist: Musculoskeletal Ultrasound)

Purpose of the study

Muscle has been shown to undergo changes in Duchenne Muscular Dystrophy. Studies have focused on the microscopic changes that occur in the muscle. In this study we will examine the muscle fiber bundle organization throughout two calf muscles of children with Duchenne muscular dystrophy, using ultrasound. These results will be compared to data from similarly aged children with no history of muscular disease. Ultrasonography enables us to look at differences in fiber length and fiber angle in several parts of two calf muscles (gastrocnemius and soleus). The muscles will be studied in relaxed and contracted states. This study will enable us to document changes that have taken place in muscle organization in Duchenne muscular dystrophy, and how those changes may affect muscle function.

What does participation in the study involve?

Our principal investigator will briefly explain the study to you when he contacts you by phone. The study will be explained to you again on the day of your participation. You will be given a copy of the consent form to keep. The study itself will consist of one visit, of 60 minutes duration, to the Medical Imaging Department and gait lab at the Bloorview MacMillan Center. The fiber organization of two calf muscles will be studied using ultrasound. Ultrasound is a painless noninvasive technique, with no known side effects. You and your child will be shown the ultrasound machine and given an explanation of how it works.

We will begin by looking at two of your child's calf muscles using the ultrasound machine. We will look at the same muscles in your child's right and left legs. To do the ultrasound study your child will have to lie on a table on their stomach. Some jelly will be put on the back of their leg and a sensor (transducer) will be run over the surface of the skin. Sound waves will pass through the skin into the muscle and an image of the muscle fiber bundles will appear on a computer screen. Film will be taken of many parts of each muscle, first when the muscle is relaxed and secondly when the muscle is active (contracted). Later the images will be used to measure relevant muscle parameters. Your child will be asked what activities he/she does and their right and left leg length will be measured with a measuring tape.

How do I get to the Bloorview MacMillan Center?

We will give you a map with instructions on how to get to Bloorview MacMillan Center, 350 Rumsey Rd., Toronto. Parking costs will be refunded.

Potential risks and benefits

Ultrasound is a painless non-invasive technique, with no known side effects.

The benefit of the study is that we will better understand changes that occur in muscle organization and function in Duchenne muscular dystrophy. We hope that this will lead to better understanding of the problems associated with gait and provide a non-invasive way to assess the effects of treatments to optimize gait.

Confidentiality

All the information which we collect about your child will be kept confidential. No information about your child will be given out to anyone without your written permission, unless this information is required by law.

A number will be assigned to your child at the outset of the study, so that your child's name will remain confidential. In our data bank all scans and recorded information will be referred to by subject number only. Data from subjects in each study group will be combined, therefore making it impossible to identify any individual.

The original consent/assent form(s) will be filed in your child's medical chart (for patients of Bloorview MacMillan). One photocopy of the form(s) will be filed in your

child's research file. You will be given a photocopy of the consent/assent forms for your own records.

Participation

Participation in this study is voluntary. You have the right to decide not to allow your child to be part of this study. You also have the right to withdraw your child from this study at any time. If you don't want to participate or you choose to withdraw at a later date, you and your family will continue to have access to quality care at Bloorview MacMillan Centre.

For questions and further information

Please do not hesitate to contact Chris Yuen (416-978-8855), Anne Agur (416-978-8855), Dr. McKee (416-978-2965) with any questions or concerns you may have in regards to this study, Monday to Friday (9:00AM-4:30PM). If you reach voice mail, please leave your name and phone number. We will call you as soon as we can.

